THE UNIVERSITY OF MICHIGAN

AFAL-TR-66-169 7274-1-F

INVESTIGATION OF MEASUREMENT TECHNIQUES FOR OBTAINING AIRBORNE ANTENNA SPECTRUM SIGNATURES

Final Technical Report
April 1965 to April 1966

June 1966

Prepared by

J. E. Ferris, W. R. DeHart, R. L. Wolford and W. B. Henry

Contract No. AF 33 (615) - 2606
Project No. 4357, Task No. 435703
K. W. Tomlinson, Contract Monitor

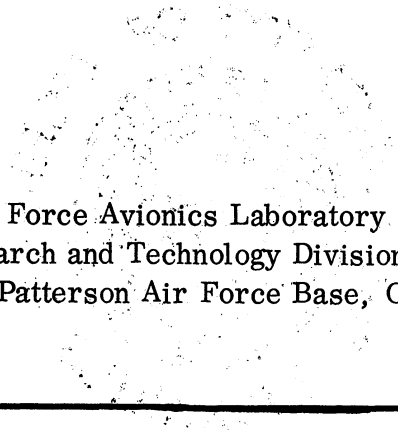

Air Force Avionics Laboratory AVWE
Research and Technology Division, AFSC
Wright-Patterson Air Force Base, Ohio 45433

FOREWORD

This report was prepared by The University of Michigan, under USAF Contract No. AF 33 (615) - 2606. The contract was initiated under Project No. 4357, "Electromagnetic Compatibility Techniques" and Task No. 435703, "Interference Measurement Techniques." This was administered under the direction of the Electronics Warfare Division, Air Force Avionics Laboratory at Wright Patterson Air Force Base, Ohio, with Mr. H. M. Bartman as Project Manager and Mr. K. W. Tomlinson as Contract Monitor. This report covers work conducted from April 1965 to April 1966.

This report was submitted by the authors, 15 April 1966.

PUBLICATION REVIEW

This technical report has been reviewed and is approved.

JOSEPH A. DOMBROWSKI
Lt. Colonel, USAF
Chief, Electronic Warfare Division

TABLE OF CONTENTS

LIST OF FIGURES

LIST OF FIGURES
(continued)

LIST OF FIGURES
(continued)

LIST OF FIGURES
(continued)

LIST OF FIGURES
(continued)

ABSTRACT

This report discusses three areas which are of importance to the Electromagnetic Compatibility program presently being conducted by the U. S. Government. The areas discussed in this report are: 1) methods for obtaining spectrum signatures at a minimum of cost, 2) data recording techniques, and 3) methods for obtaining transmitter signature characteristics.

The methods for obtaining antenna spectrum signatures discusses the use of simplifed models together with typical results for three different antenna configurations. The three antenna configurations were tested on both a simplified and a precision model of a jet aircraft at a fundamental and four harmonic frequencies. In the data recording section the data format for antenna signatures is presented. A recommendation as to the format in which the data should be collected and forwarded to ECAC for prediction analysis is made. A discussion of a technique for digitally recording signature data at a minimum of cost is presented. Under the final section, techniques for determining the signature characteristics of a communications type system are discussed and some preliminary results are presented.

I
INTRODUCTION

The present study has been divided into three areas. Each has been concerned with the determination of the Spectrum Signature of airborne electronics systems. The three areas considered during this study were: 1) methods for obtaining the antenna pattern spectrum signature at a minimum of cost, 2) data recording and reduction techniques, and 3) methods for obtaining transmitter output characteristics.

To obtain antenna spectrum signatures, consideration has been given to the use of simplified models rather than precision models or instrumented airborne systems. An extensive experimental study has been conducted to determine the feasibility of the simplified modeling technique. The initial investigation of simplified models, as they may apply to airborne antenna spectrum signatures, is presented in a report by Ferris, et al (1965) . This study has been continued, and typical results are presented. In addition to simplified models, further consideration has been given to fly-by tests (employing an instrumented full-scale aircraft). Because of costs and the complexity of the technique, it has been rejected as a practical means for obtaining spectrum signature data.

Techniques for recording spectrum signature data of airborne antennas in a digital format have also been investigated during this study. Several digital recording procedures have been considered such that the data could be efficiently stored by the Electromagnetic Compatibility Analysis Center (ECAC).

Supplement I (Dute et al 1966) of this report discusses these techniques in further detail. Digital techniques for recording and storing the original antenna signature data are desirable since ECAC prefers to use statistical procedures when making interference predictions.

Consideration has also been given to procedures that would be applicable to accurately determining the spectrum signature of airborne transmitters. Present measurement techniques employed to obtain signature data from which interference predictions may be calculated are relatively crude. Therefore, the interference predictions are generally unreliable. The present study has been directed to a level which is relatively basic in principle. From this study a better understanding of the measurement procedures as applicable to obtaining the output characteristics of the transmitter can be achieved. The study also provides a more accurate picture of the electronic phenomenon that takes place between the transmitter and antenna at the fundamental, spurious and harmonic frequencies.

II
SIMPLIFIED MODELING

In a previous report, Ferris et al (1965), op. cit. it was shown that the technique of simplified modeling appeared feasible. Therefore, the present contract was initiated to complete the study. During the period covered by the present contract, three antennas located on both the simplified and precision models have been considered. In addition to the study of simplified and precision models, the need for employing full scale aircraft antenna techniques has been considered.

2.1 Antenna Configurations

Two VHF and one UHF antenna configurations were employed during the study of the simplified modeling technique. The VHF antennas were a modified monopole and a conventional $\lambda/4$ monopole antenna. The full-scale modified monopole antenna is designed to operate over a 2:1 frequency range of 200 to 400 MHz, and the simple full-scale $\lambda/4$ monopole is a narrow-band antenna that operates at 300 MHz. Both of these antennas were scaled by a factor of 8 so that they operated in the UHF frequency range at approximately 2.4 GHz center frequency.

The modified monopole was located on scale models of a jet aircraft directly beneath the wings. Three-dimensional antenna spectrum signatures were collected at the fundamental and four harmonic frequencies. The $\lambda/4$ monopole was located on the underside of the nose of the aircraft. Three-dimensional data was collected at the fundamental frequency and principal plane patterns were obtained at four harmonic frequencies.

The UHF antenna simulated a full-scale 1.0 GHz antenna. The scale model antenna consisted of a short section of open ended X-band waveguide operating at a fundamental frequency of 8.0 GHz. Principal plane pattern data was collected at the fundamental and four harmonic frequencies. This antenna was located in the underside of the fuselage midway between the wings.

Pattern data was collected both on the simplified and precision models of the jet aircraft. This data was reduced to typical statistical formats used by ECAC. The statistical data was compared to determine the validity of simplified model data.

2.2 Modified Monopole

Figures 1a and 1b show the modified monopole located on the precision and simplified models respectively. Some data, demonstrating the feasibility of the simplified modeling technique for the modified monopole, was presented in a previous report (Ferris, et al 1965). During the period covered by the present contract, additional data was obtained for the modified monopole antenna at the fundamental and four harmonic frequencies. This data was collected such that the three-dimensional pattern characteristics of the antenna were obtained at each of the above frequencies.

All pattern data collected with the aircraft employed the spherical coordinate system shown in Fig. 2. The three-dimensional antenna patterns were recorded in the θ-variable plane with ϕ varied in increments of 10^{o}. The polarization of the transmitting antenna was constant E_{θ}.

A typical set of three-dimensional pattern data is shown in Figs. 3-22. The data is for 7.2 GHz and alternate patterns show results first for the simplified and then for the precision model for various values of θ and ϕ. This data was reduced to a cumulative gain distribution (statistical) format for further comparison. Typical cumulative gain distributions for the above patterns are shown in Figs. 23-32.

An example of an alternate data reduction technique that was employed to compare the simplified and precision models is illustrated in Figure 33a. The conventional antenna patterns shown in Figs. 3 and 4 have been reduced to statistical patterns in Fig. 33a. Pattern data, when placed in this statistical format by an averaging process, may be effectively compared due to the smoothing of the pattern in cluttered, narrow-lobe regions. This alternate technique employs a sliding sector as illustraged in Fig. 33b. Here it is seen that the sector width (in degrees) is denoted as α, and the sector slide increment (in degrees) as β. The sector α is

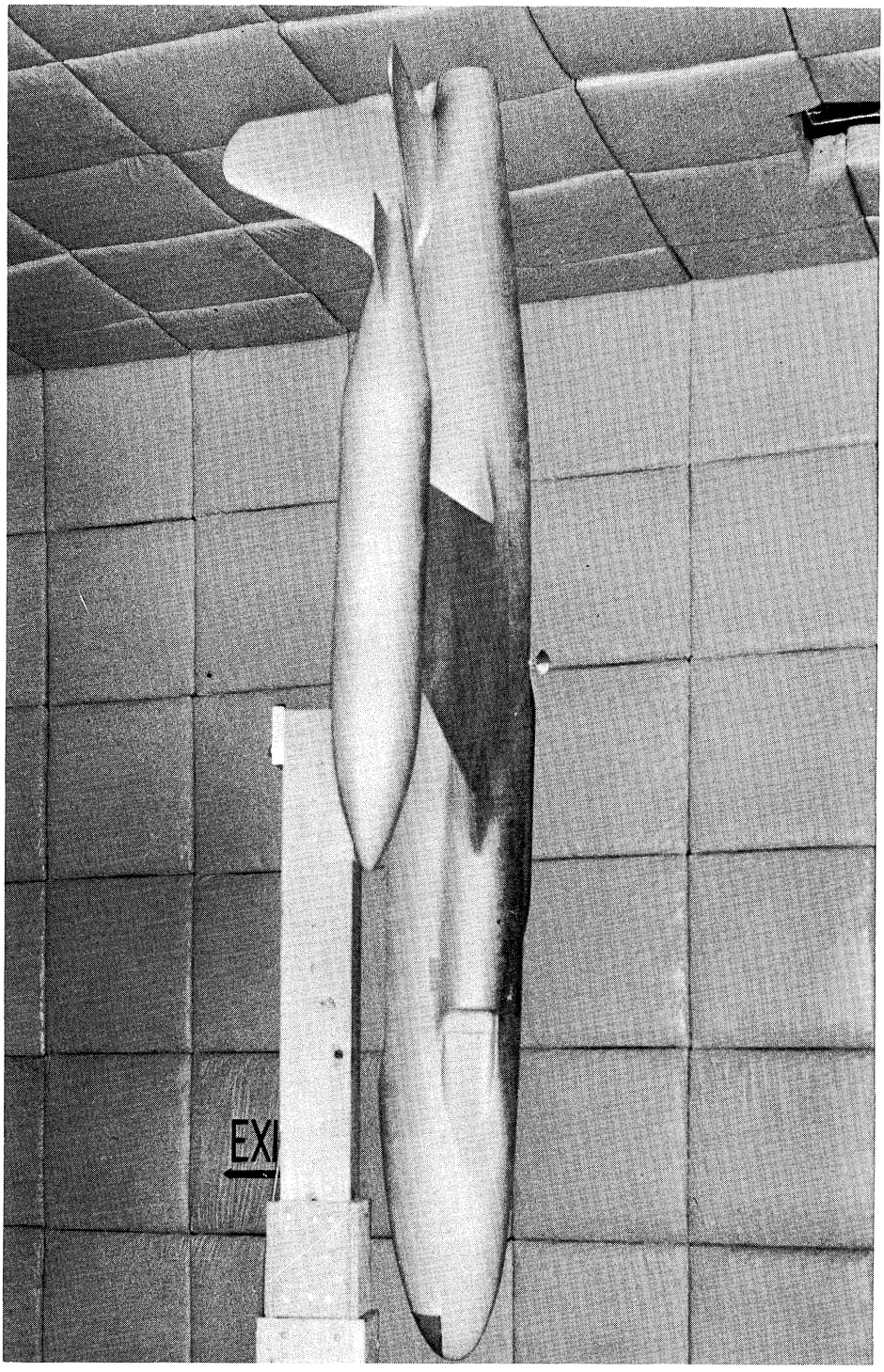

FIG. 1a: PRECISION T-33 MODEL

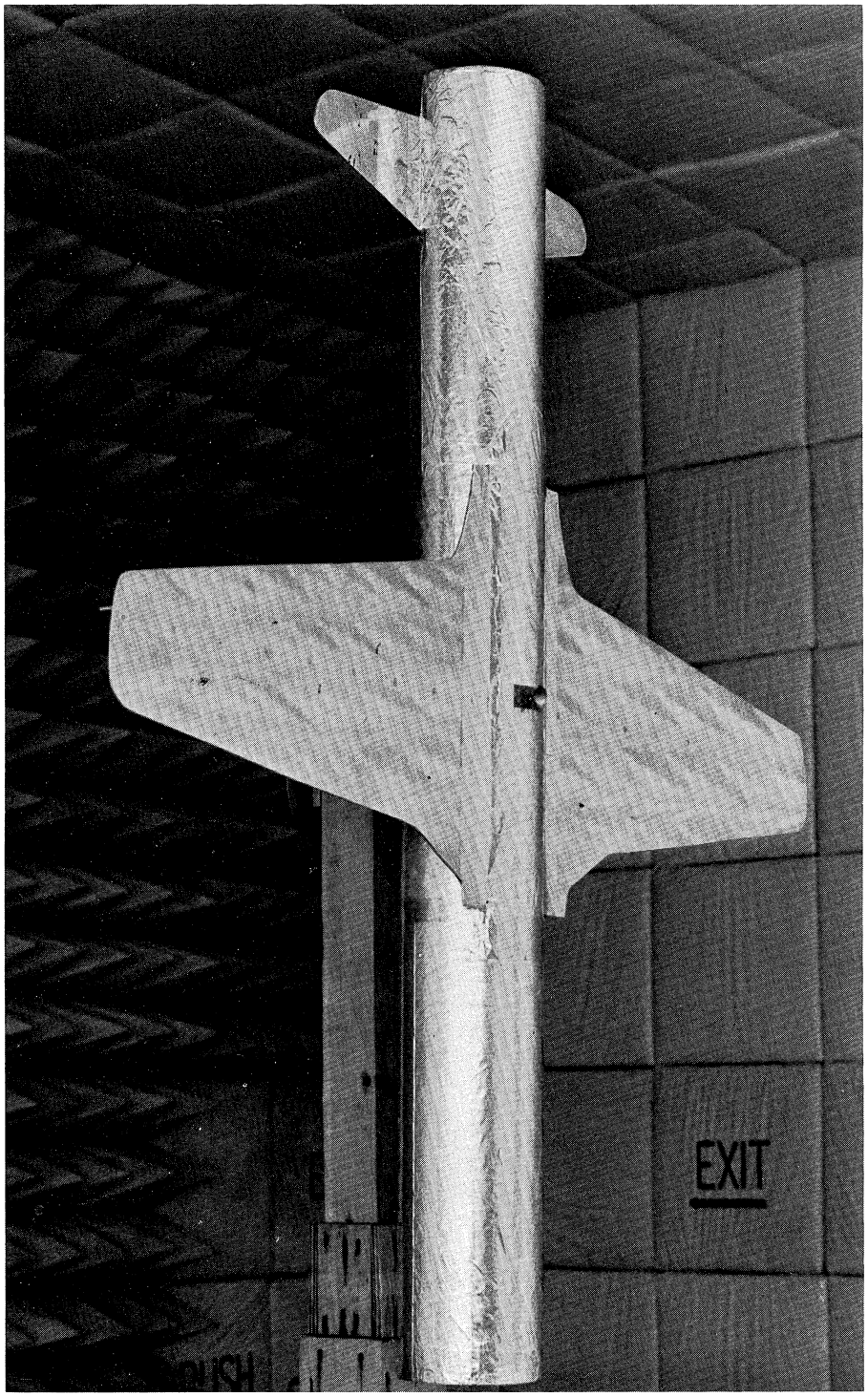

FIG. 1b: SIMPLIFIED T-33 MODEL

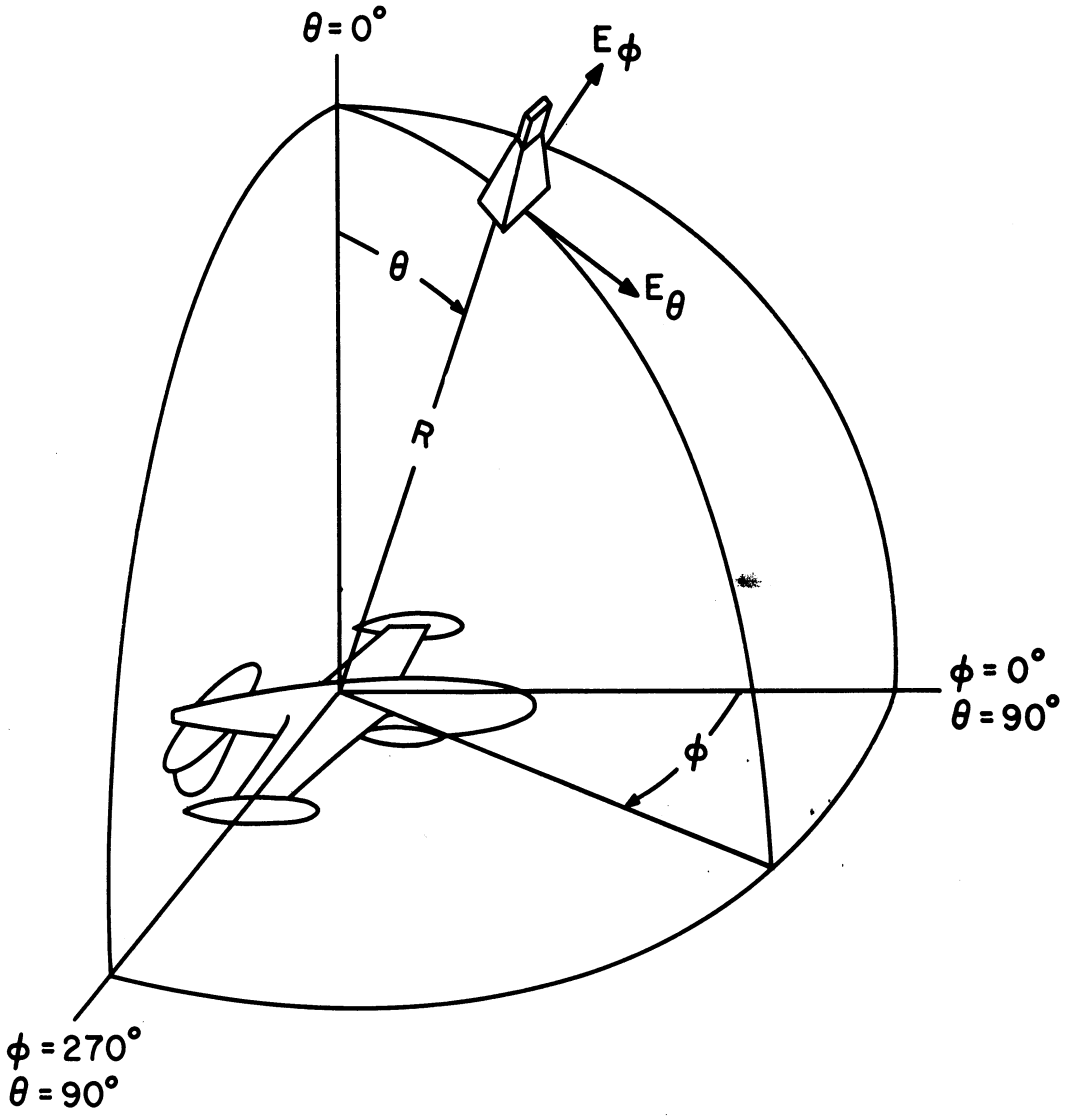

FIG. 2: SPHERICAL COORDINATE SYSTEM

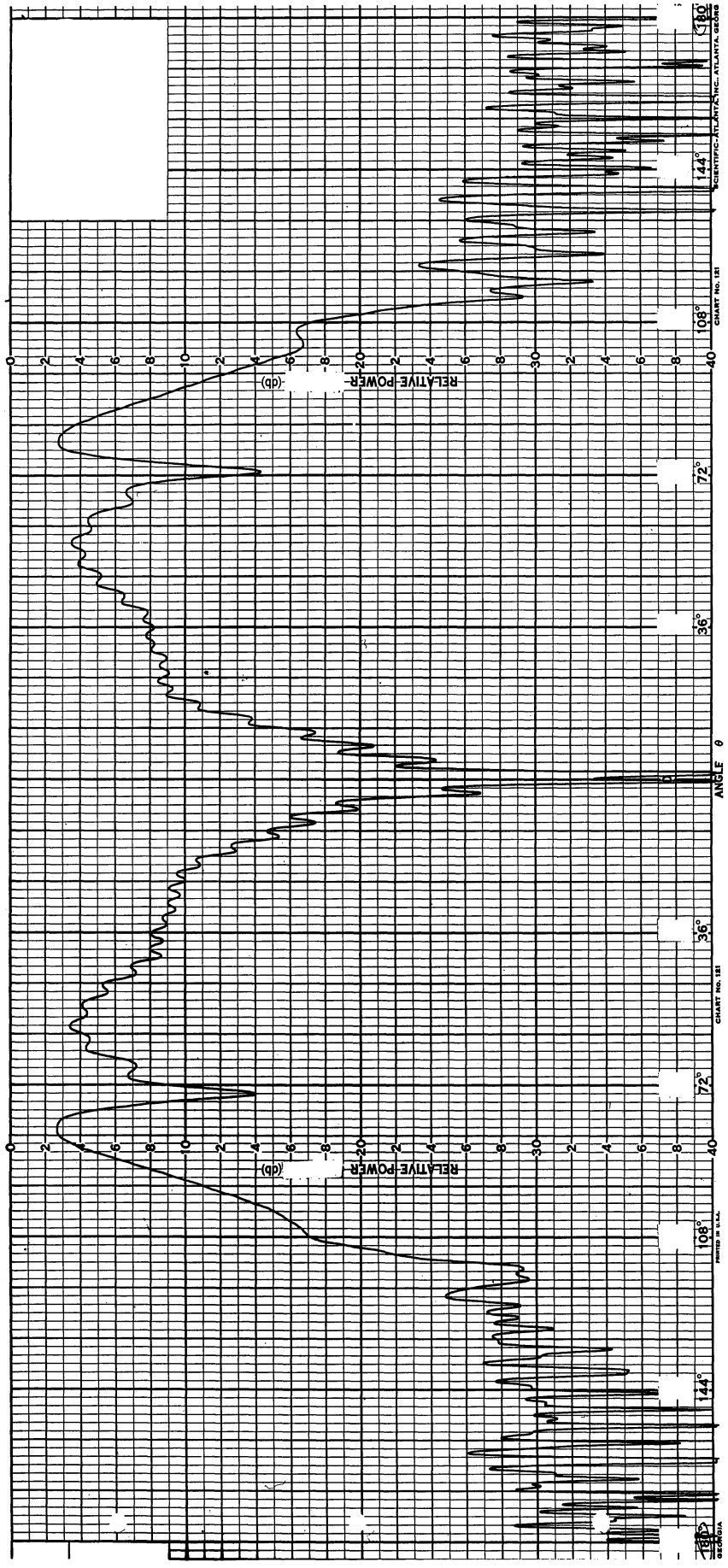

FIG. 3: MODIFIED MONOPOLE 7.2 GHz SIMPLIFIED T-33

$\phi = 90°/\phi = 270°$

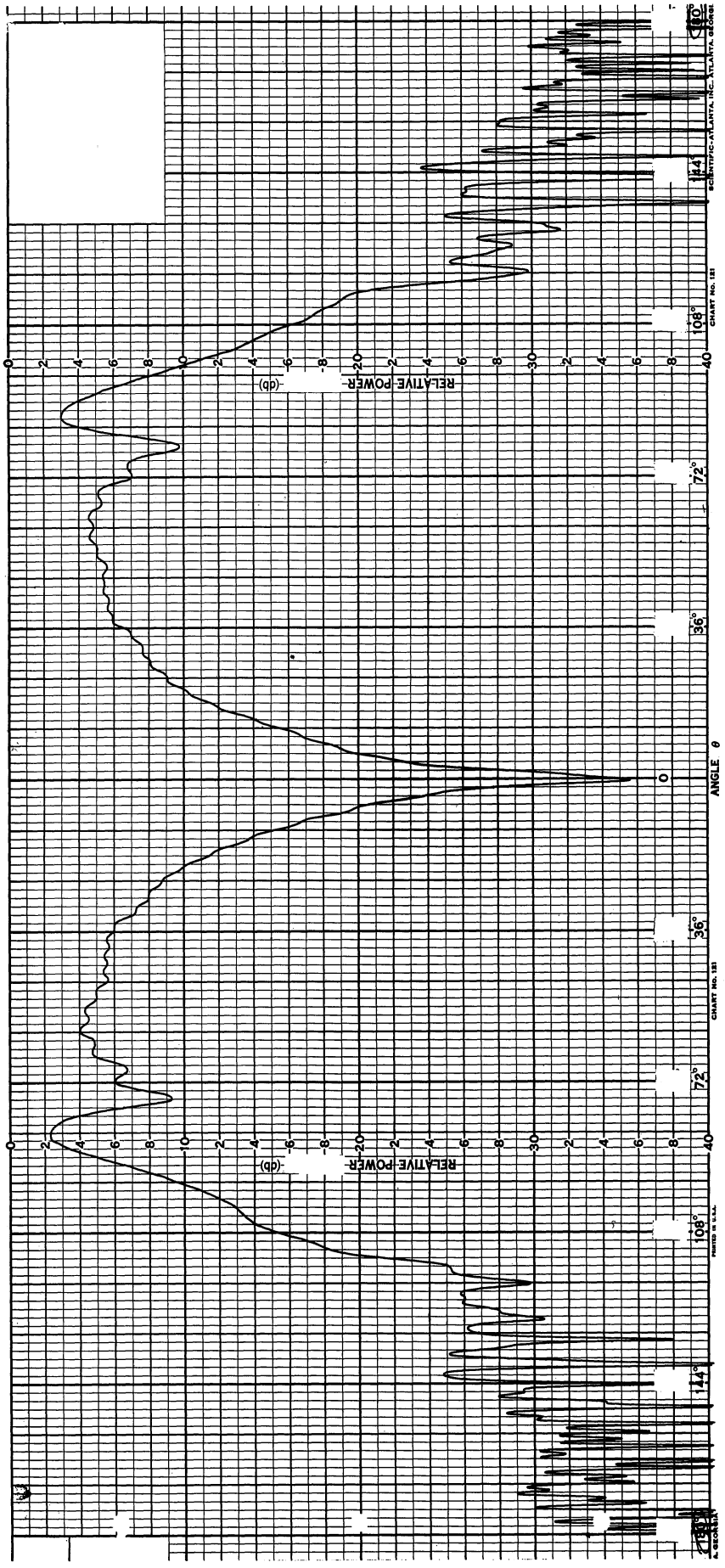

FIG. 4: MODIFIED MONOPOLE 7.2 GHz PRECISION T-33

$\phi = 90^{\circ}/\phi = 270^{\circ}$

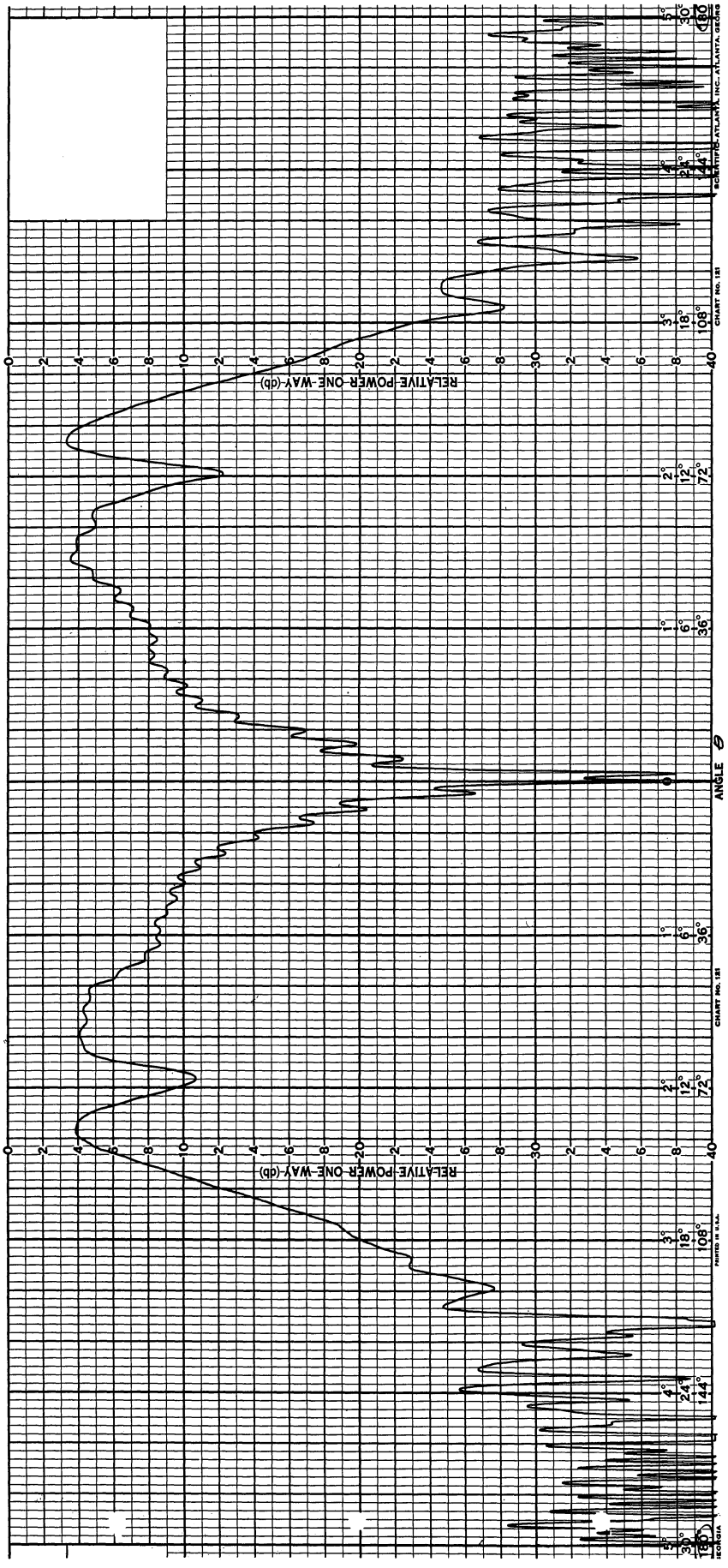

FIG. 5: MODIFIED MONOPOLE 7.2 GHz SIMPLIFIED T-33

$\phi = 100^{o}/\phi = 280^{o}$

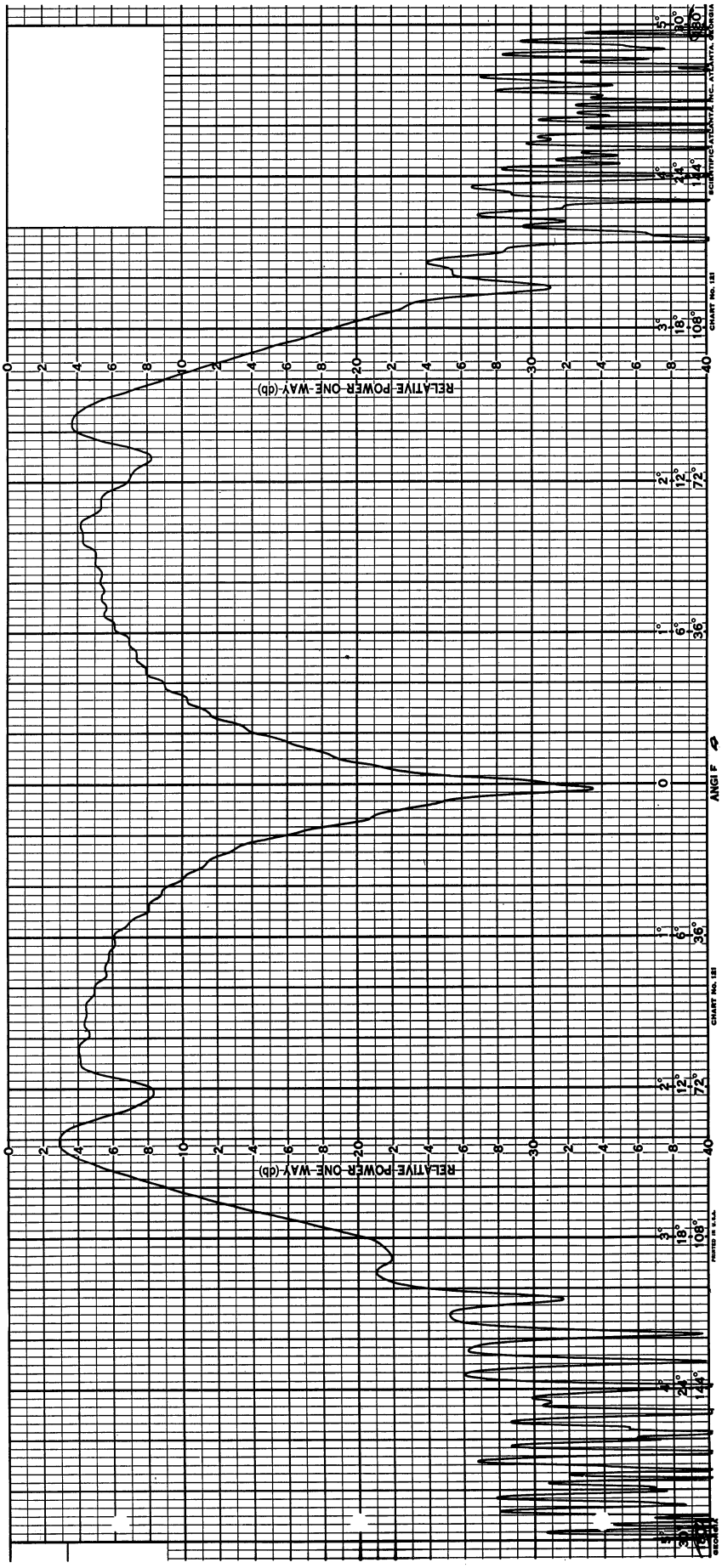

FIG. 6: MODIFIED MONOPOLE, 7.2 GHz, PRECISION T-33

$\phi = 100^{o}/\phi = 280^{o}$

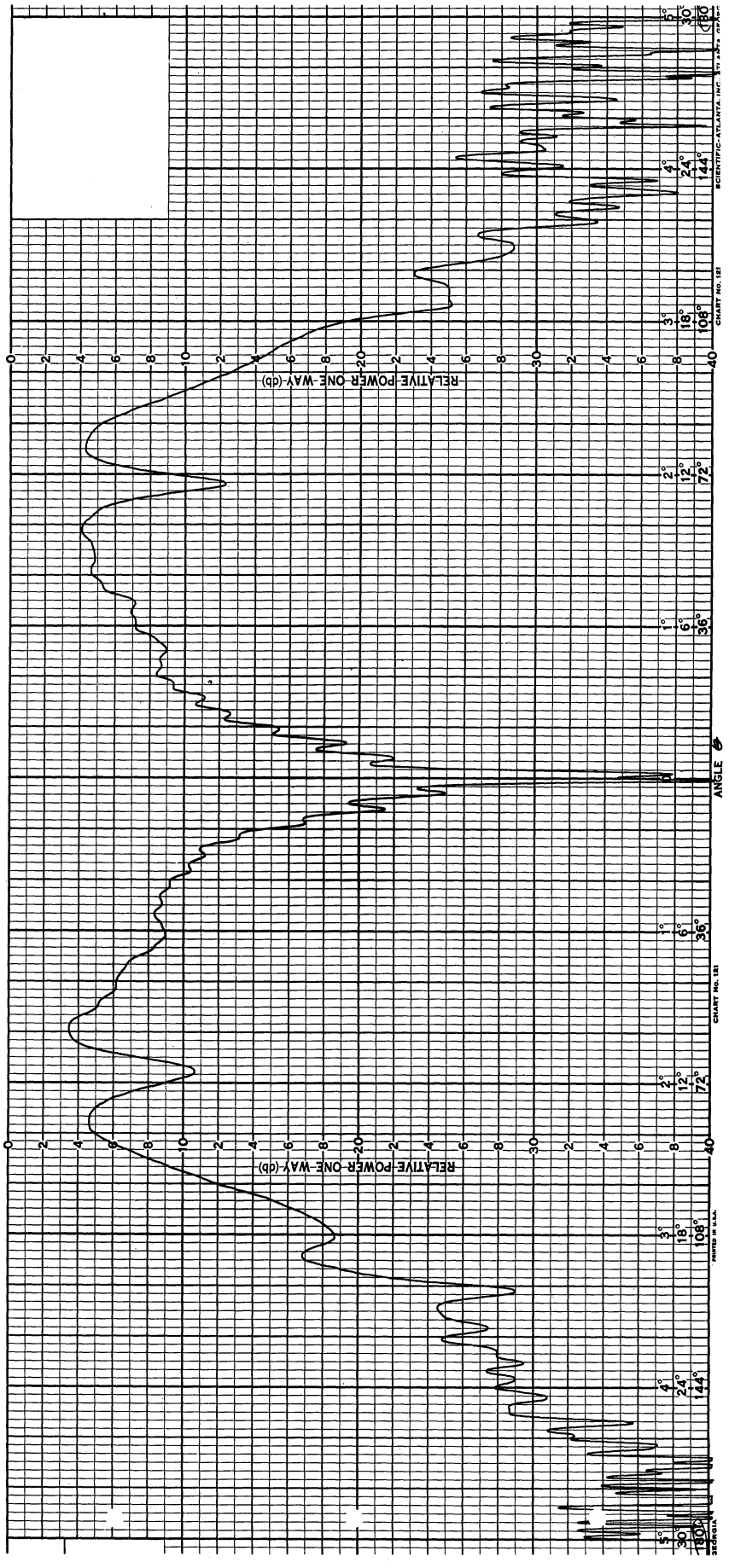

FIG. 7: MODIFIED MONOPOLE, 7.2 GHz, SIMPLIFIED T-33

$\phi = 110^{\circ}/\phi = 290^{\circ}$

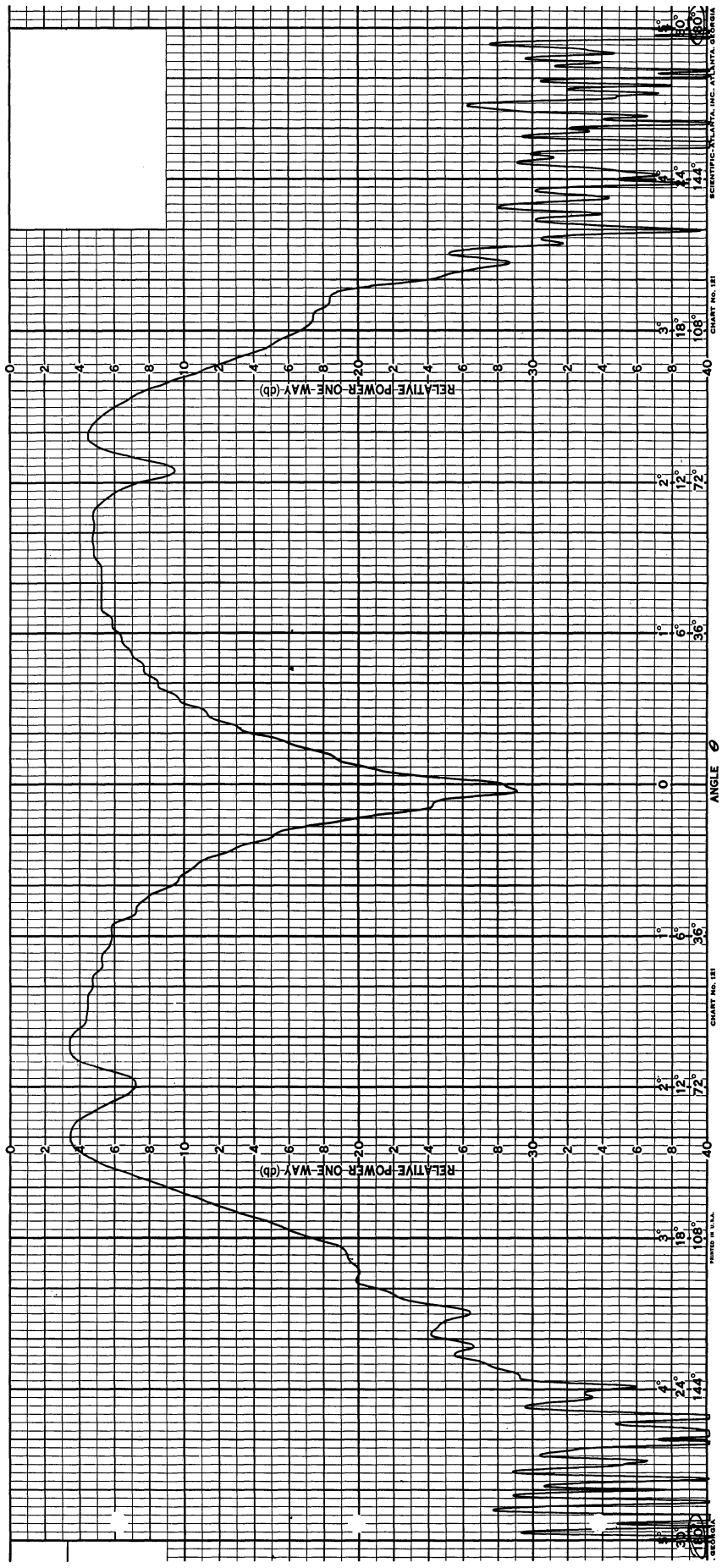

$\phi = 110^{o}/\phi = 290^{o}$

FIG. 8: MODIFIED MONOPOLE, 7.2 GHz, PRECISION T-33

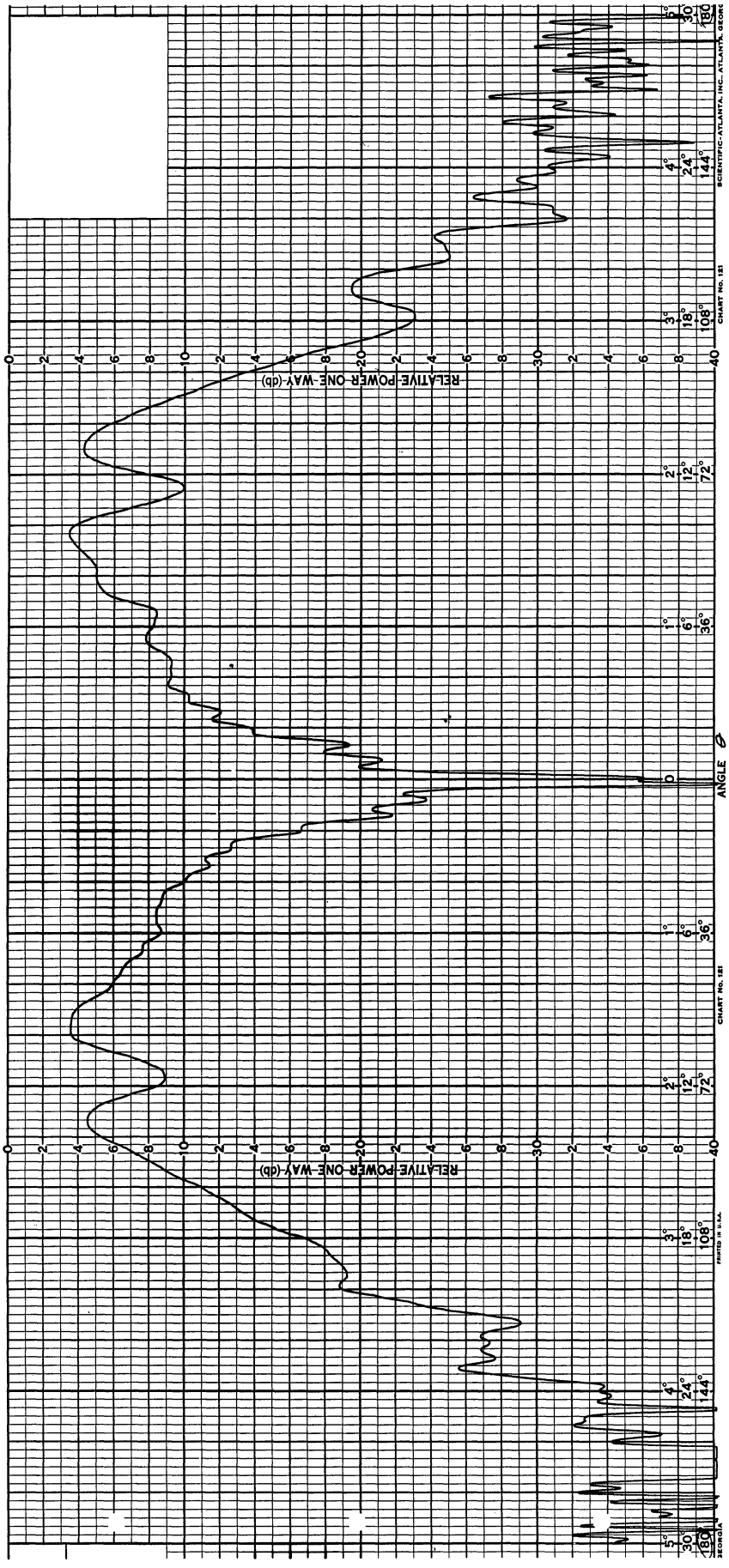

$\phi = 120^{o}/\phi = 300^{o}$

FIG. 9: MODIFIED MONOPOLE, 7.2 GHz, SIMPLIFIED T-33

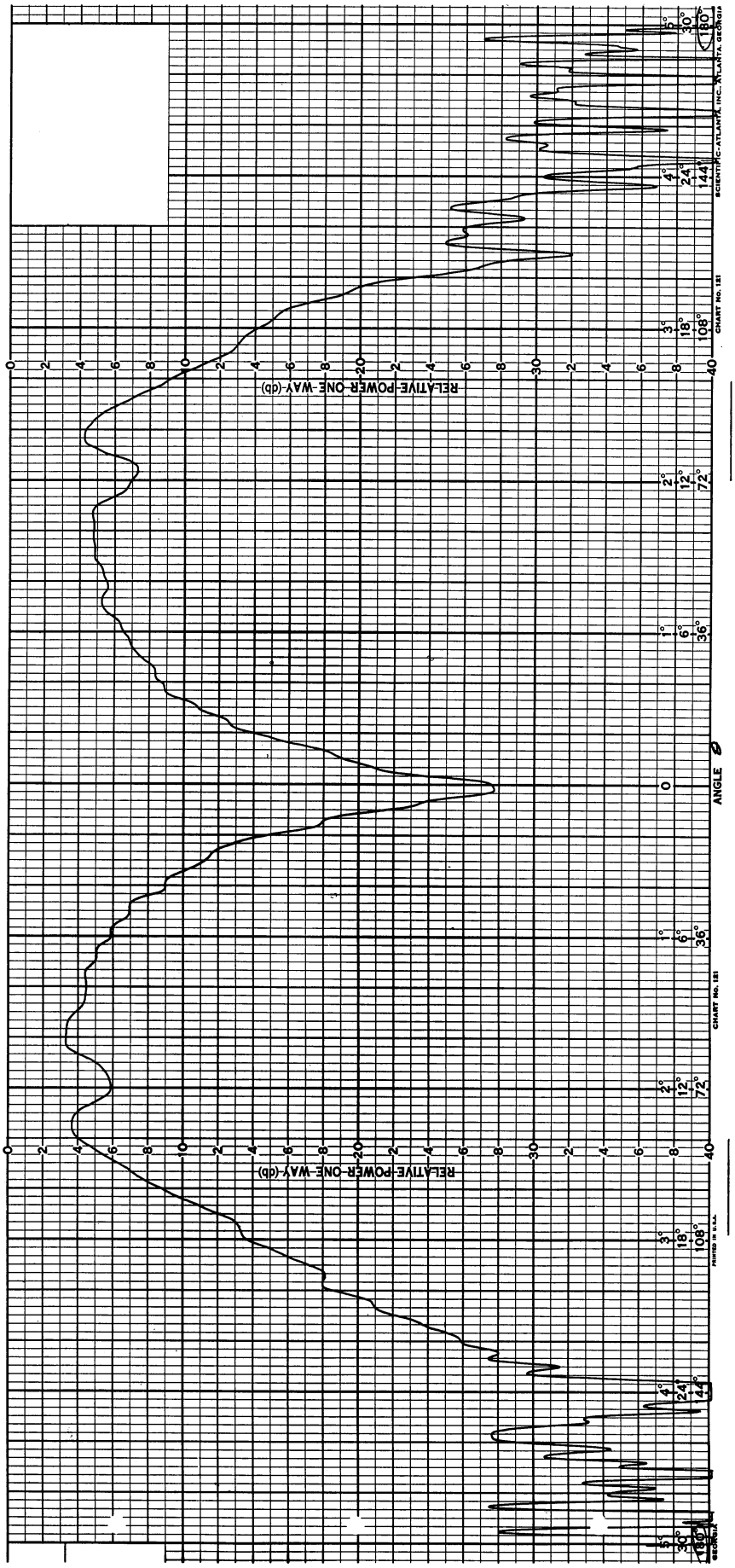

$\phi = 120^{\circ}/\phi = 300^{\circ}$

FIG. 10: MODIFIED MONOPOLE, 7.2 GHz, PRECISION T-33

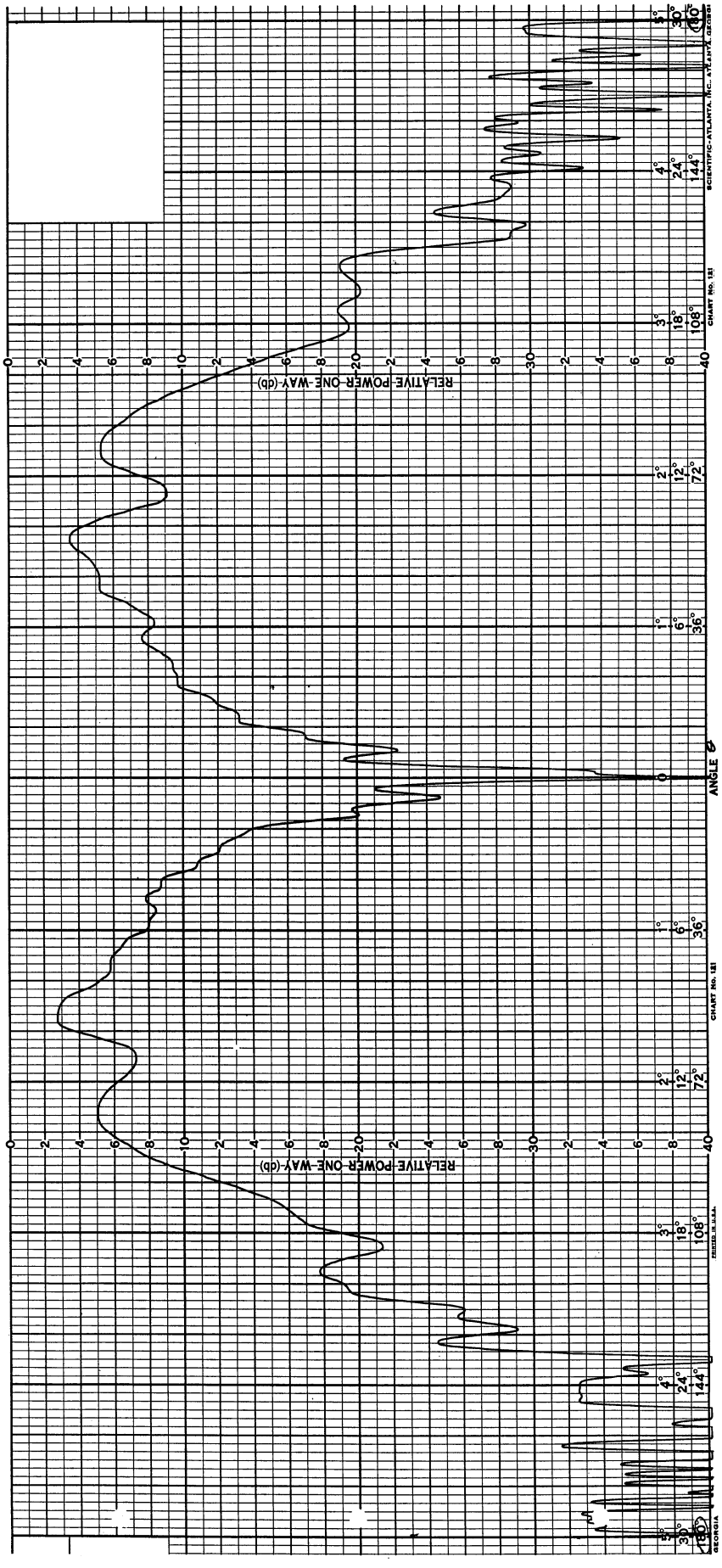

$\phi = 130^{o}/\phi = 310^{o}$

FIG. 11: MODIFIED MONOPOLE, 7.2 GHz, SIMPLIFIED T-33

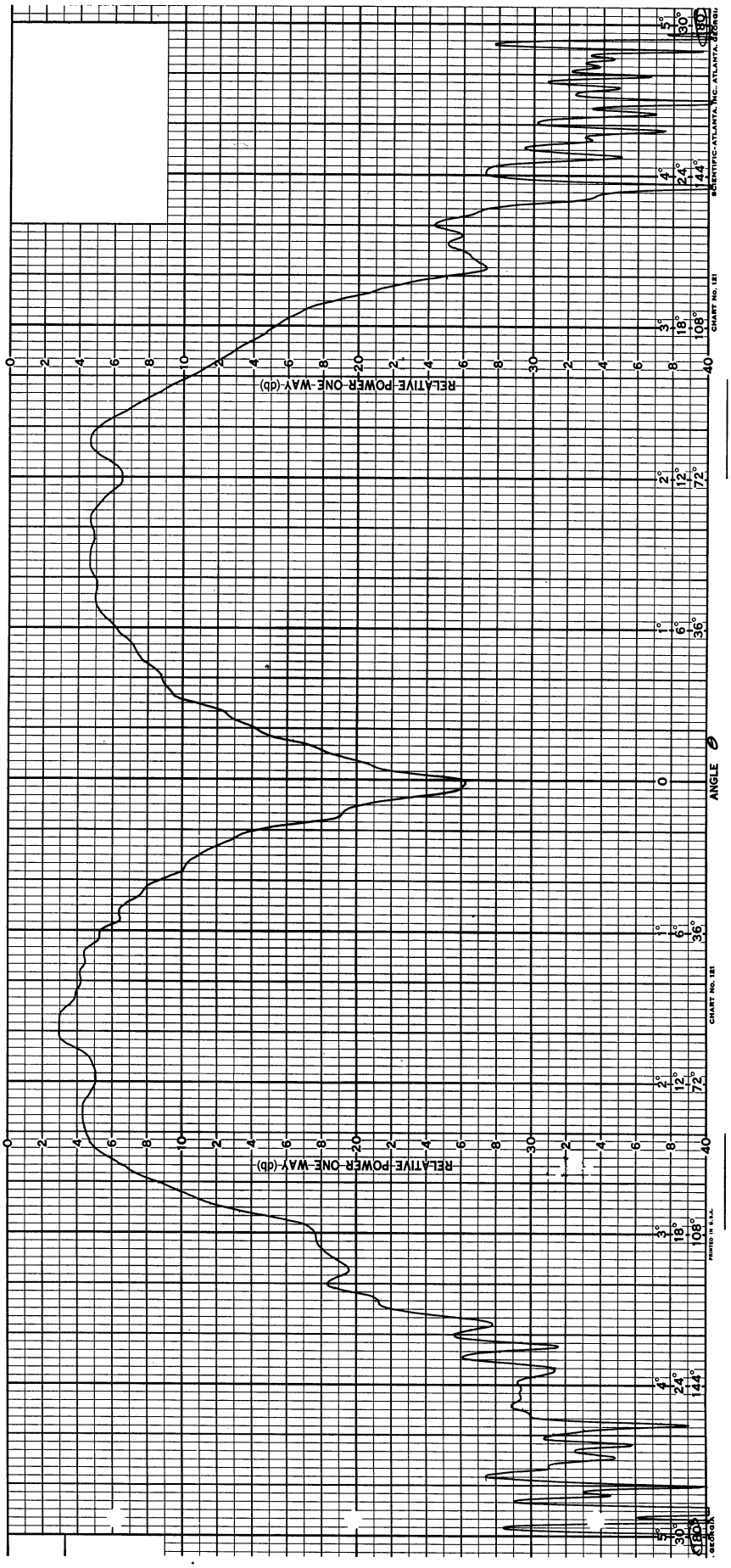

$\phi = 130^{\circ}/\phi = 310^{\circ}$

FIG. 12 : MODIFIED MONOPOLE, 7.2 GHz, PRECISION T-33

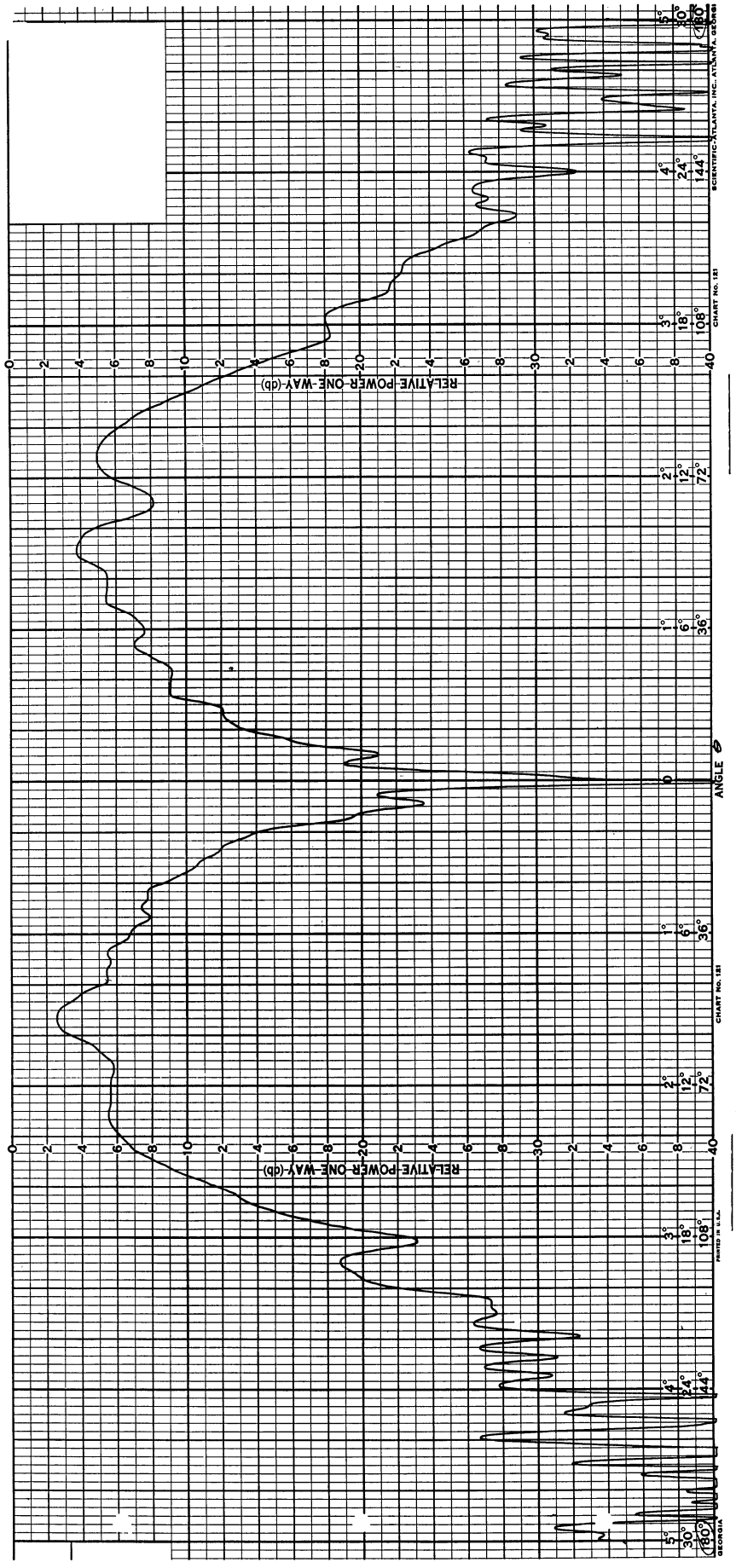

$\phi = 140^{o}/\phi = 320^{o}$

FIG. 13 : MODIFIED MONOPOLE, 7.2 GHz, SIMPLIFIED T-33

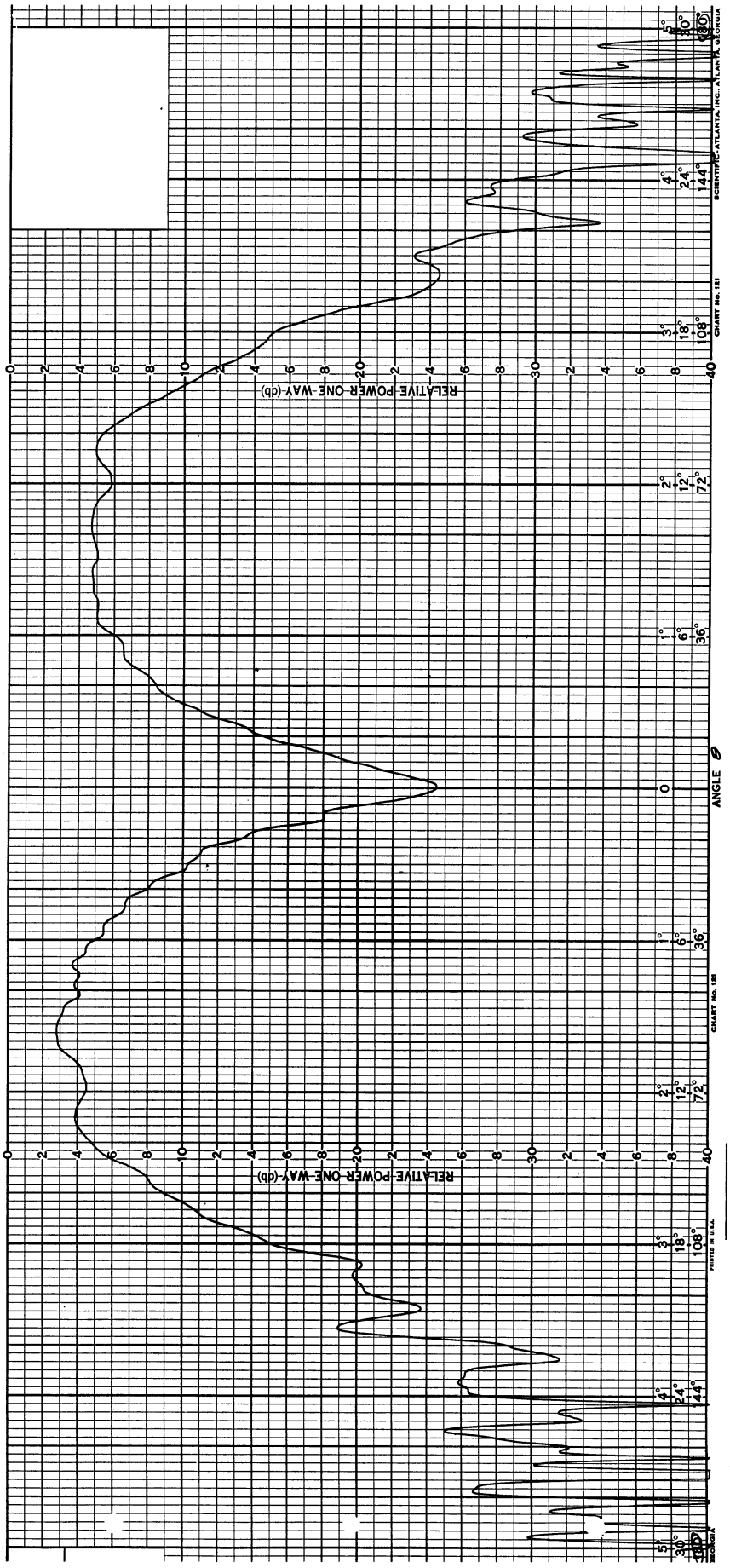

$\phi = 140^{o}/\phi = 320^{o}$

FIG. 14: MODIFIED MONOPOLE, 7.2 GHz, PRECISION T-33

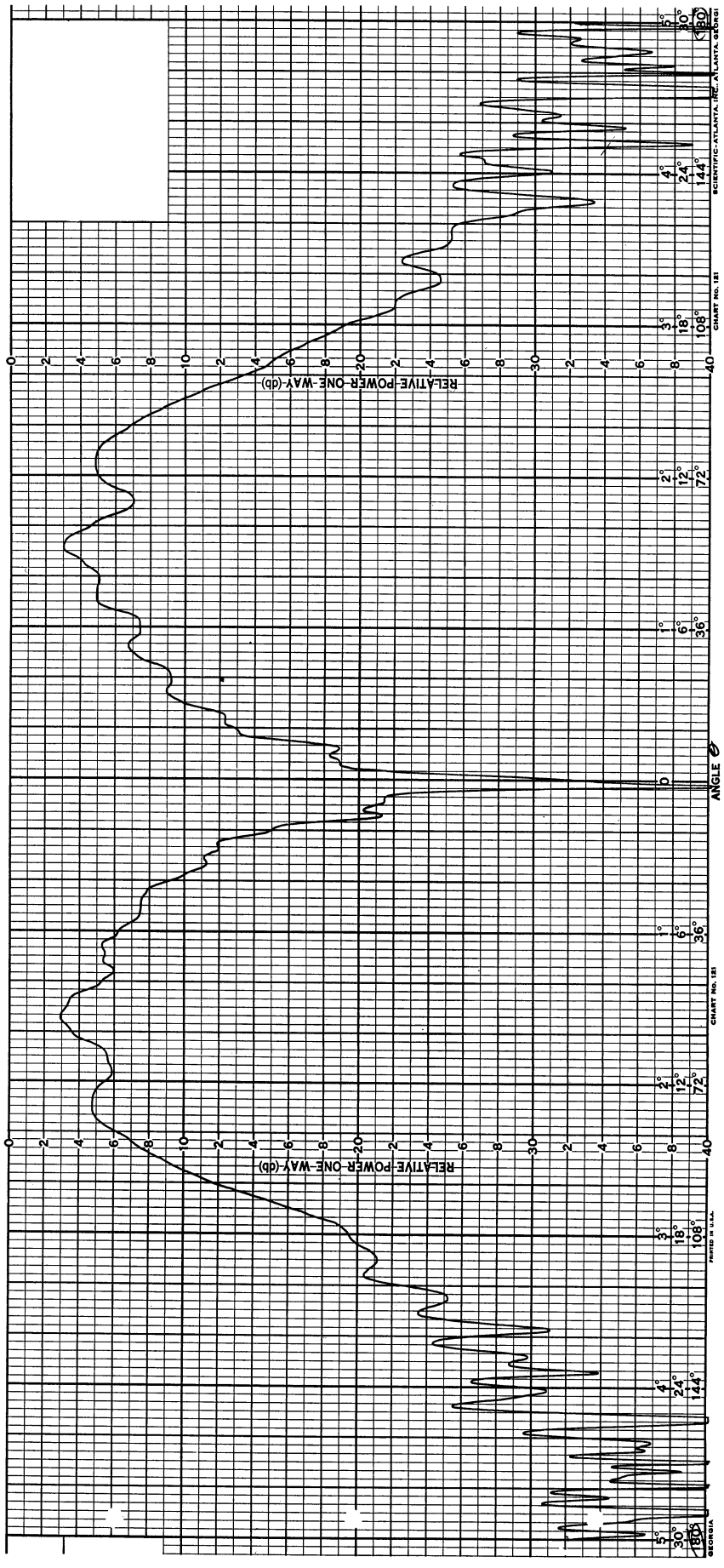

$\phi = 150^{\circ}/\phi = 330^{\circ}$

FIG. 15 : MODIFIED MONOPOLE, 7.2 GHz, SIMPLIFIED T-33

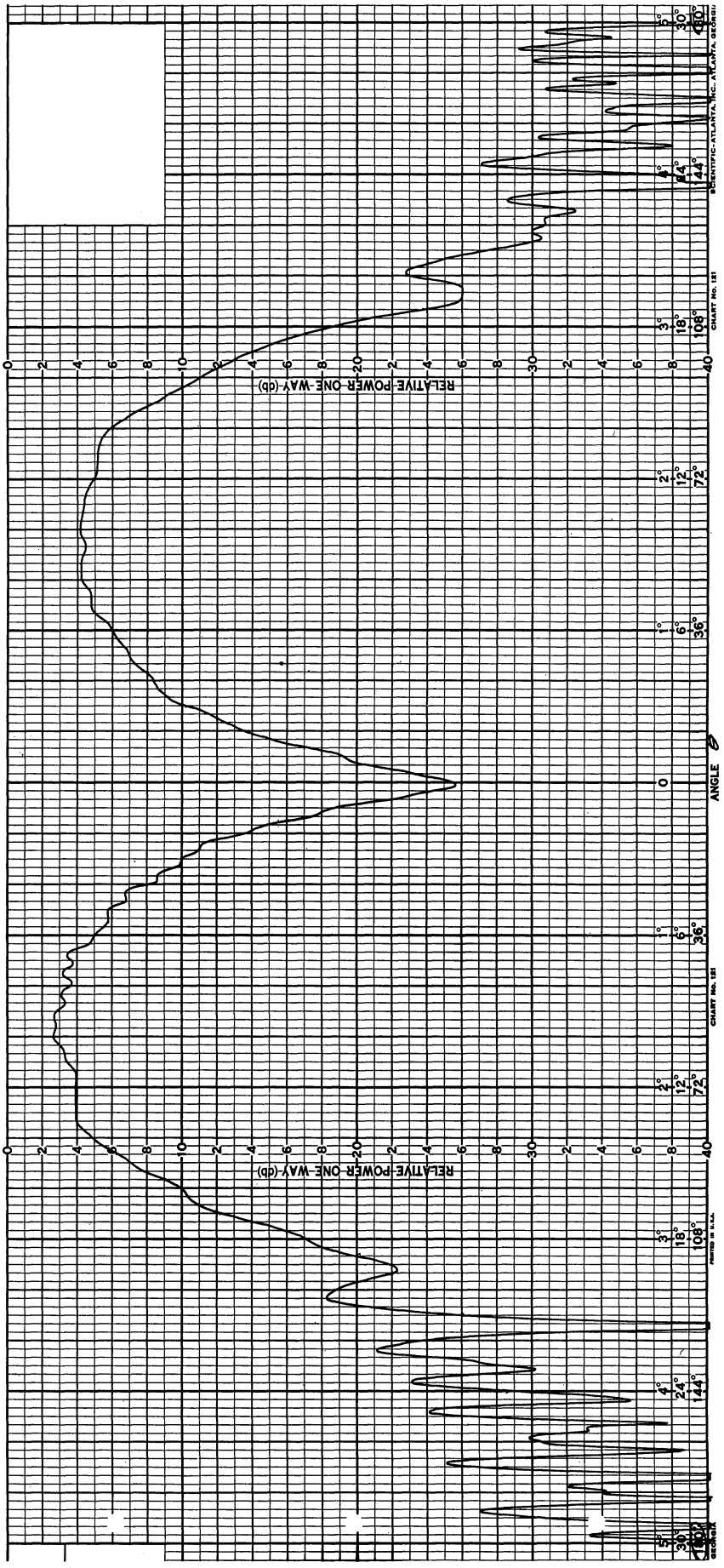

$\phi = 150^{\circ}/\phi = 330^{\circ}$

FIG. 16: MODIFIED MONOPOLE, 7.2 GHz, PRECISION T-33

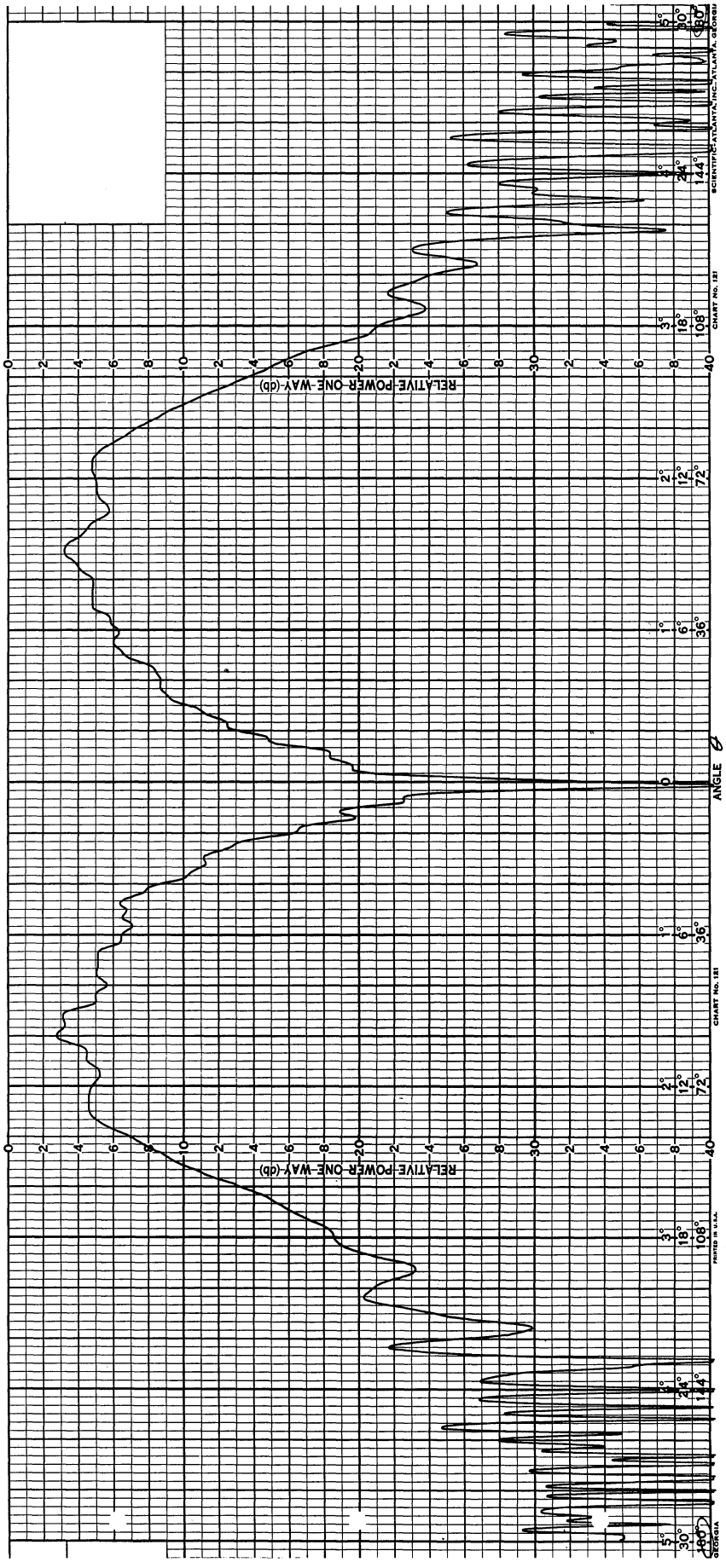

$\phi = 160^{\circ}/\phi = 340^{\circ}$

FIG. 17: MODIFIED MONOPOLE, 7.2 GHz, SIMPLIFIED T-33

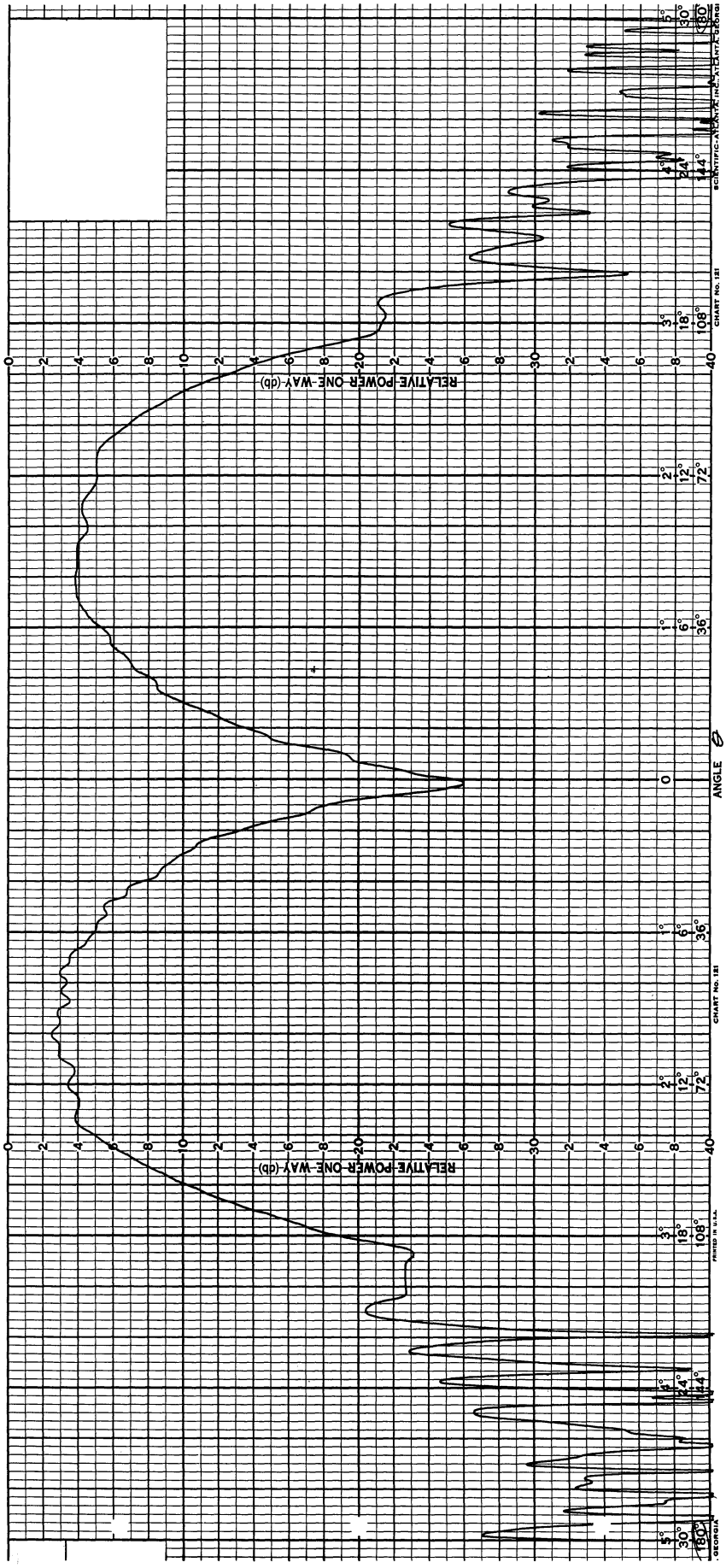

$\phi = 160^{o}/\phi = 340^{o}$

FIG. 18: MODIFIED MONOPOLE, 7.2 GHz, PRECISION T-33

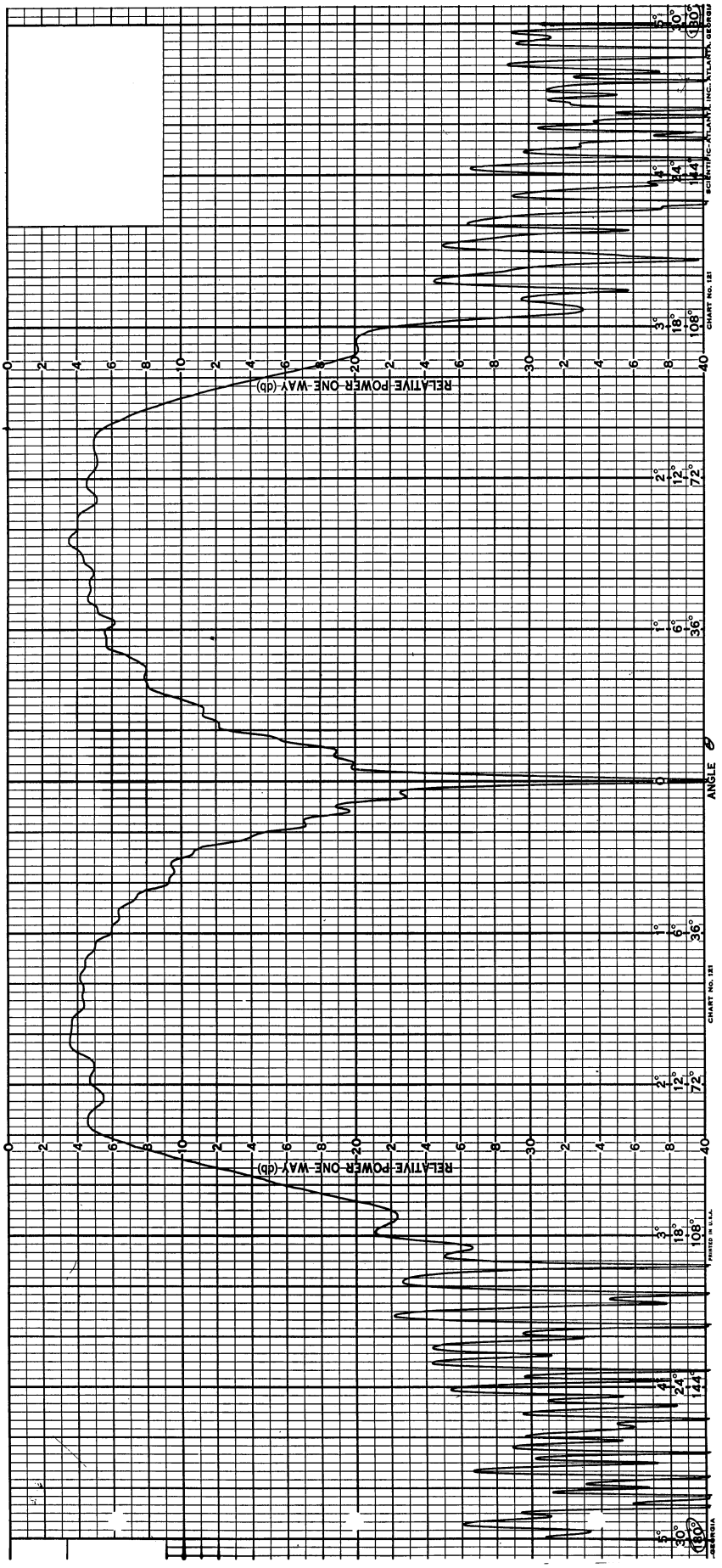

$\phi = 170^{\circ}/\phi = 350^{\circ}$

FIG. 19: MODIFIED MONOPOLE, 7.2 GHz, SIMPLIFIED T-33

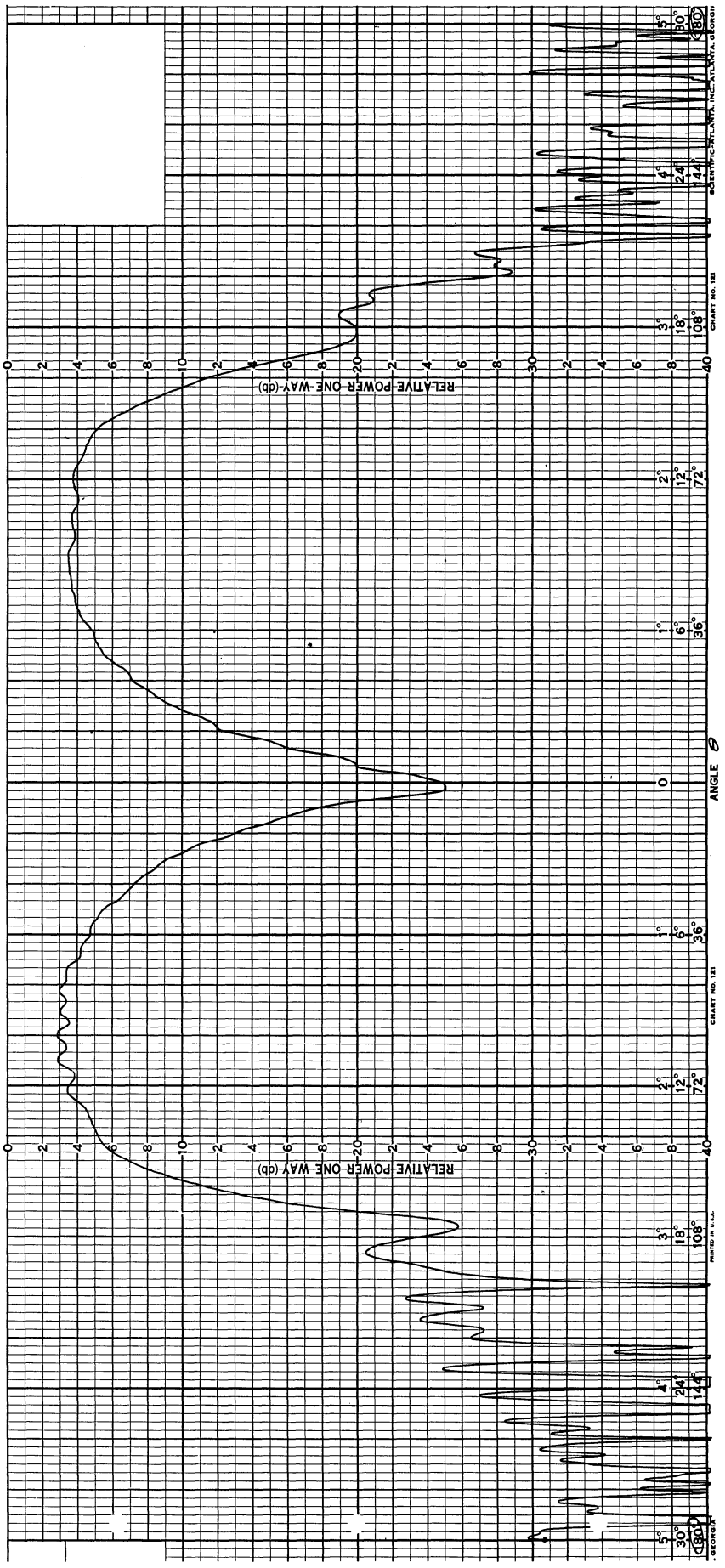

$\phi = 170^{o}/\phi = 350^{o}$

FIG. 20: MODIFIED MONOPOLE, 7.2 GHz, PRECISION T-33

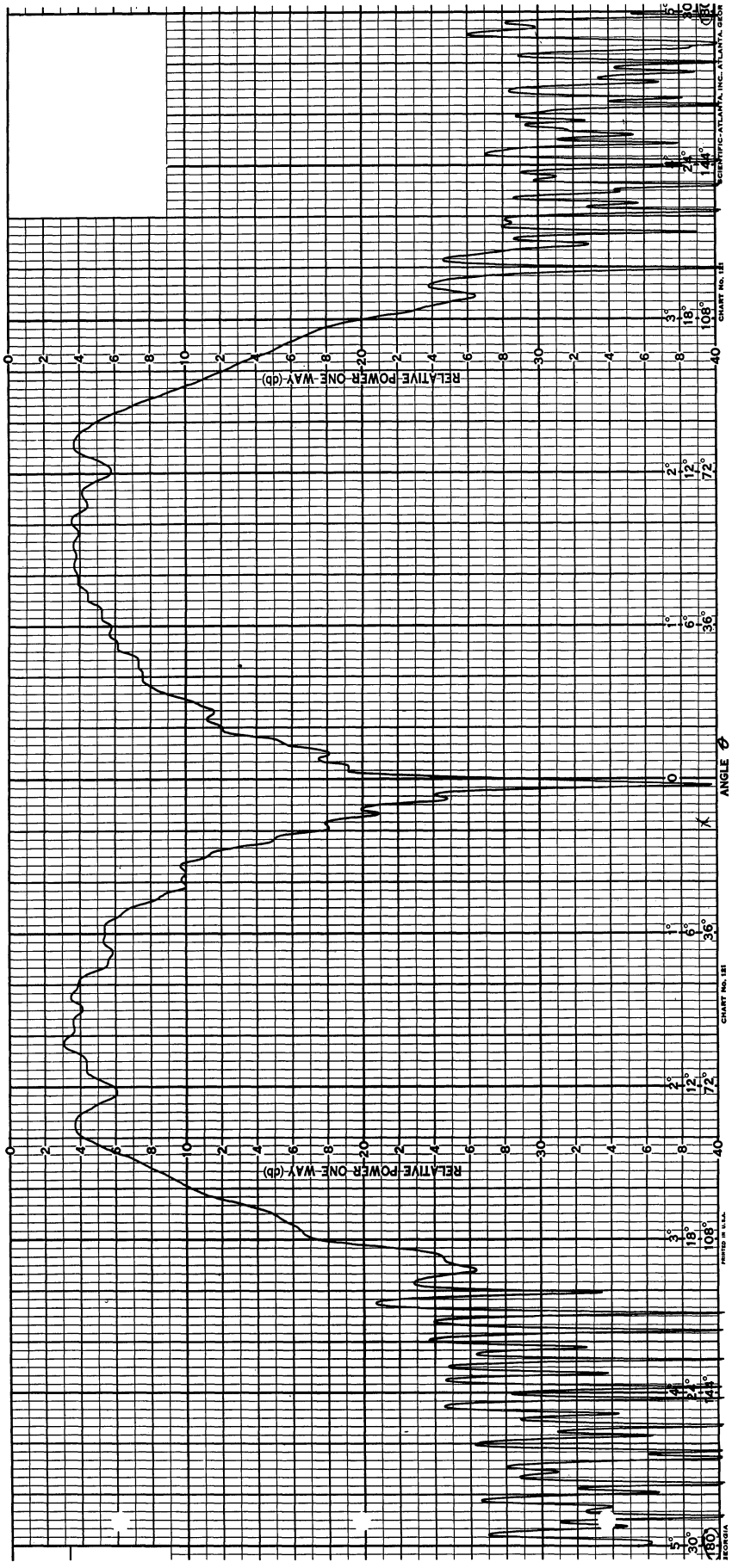

$\phi = 180^{o}/\phi = 0^{o}$

FIG. 21: MODIFIED MONOPOLE, 7.2 GHz, SIMPLIFIED T-33

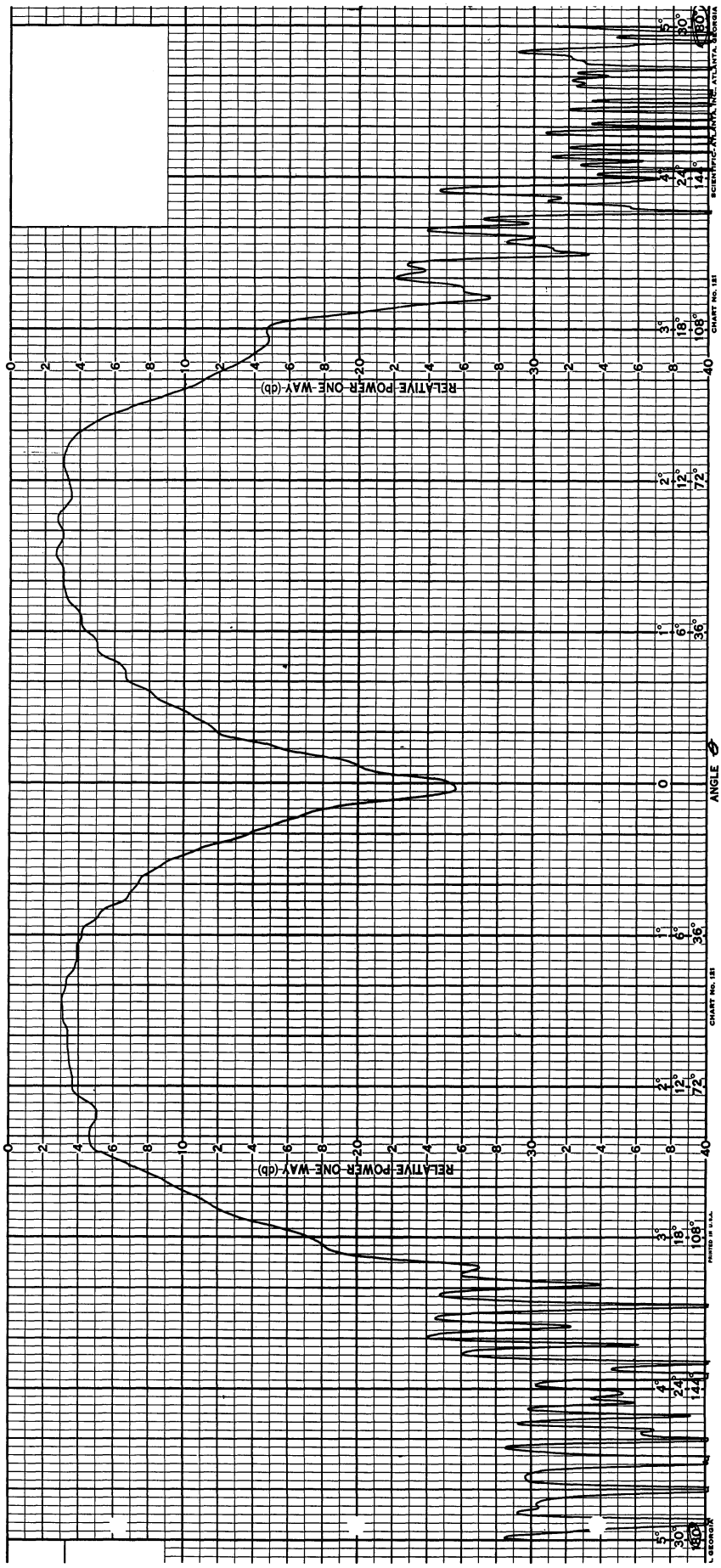

$\phi = 180^{\circ}/\phi = 0^{\circ}$

FIG. 22 : MODIFIED MONOPOLE, 7.2 GHz, PRECISION T-33

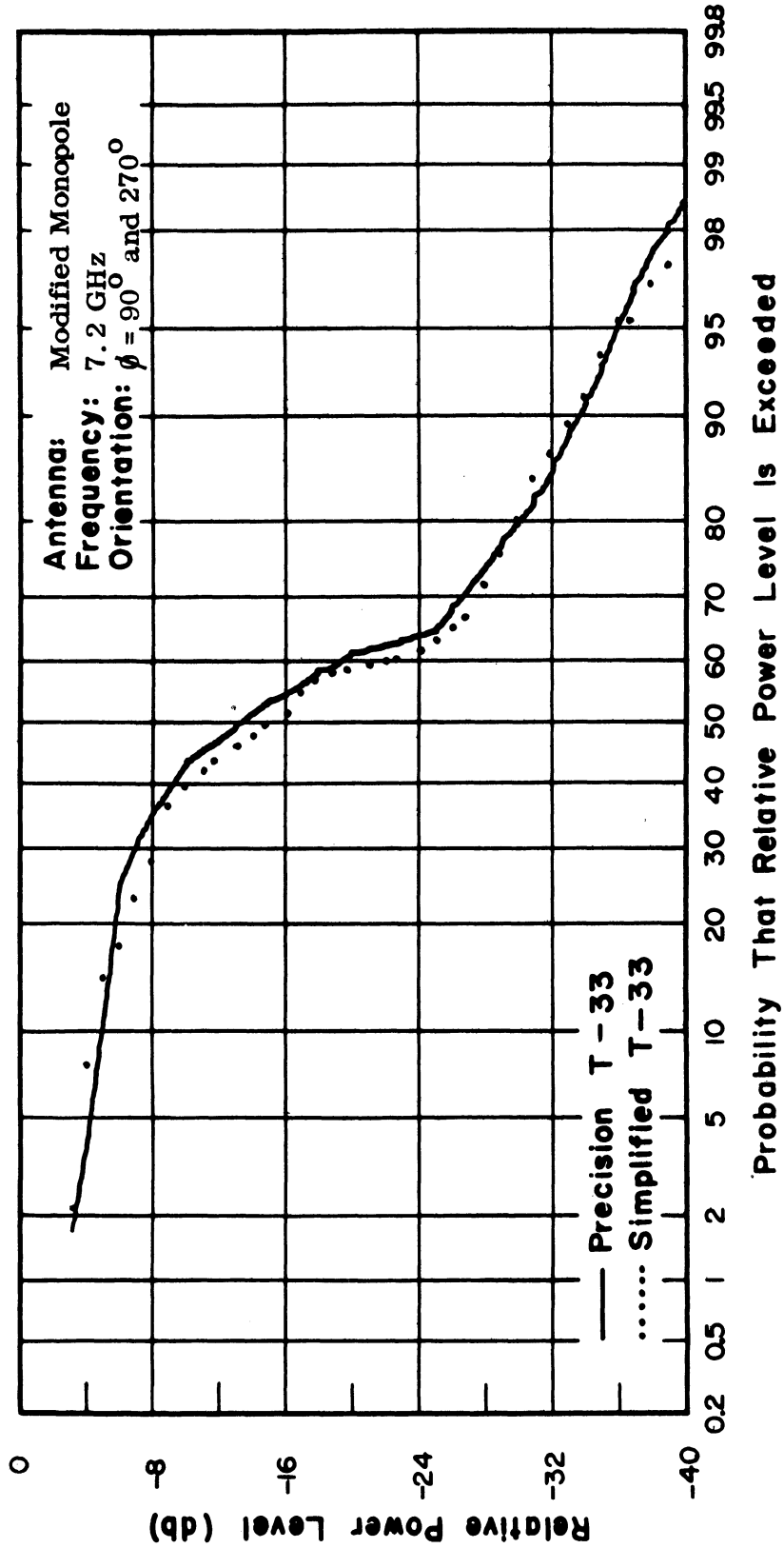

FIG. 23: CUMULATIVE GAIN DISTRIBUTIONS OF PRECISION AND SIMPLIFIED MODELS

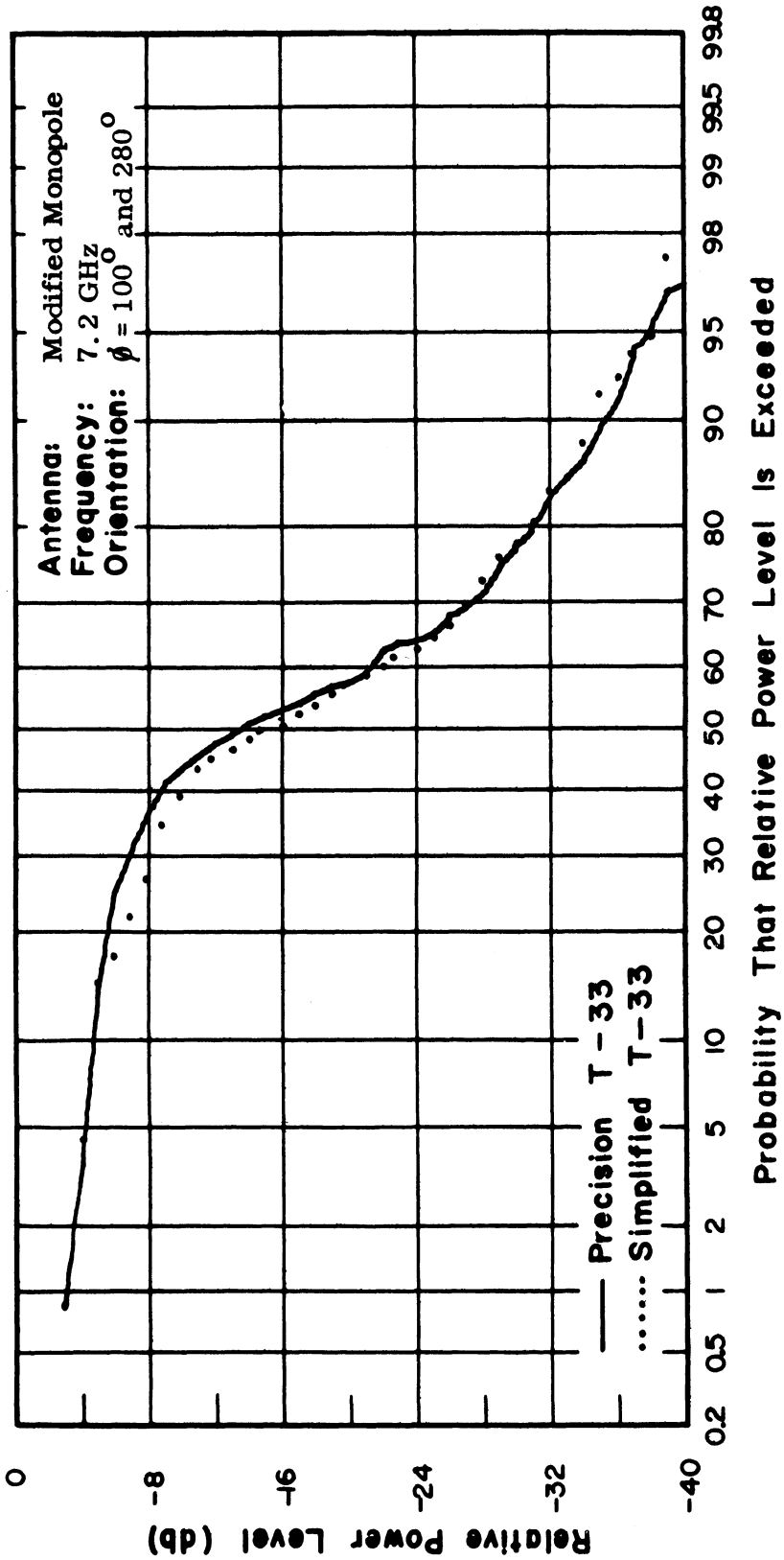

FIG. 24: CUMULATIVE GAIN DISTRIBUTIONS OF PRECISION AND SIMPLIFIED MODELS

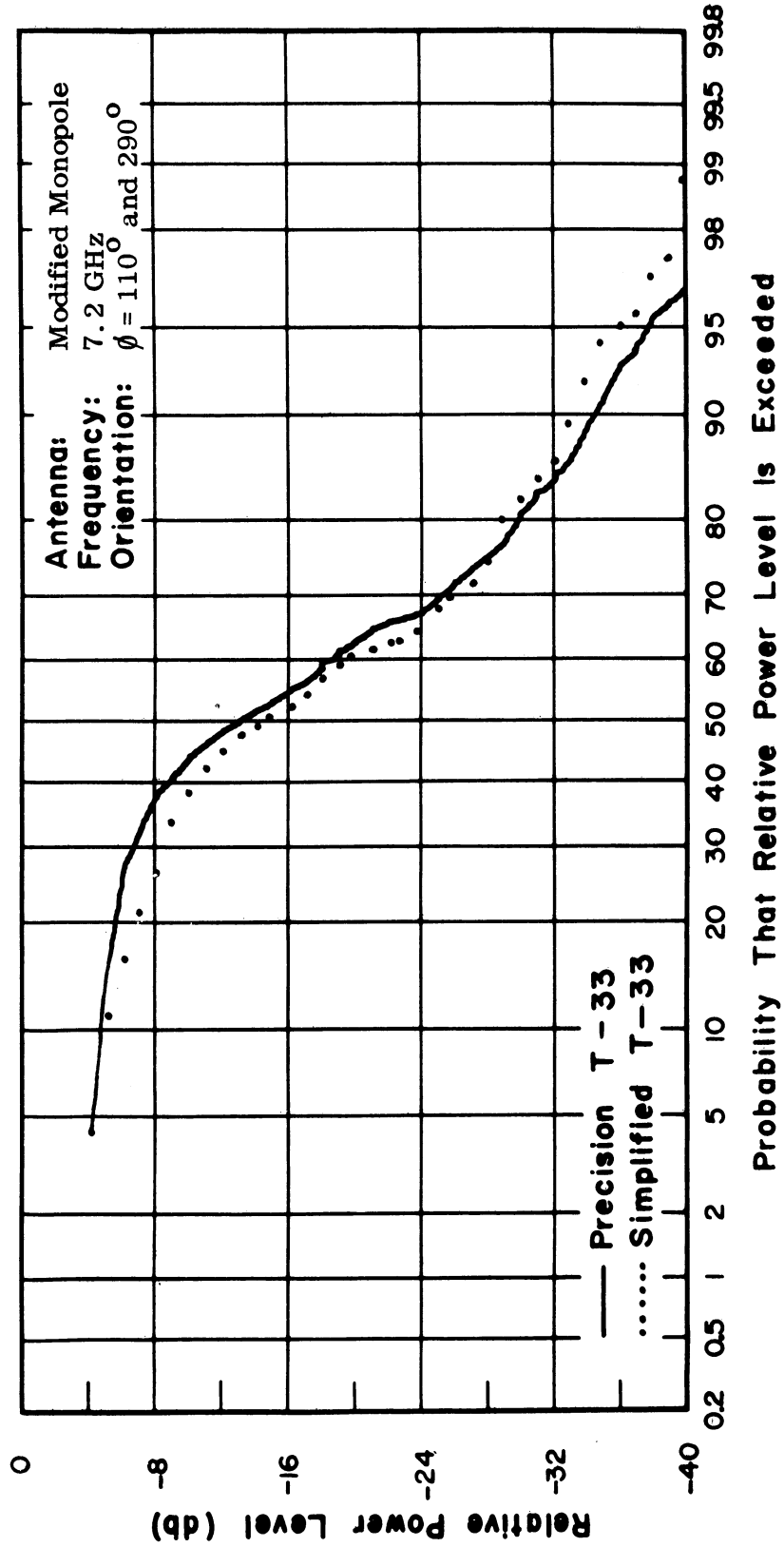

FIG. 25: CUMULATIVE GAIN DISTRIBUTIONS OF PRECISION AND SIMPLIFIED MODELS

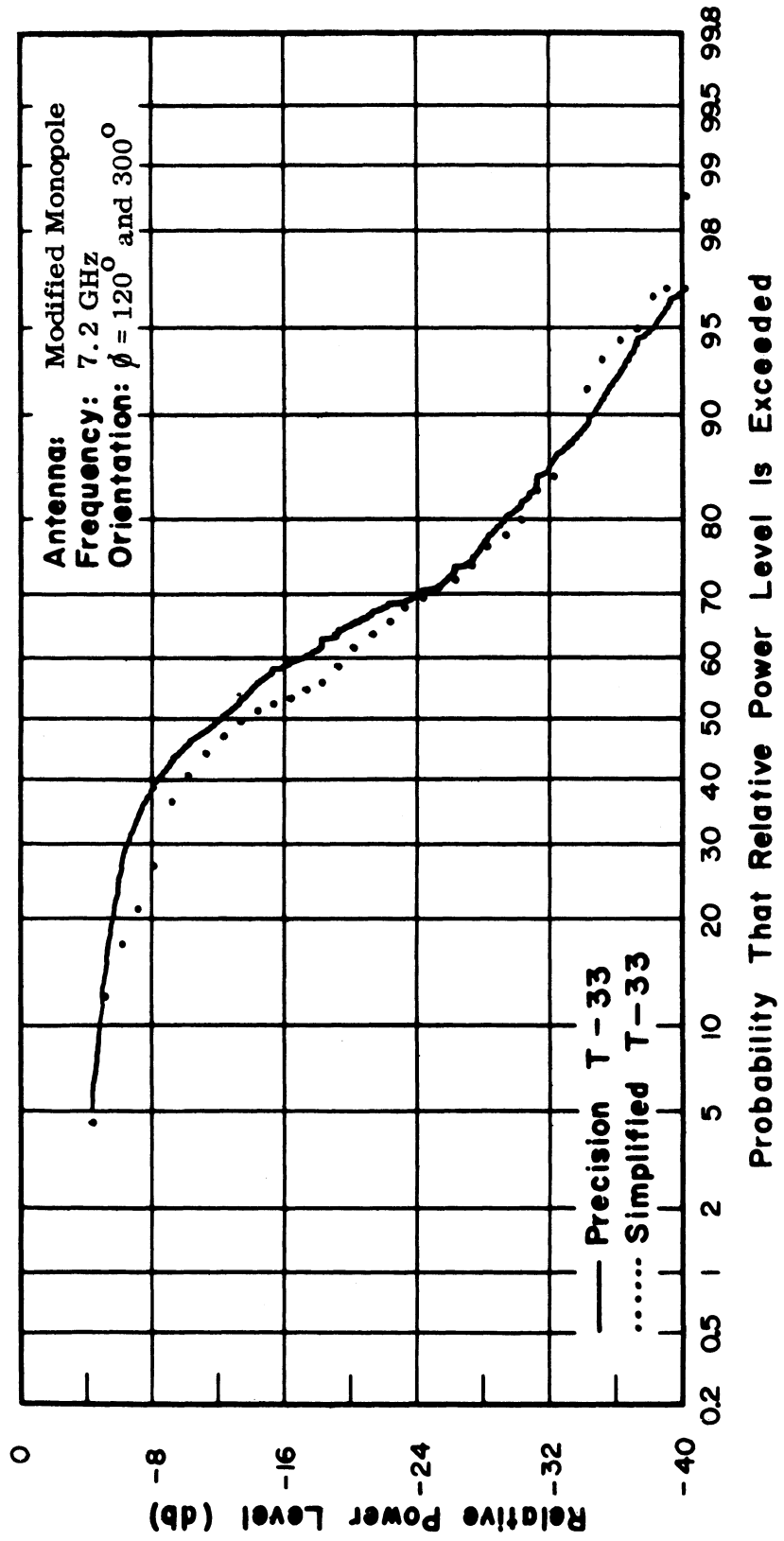

FIG. 26: CUMULATIVE GAIN DISTRIBUTIONS OF PRECISION AND SIMPLIFIED MODELS

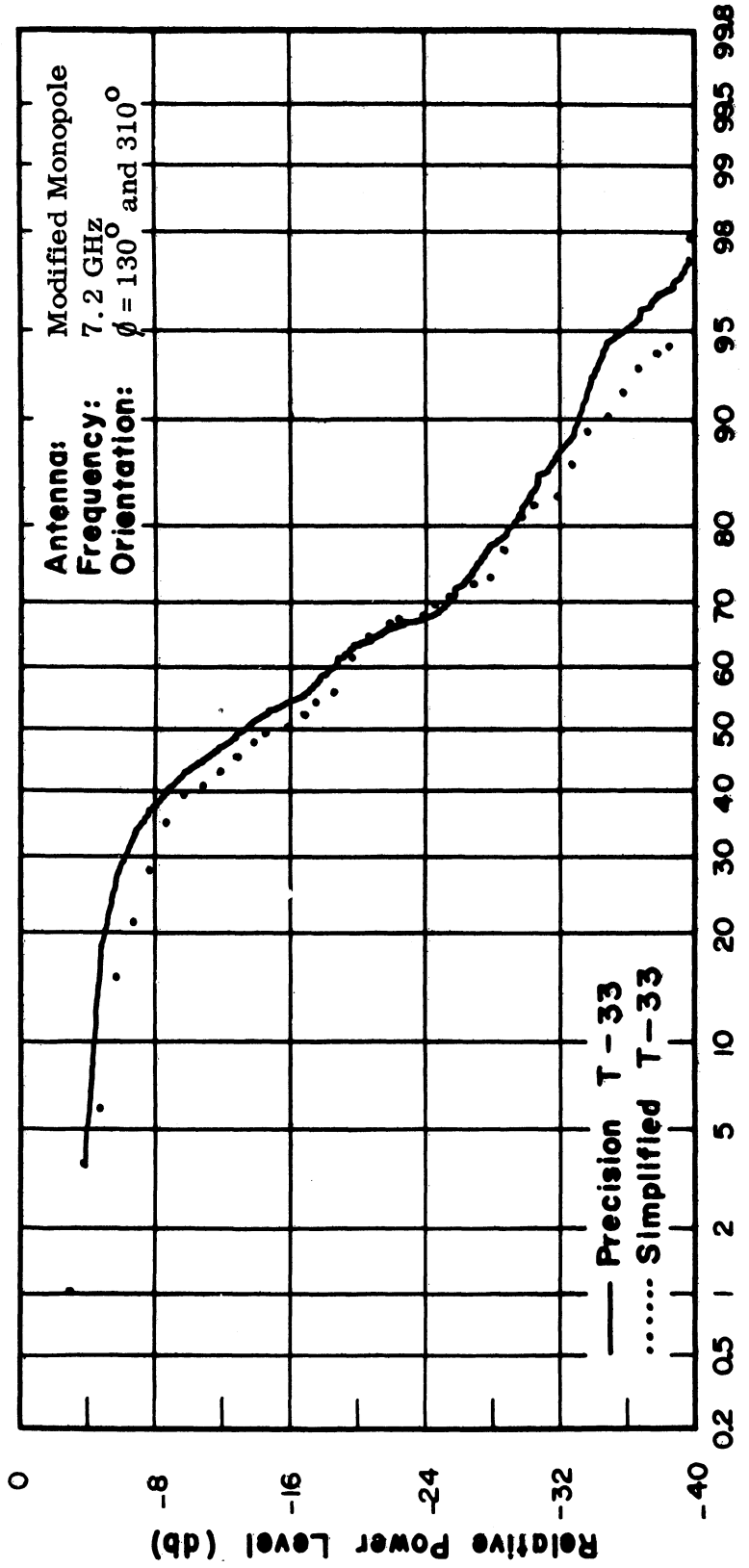

FIG. 27: CUMULATIVE GAIN DISTRIBUTIONS OF PRECISION AND SIMPLIFIED MODELS

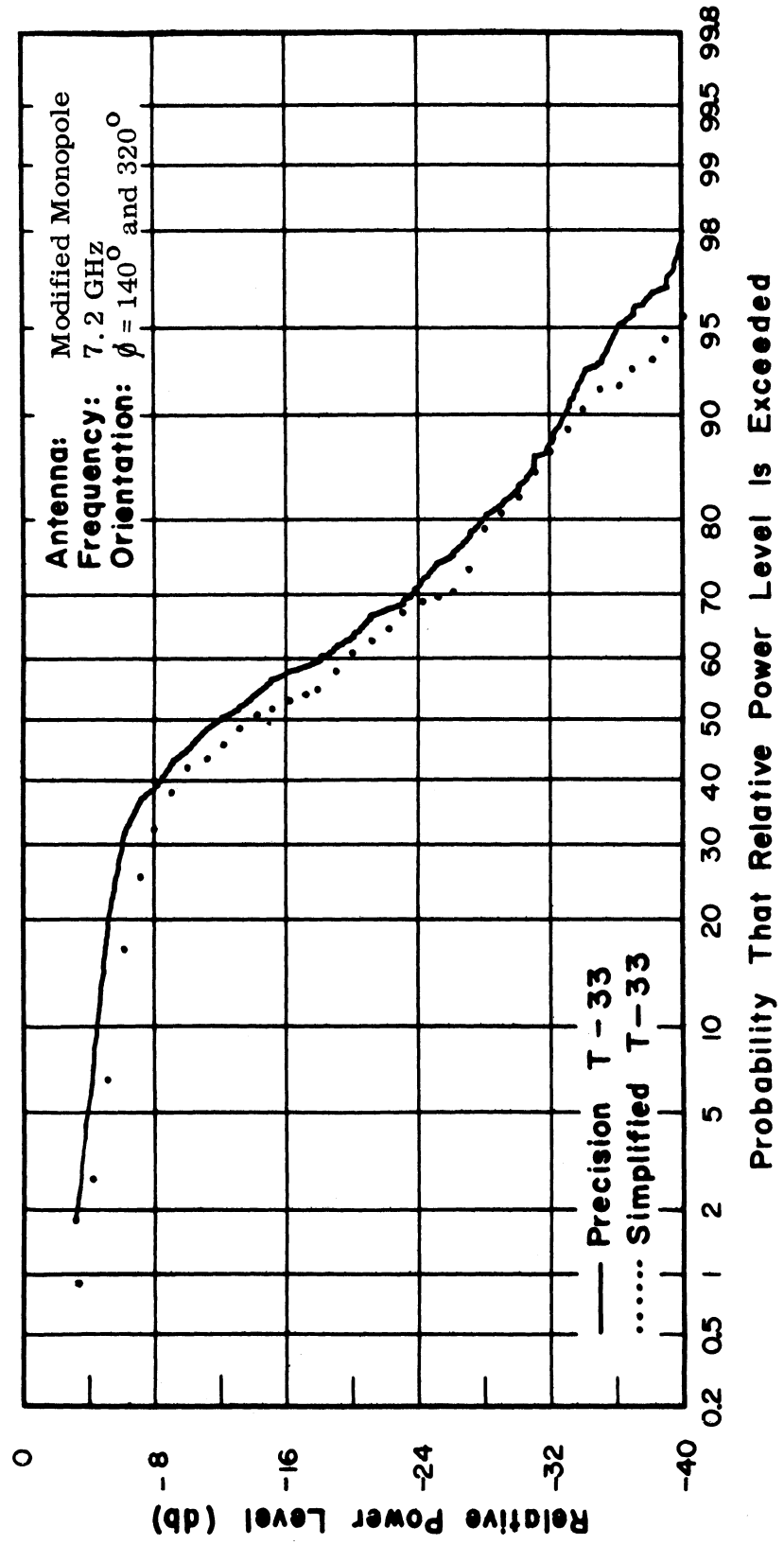

FIG. 28: CUMULATIVE GAIN DISTRIBUTIONS OF PRECISION AND SIMPLIFIED MODELS

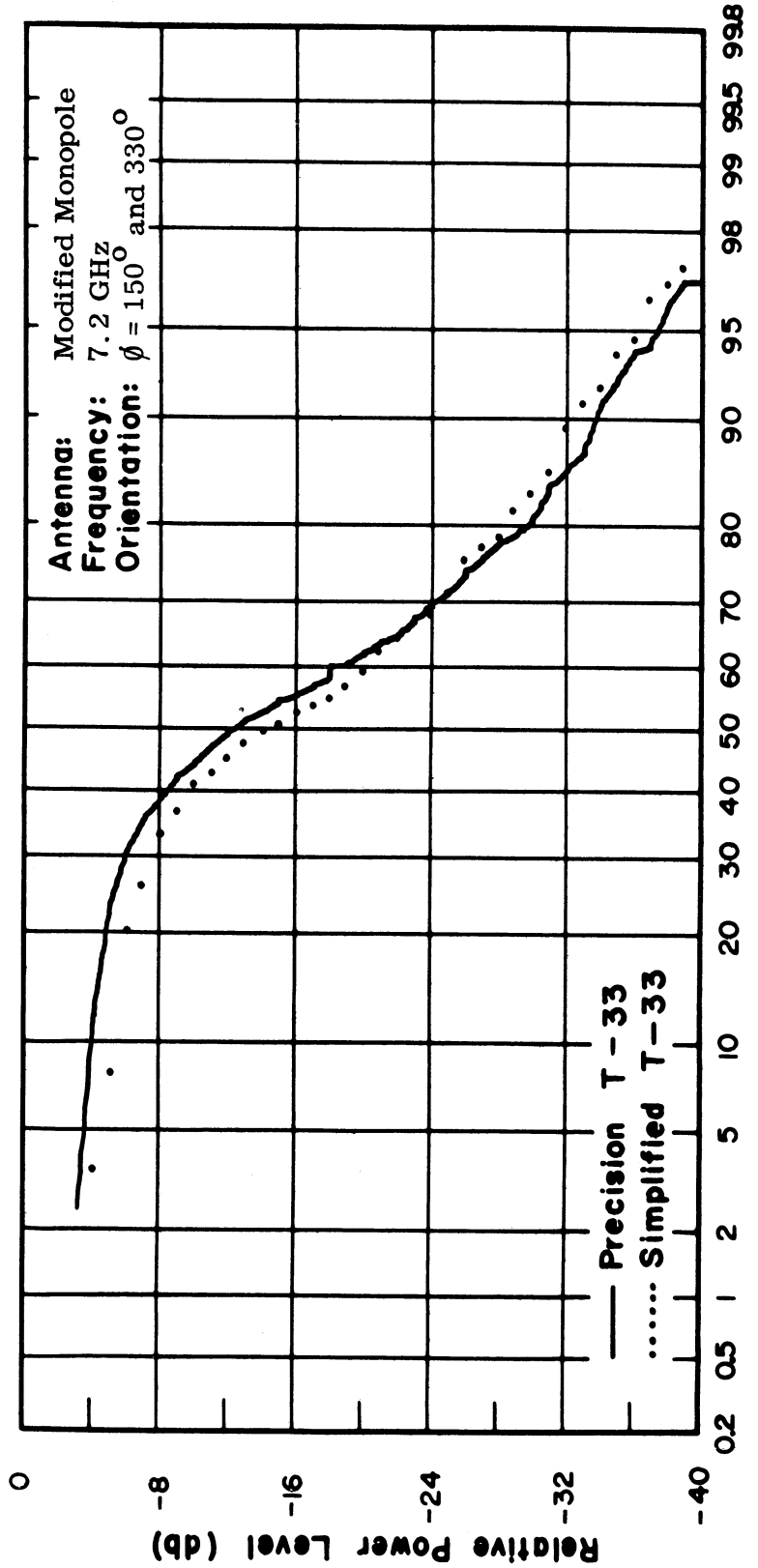

FIG. 29: CUMULATIVE GAIN DISTRIBUTIONS OF PRECISION AND SIMPLIFIED MODELS

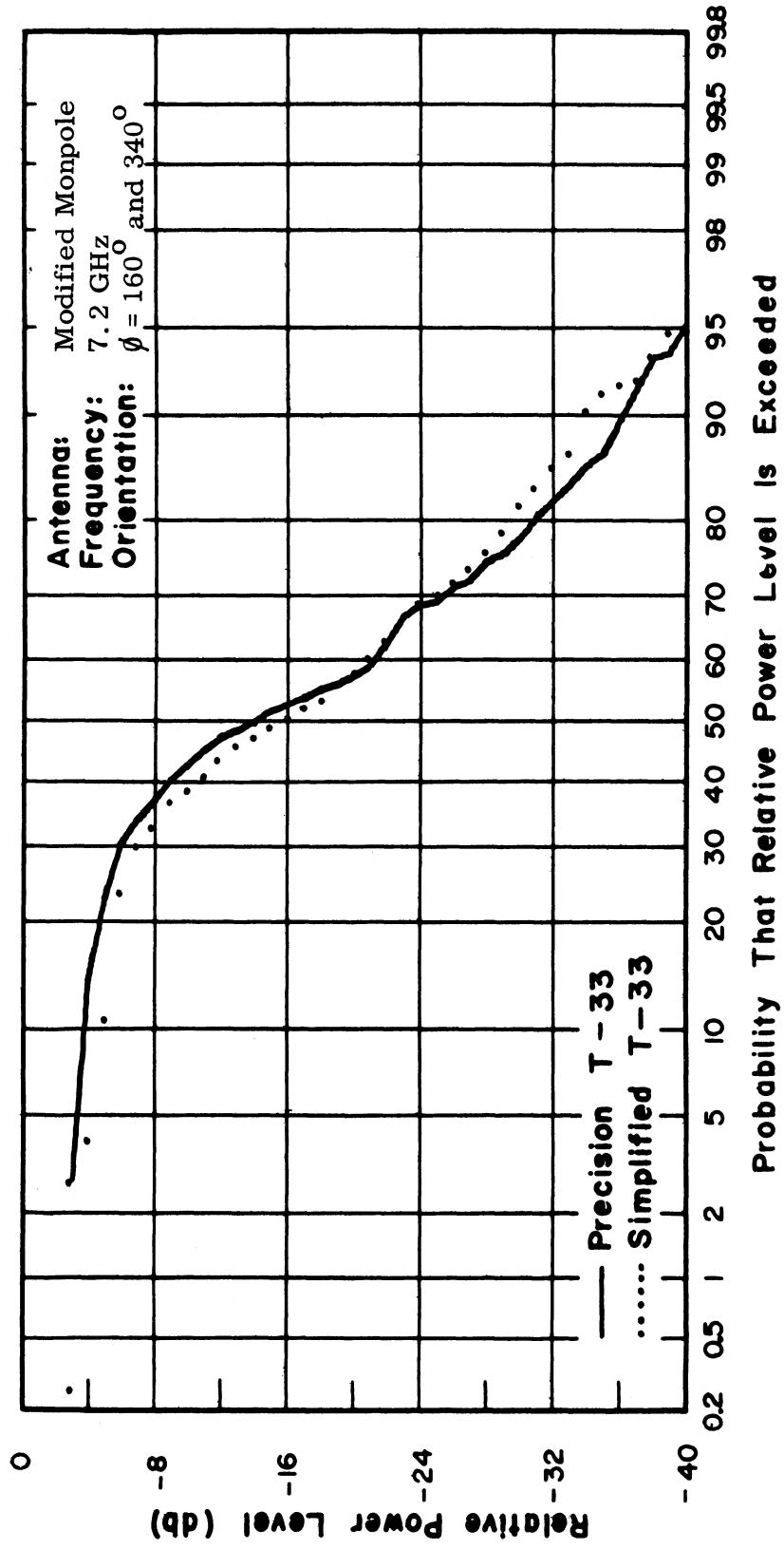

FIG. 30: CUMULATIVE GAIN DISTRIBUTIONS OF PRECISION AND SIMPLIFIED MODELS

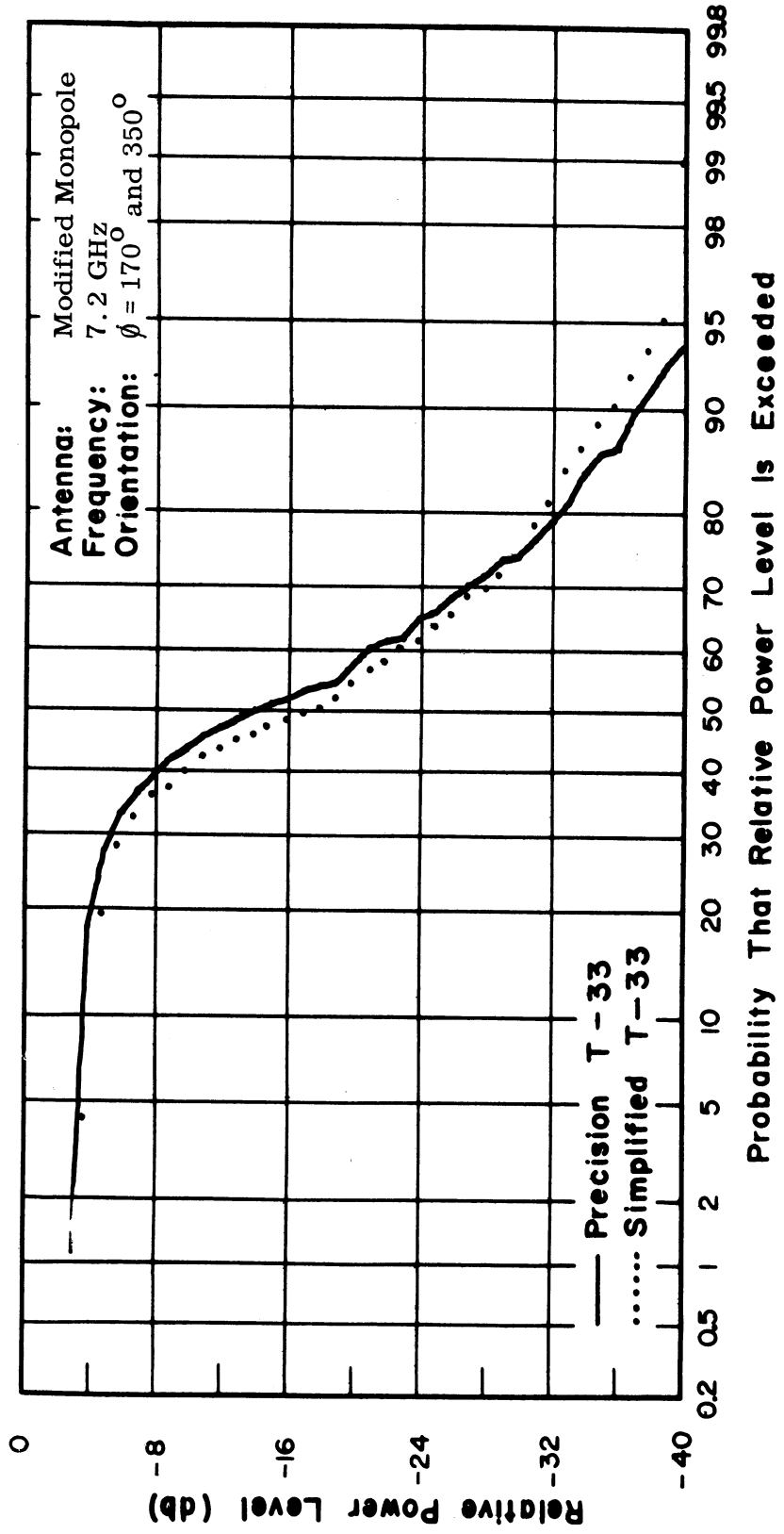

FIG. 31: CUMULATIVE GAIN DISTRIBUTIONS OF PRECISION AND SIMPLIFIED MODELS

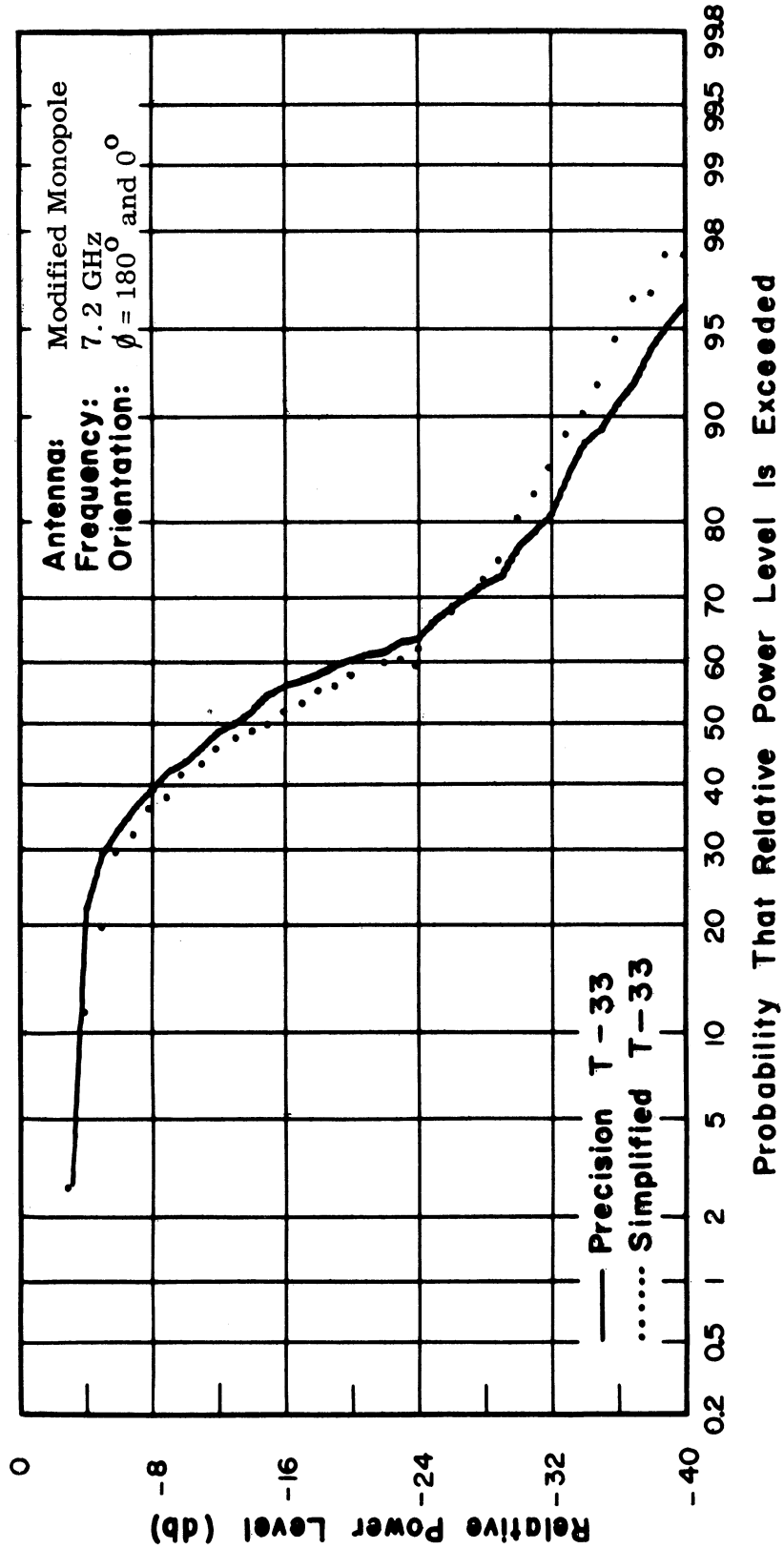

FIG. 32: CUMULATIVE GAIN DISTRIBUTIONS OF PRECISION AND SIMPLIFIED MODELS

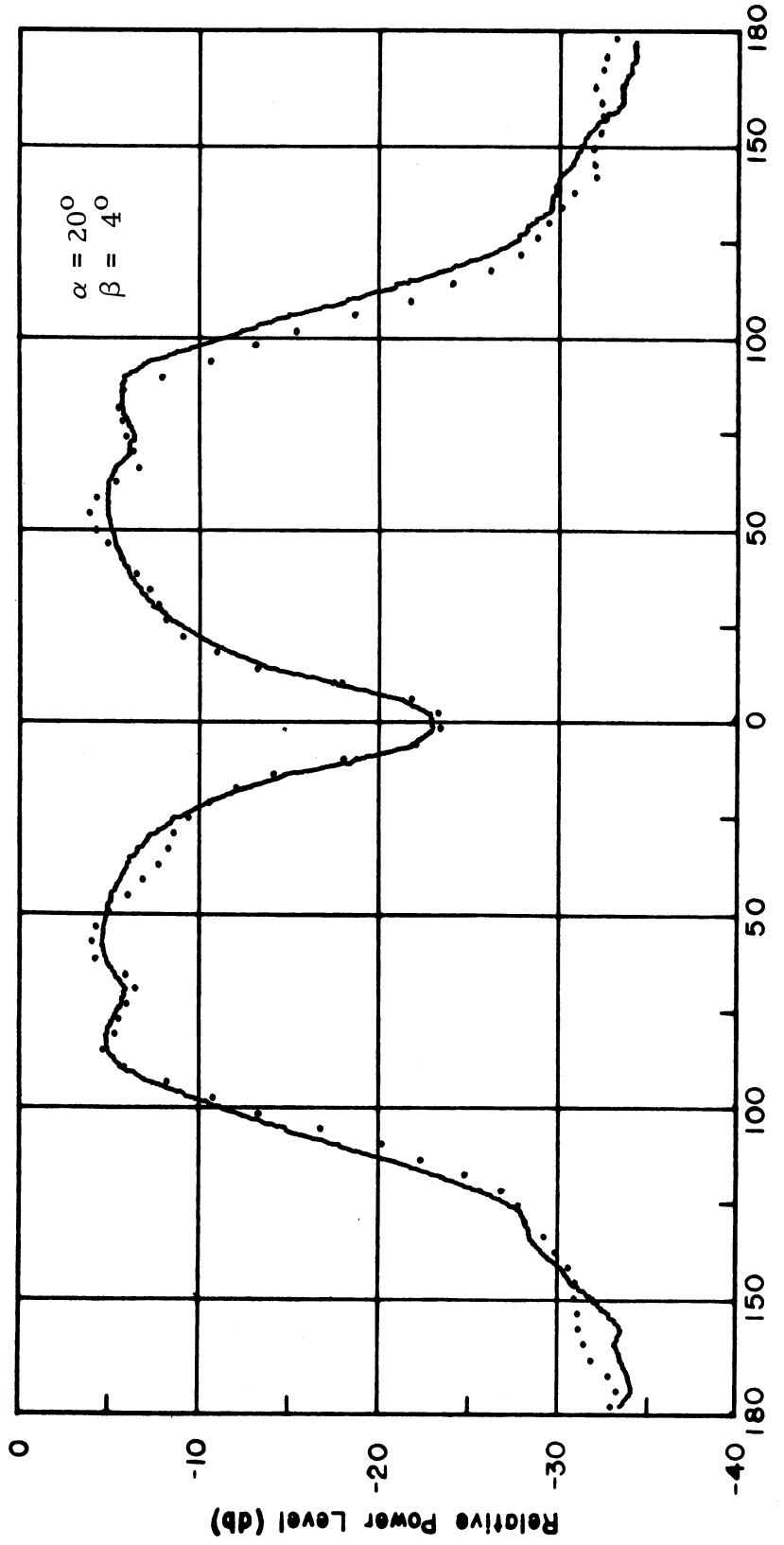

FIG. 33a: AVERAGE OF SLIDING SECTOR OF PRECISION AND SIMPLIFIED MODELS.
Antenna: Modified Monopole. Freq. = 7.2 Gc.

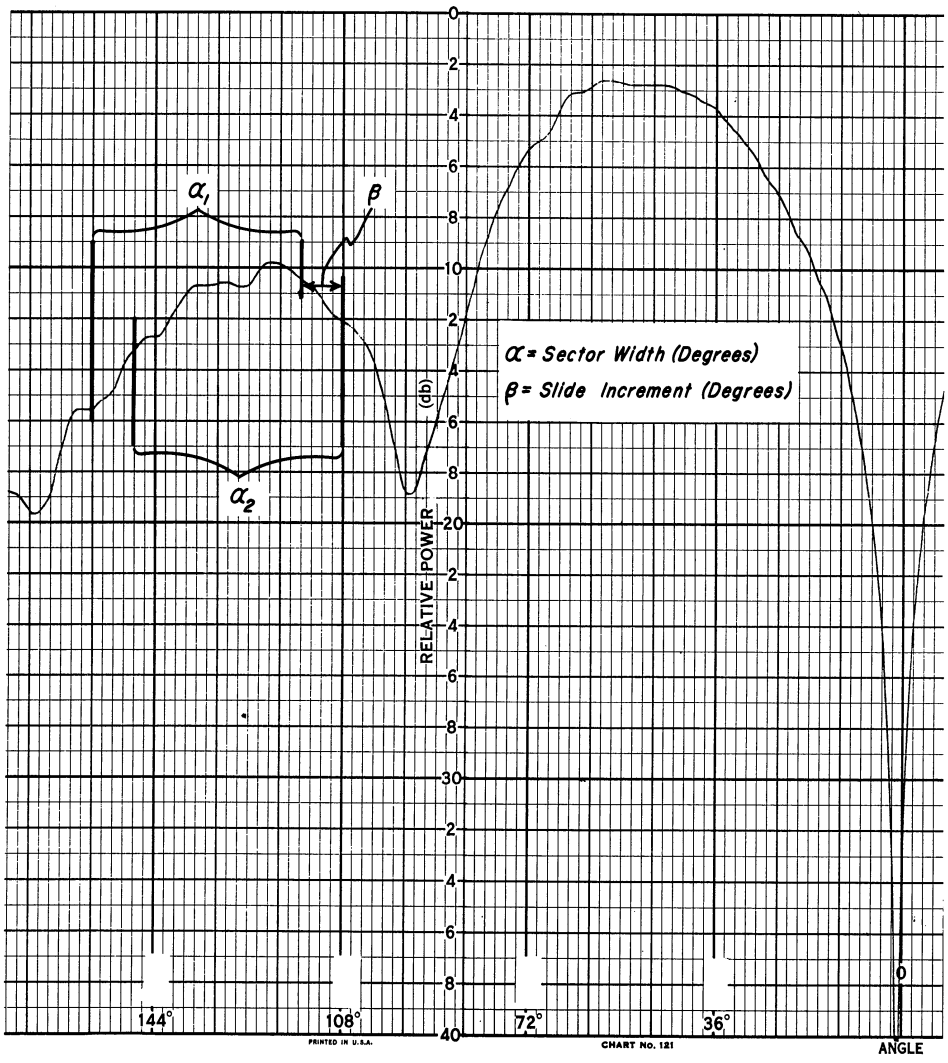

FIG. 33b: SLIDING SECTOR DESCRIPTION

is slid in steps of β across the 360-degree width of the conventional antenna pattern. As the sector is slid, statistical data is calculated and plotted as follows: (1) the average gain within the sector α_1 is determined and recorded at $\alpha_1/2$; (2) the sector α_1 is slid β^o becoming α_2 and the above calculation repeated and plotted at $\alpha_2/2 = \alpha_1/2 + \beta$; (3) the process is repeated for α_3, α_4, etc. across the pattern (Note: $\alpha_1 = \alpha_2 = \alpha_3$, etc.). Figure 33a is a composite (precision versus simplified model) of average data for the modified monopole with $\alpha = 20^o$ and $\beta = 4^o$.

To aid in the reduction of the data into statistical formats all data has been recorded in a digital, as well as analog, format (the pattern data in this report is in analog format). The instrumentation employed to obtain the digital data is discussed in a later section of the report.

2.3 $\lambda/4$ Monopole

The $\lambda/4$ monopole was also discussed in the previous report (Ferris et al 1965). Since the writing of that report, additional data has been obtained at the fundamental and harmonic frequencies. A complete set of three-dimensional data has been obtained for the $\lambda/4$ monopole at the scaled fundamental frequency of 2.4 GHz. Figures 34a and 34b show the antenna mounted on the underside of the nose of the precision and simplified jet aircraft models. Figures 35-54 constitute a set of three-dimensional data for the $\lambda/4$ monopole at 2.4 GHz. It is interesting to note the similarity between the patterns of the precision and simplified models in spite of the streamlined contour of the precision model. Cumulative gain distributions (statistical) were plotted to aid in their comparison as shown in Figs. 55-64.

The University of Michigan analog-to-digital converter was employed to record the above antenna pattern data in digital form on magnetic tape as the analog pattern was being plotted on chart paper. The digitalized data was later automatically processed, reduced and plotted in a form of cumulative gain distributions as will be discussed later in this report. During the period covered by the present contract, the recording system was modified to include a 60 db dynamic range and this was employed to obtain the above patterns.

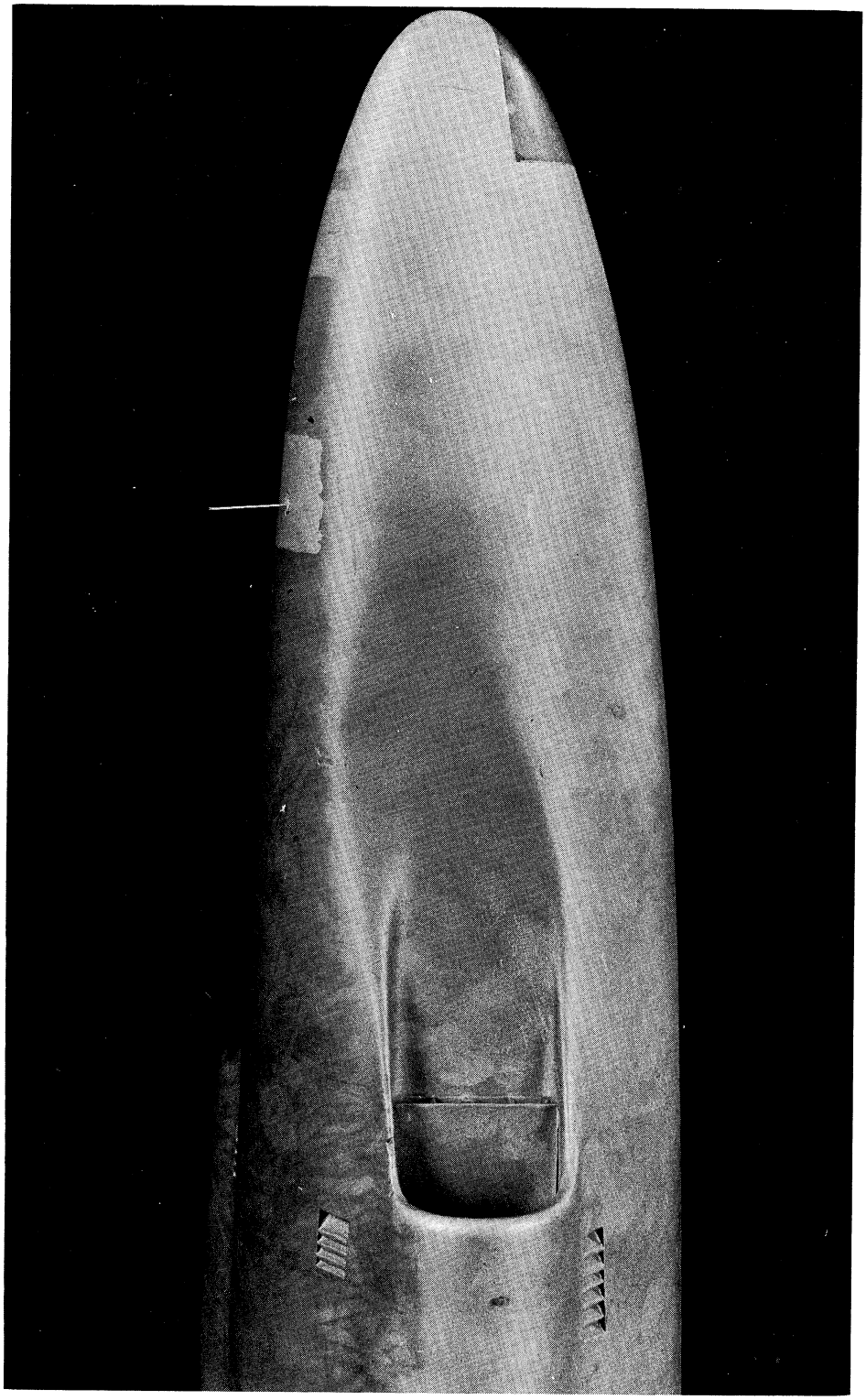

FIG. 34a: $\lambda/4$ MONOPOLE ANTENNA ON PRECISION MODEL T-33

FIG. 34b: $\lambda/4$ MONOPOLE ANTENNA ON SIMPLIFIED MODEL T-33

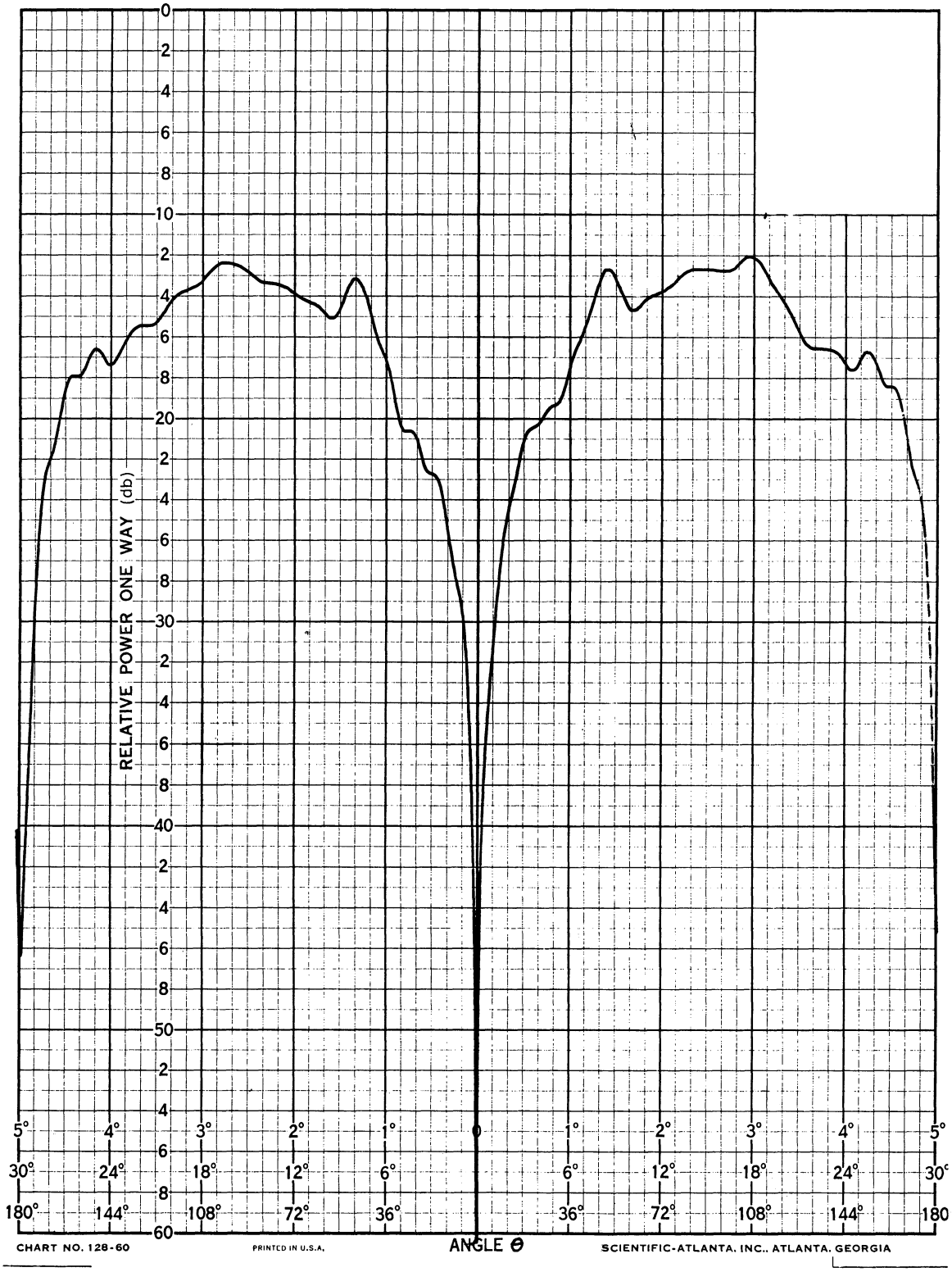

$\phi = 90^{o}$ and 270^{o}

FIG. 35: $\lambda/4$ MONOPOLE, 2.4 GHz, PRECISION T-33

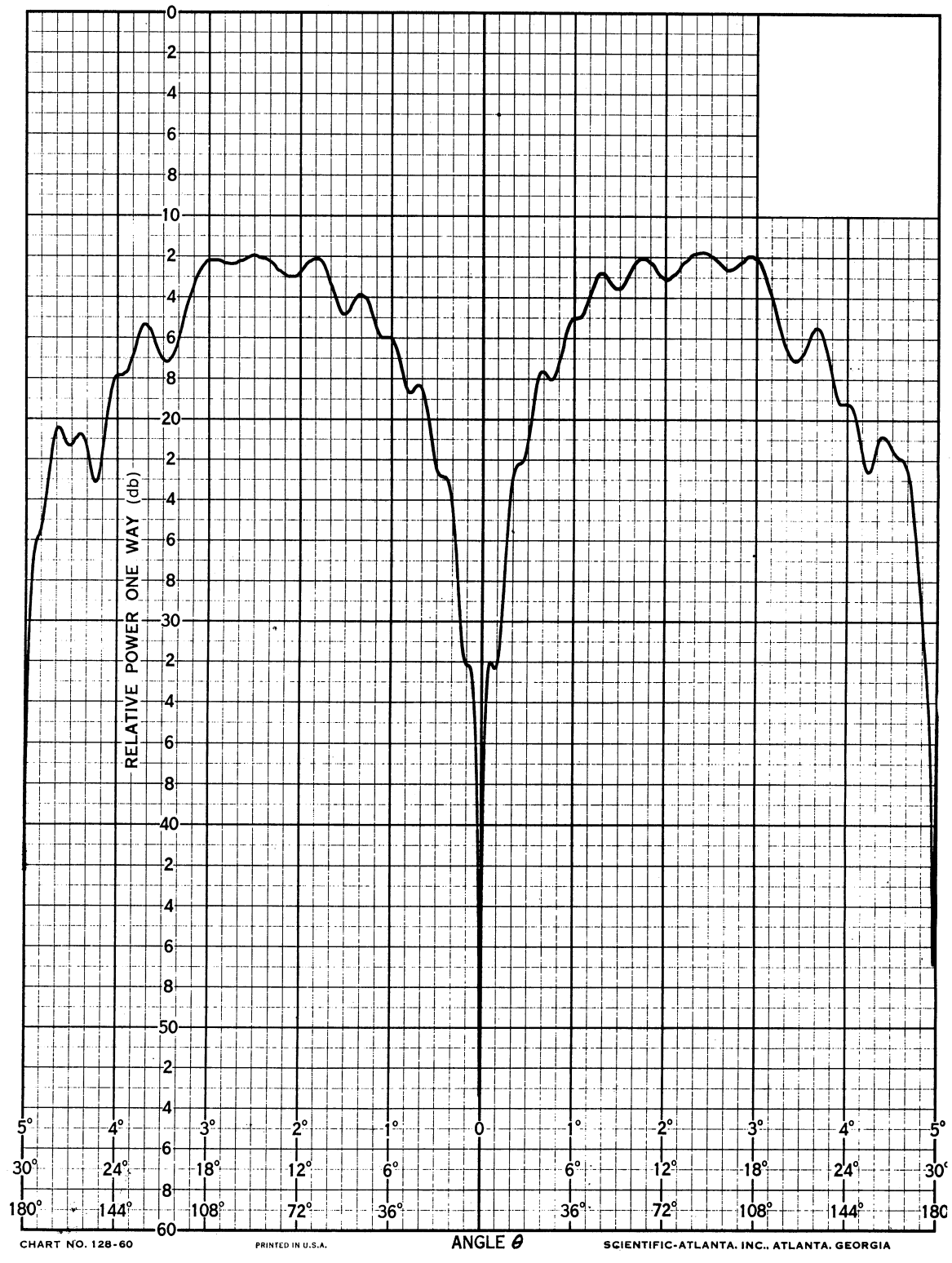

$\phi = 90^{o}$ and 270^{o}

FIG. 36: $\lambda/4$ MONOPOLE, 2.4 GHz, SIMPLIFIED T-33

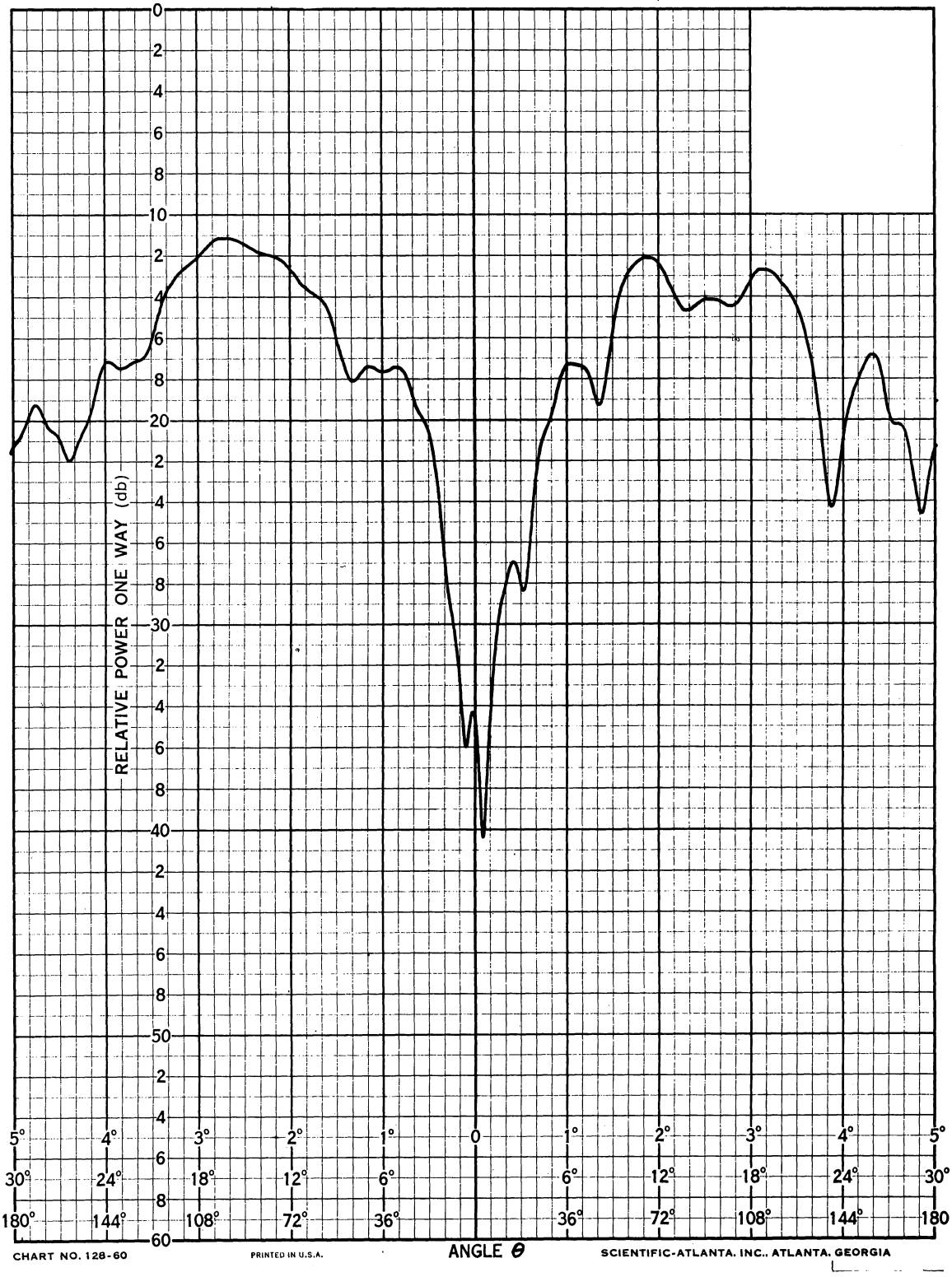

ϕ = 80° and 260°

FIG. 37: $\lambda/4$ MONOPOLE, 2.4 GHz, PRECISION T-33

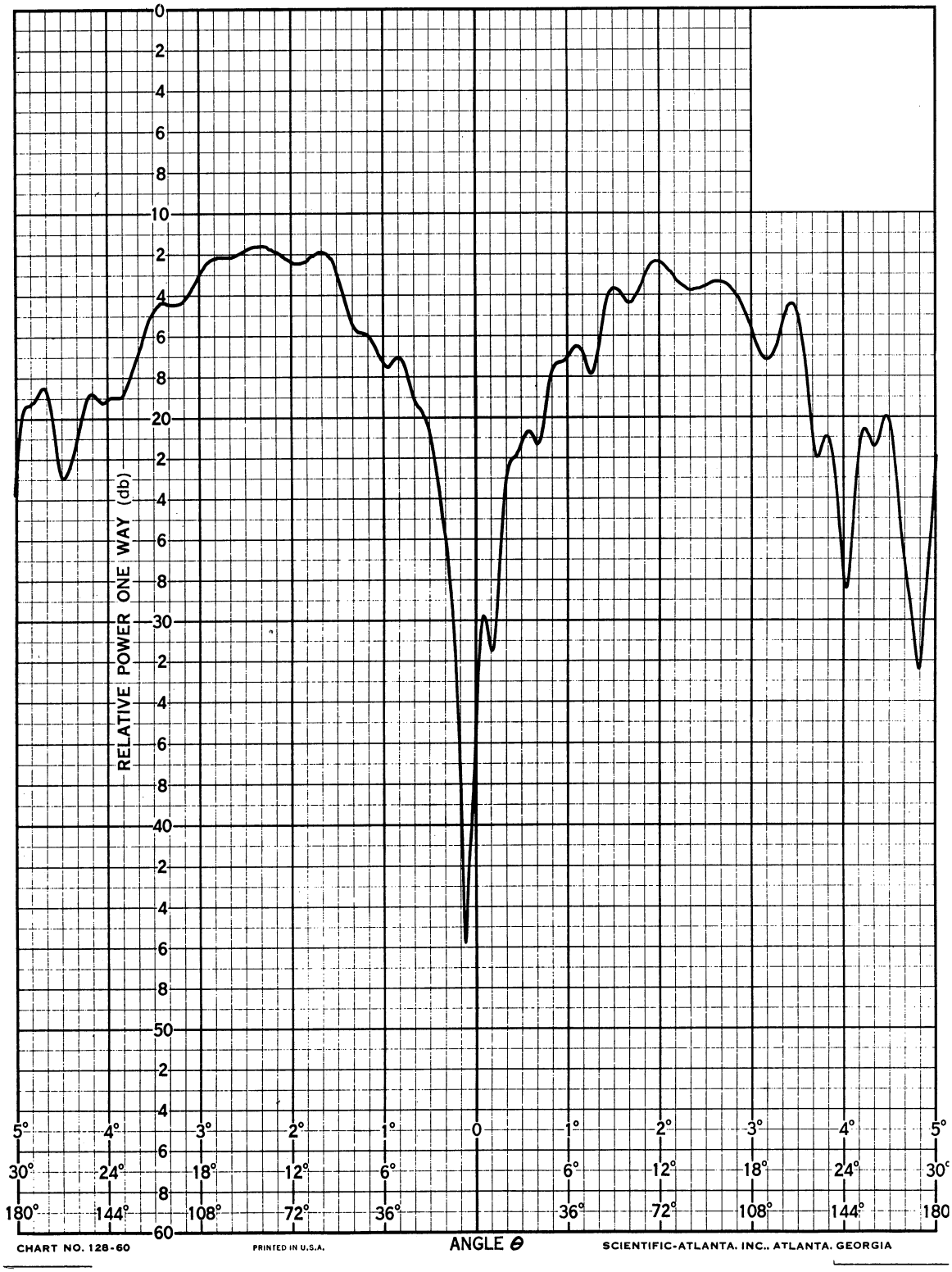

$\phi = 80^{o}$ and 260^{o}

FIG. 38: $\lambda/4$ MONOPOLE, 2.4 GHz, SIMPLIFIED T-33

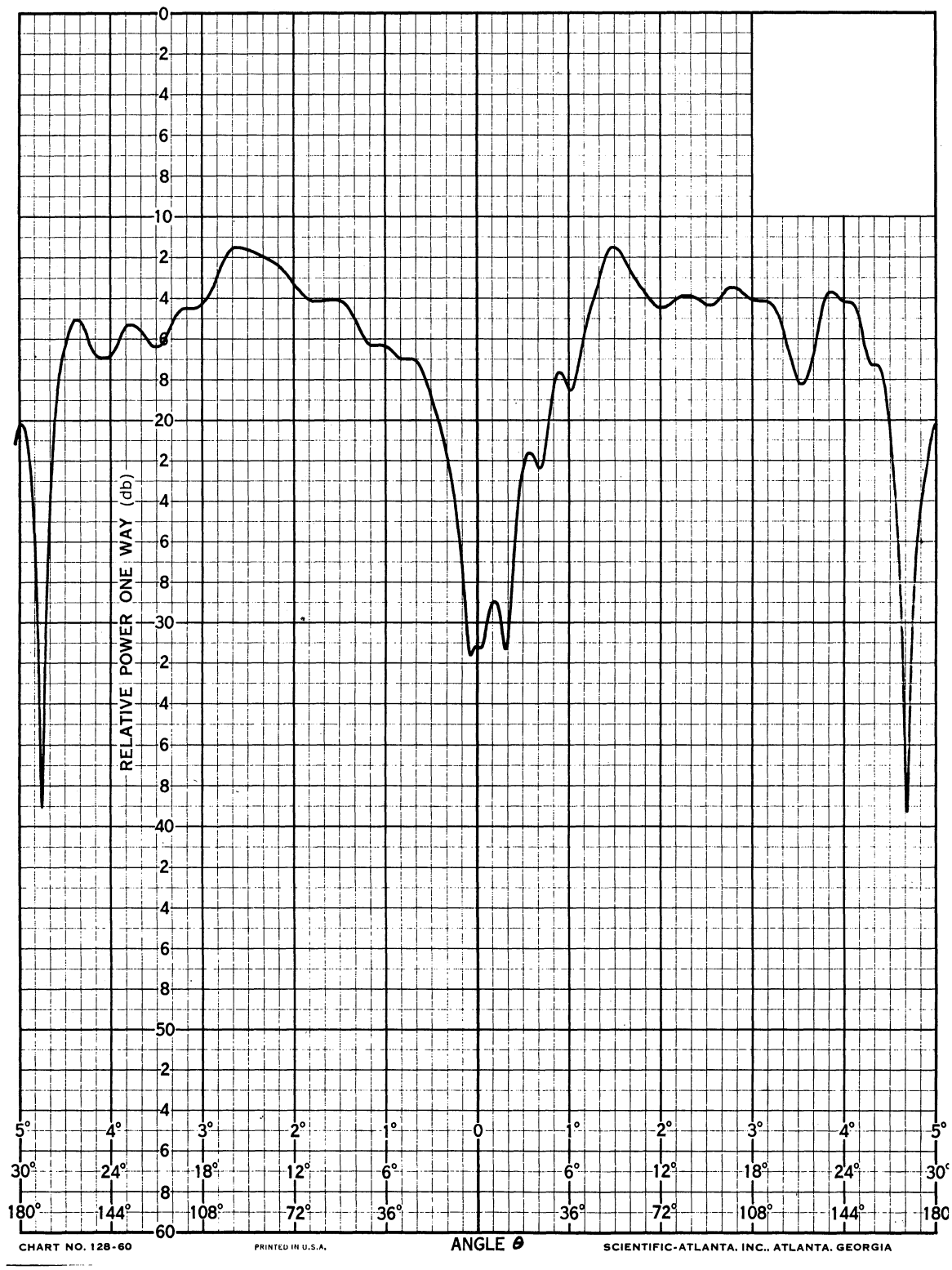

$\phi = 70^{o}$ and 250^{o}

FIG. 39: $\lambda/4$ MONOPOLE, 2.4 GHz, PRECISION T-33

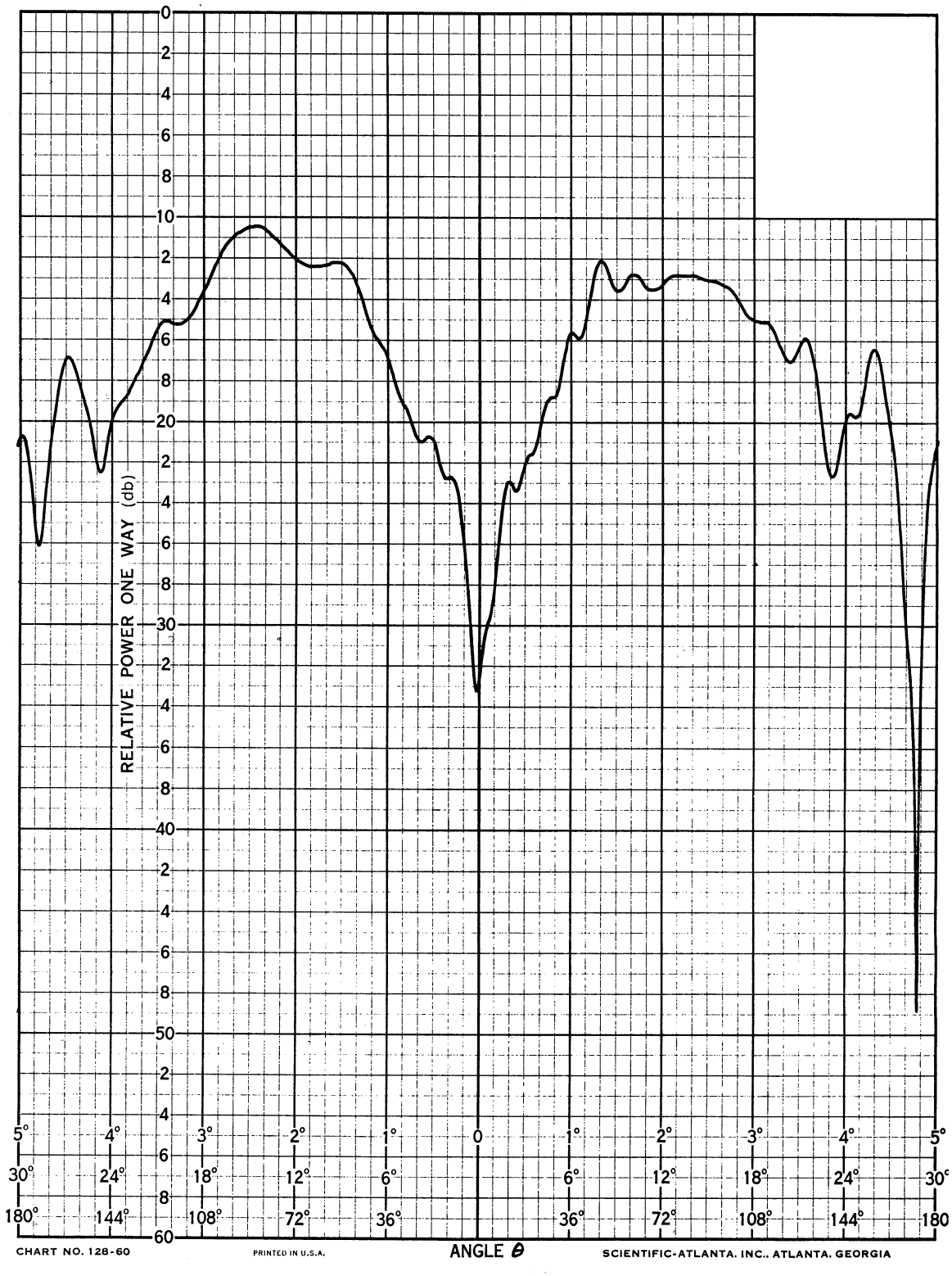

ϕ = 70° and 250°

FIG. 40: $\lambda/4$ MONOPOLE, 2.4 GHz, SIMPLIFIED T-33

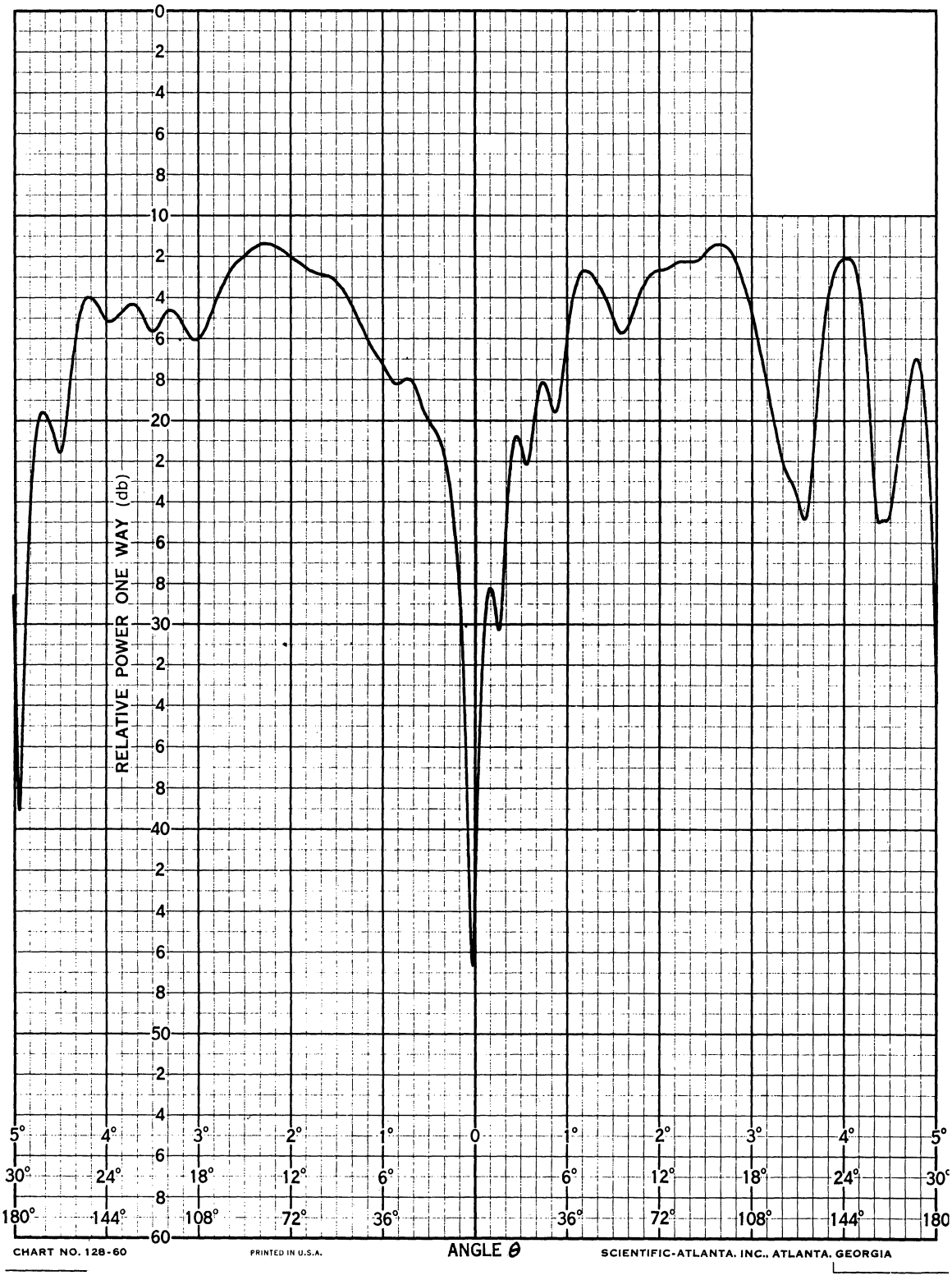

$\phi = 60^{o}$ and 240^{o}

FIG. 41: $\lambda/4$ MONOPOLE, 2.4 GHz, PRECISION T-33

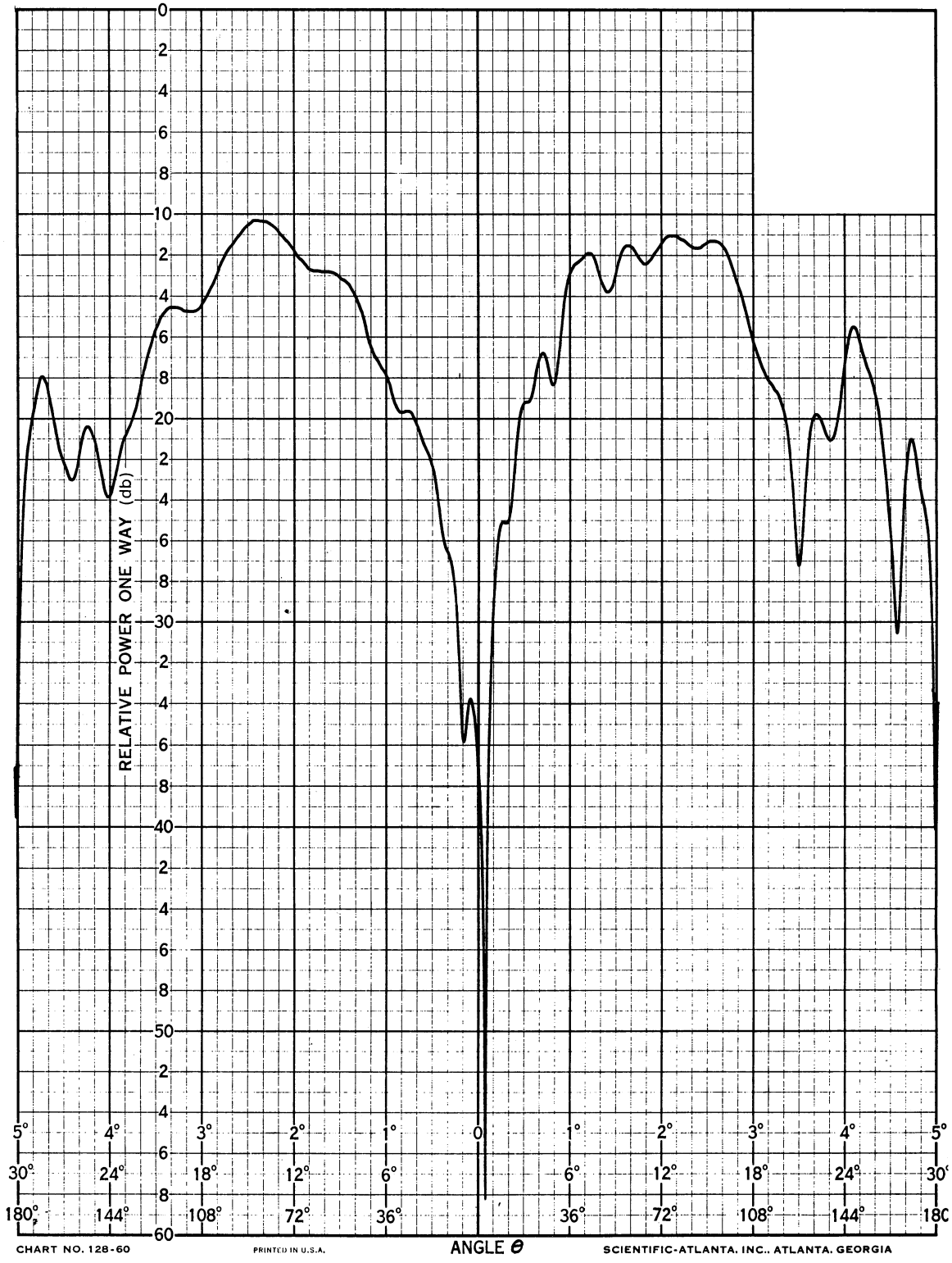

ϕ = 60° and 240°

FIG. 42: $\lambda/4$ MONOPOLE, 2.4 GHz, SIMPLIFIED T-33

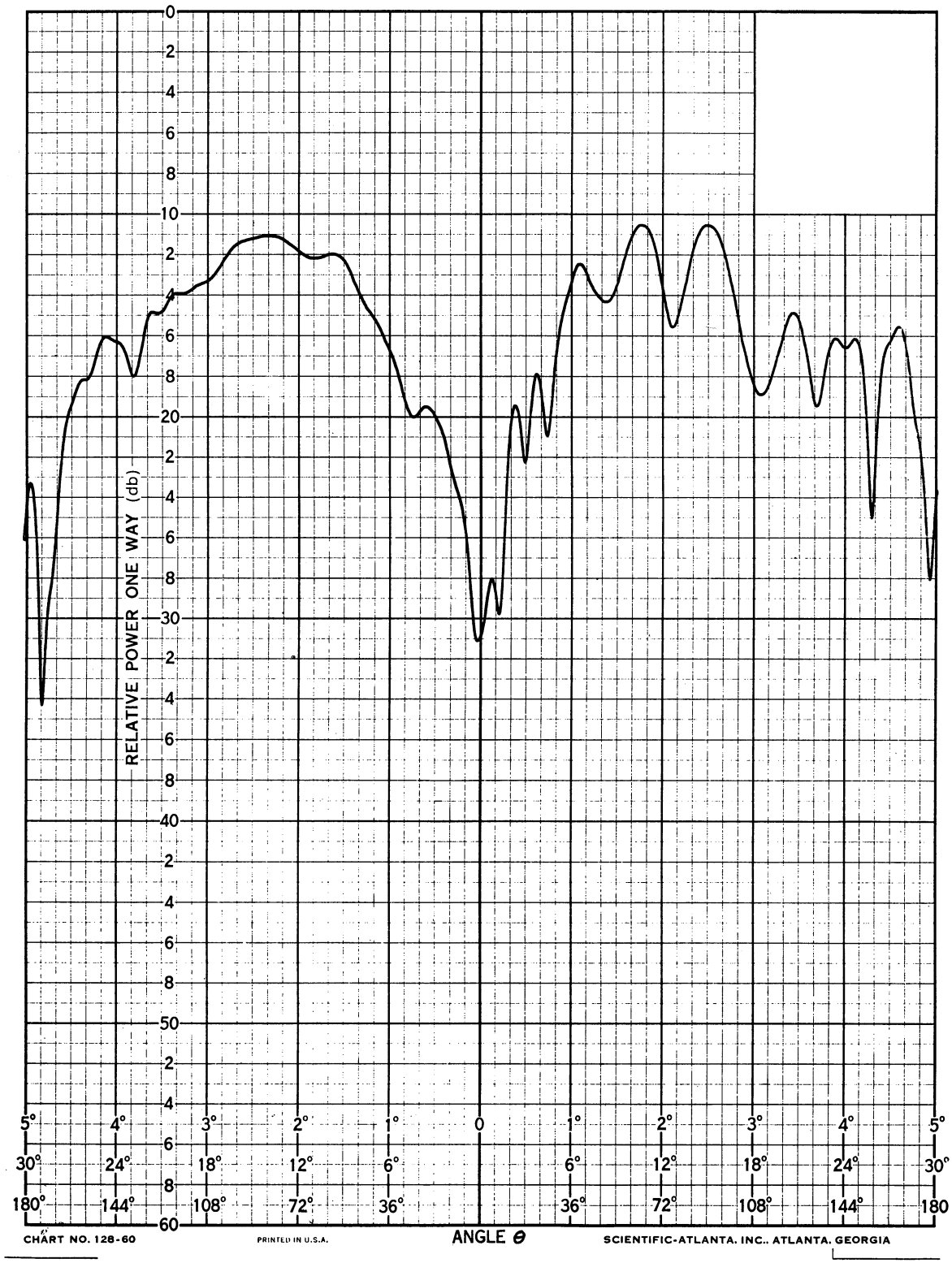

$\phi = 50^{o}$ and 230^{o}

FIG. 43: $\lambda/4$ MONOPOLE, 2.4 GHz, PRECISION T-33

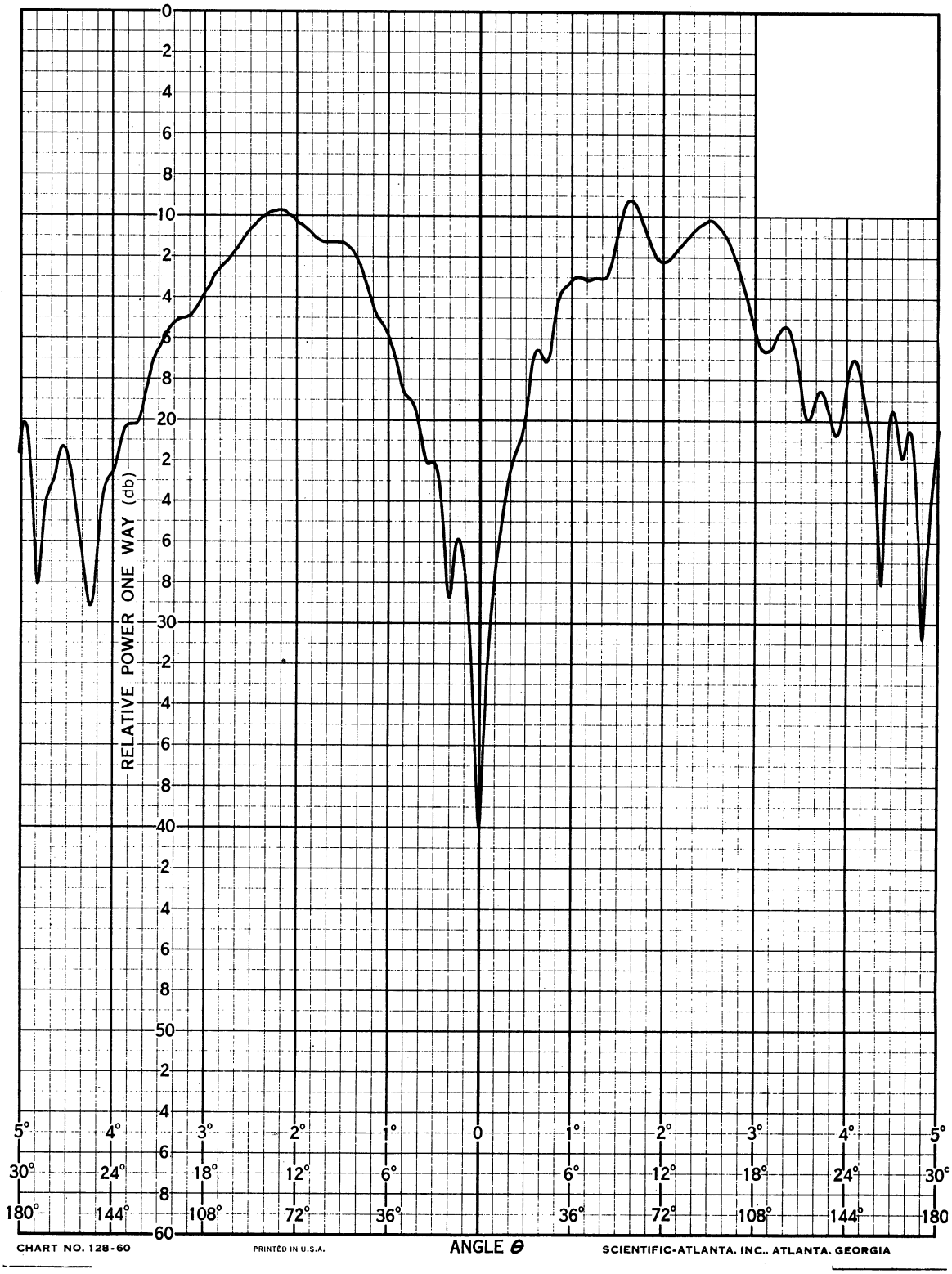

$\phi = 50^{o}$ and 230^{o}

FIG. 44: $\lambda/4$ MONOPOLE, 2.4 GHz, PRECISION T-33

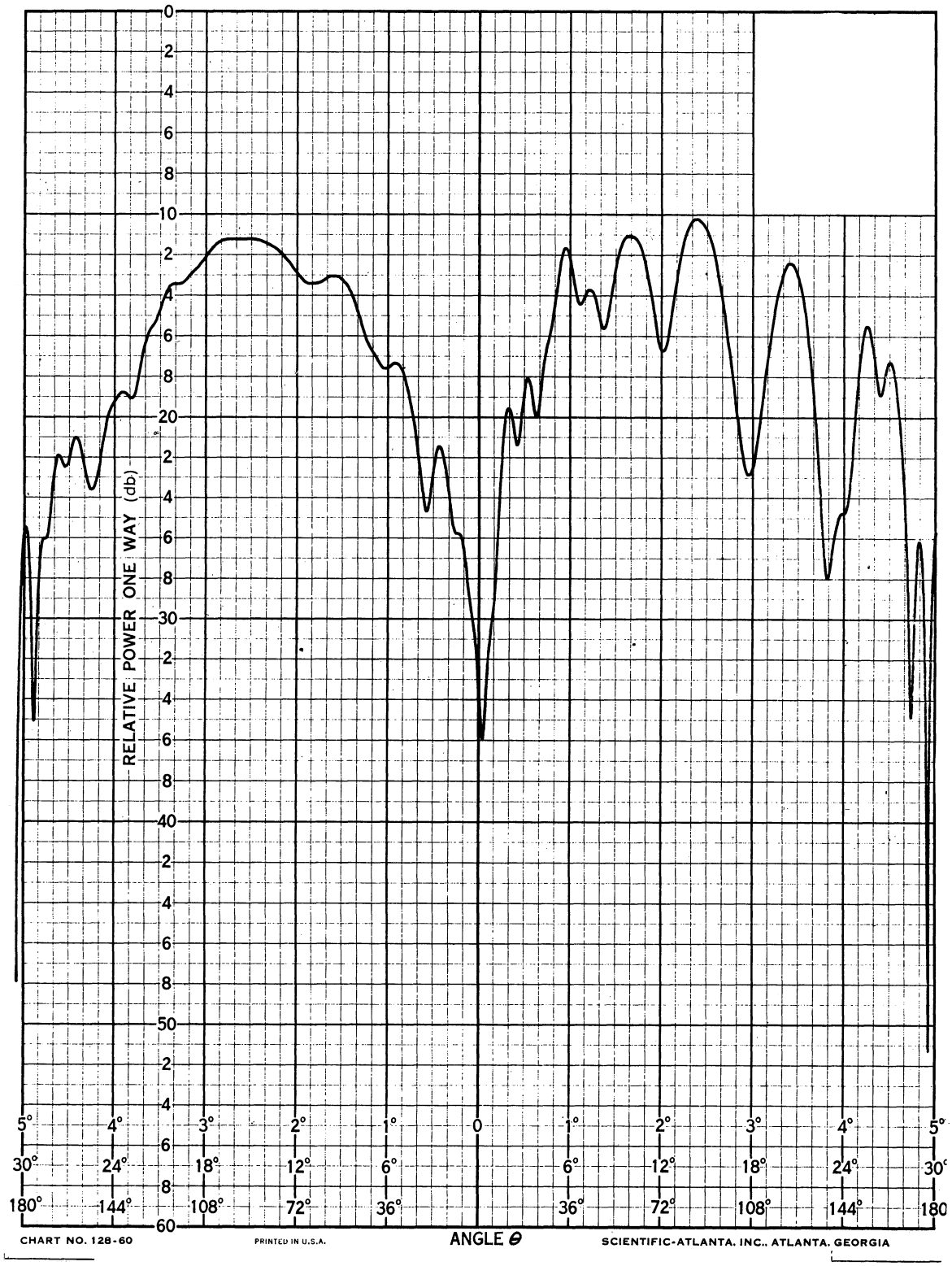

$\phi = 50^{o}$ and 230^{o}

FIG. 45: $\lambda/4$ MONOPOLE, 2.4 GHz, SIMPLIFIED T-33

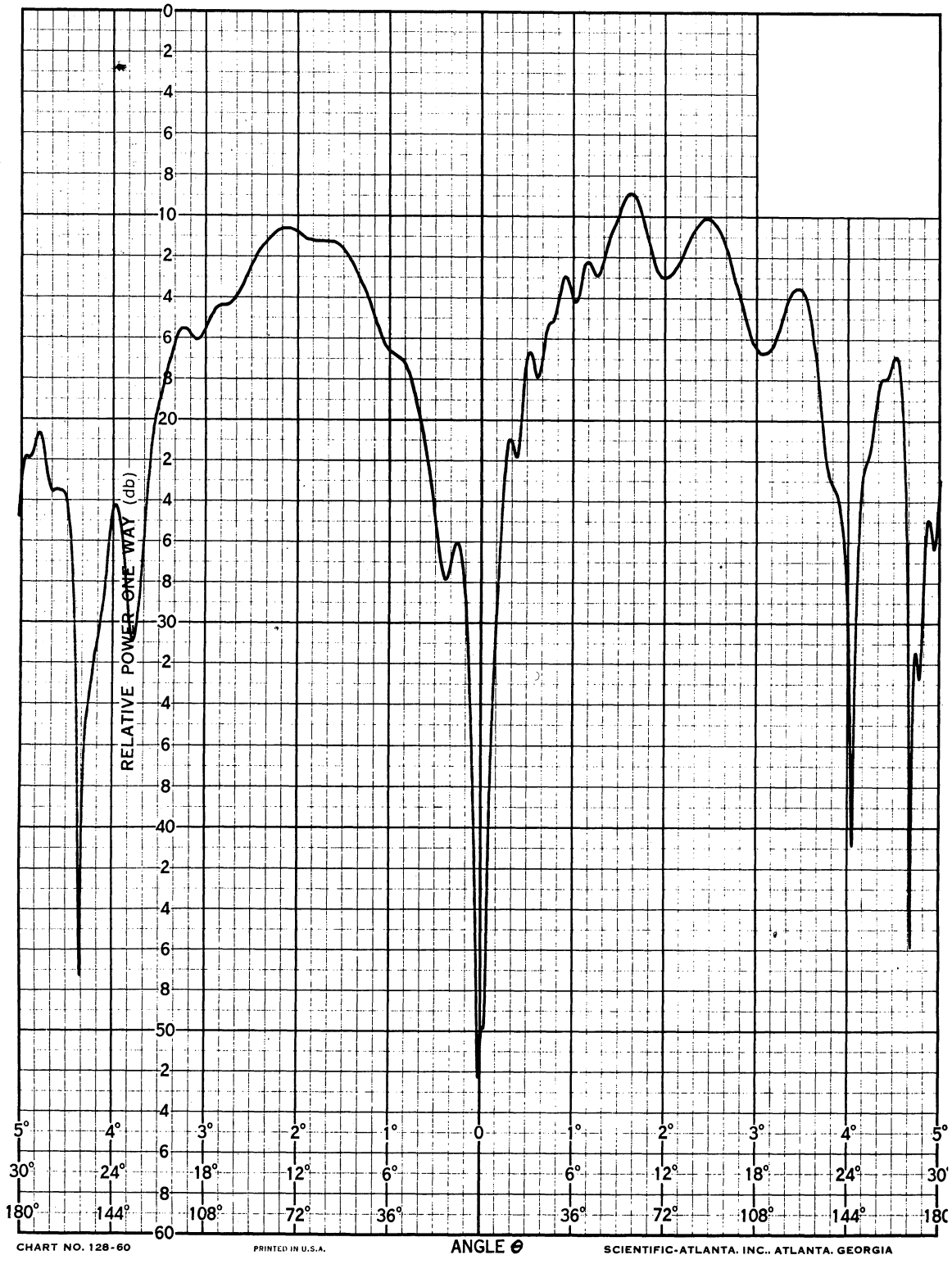

ϕ = 40° and 220°

FIG. 46: $\lambda/4$ MONOPOLE, 2.4 GHz, PRECISION T-33

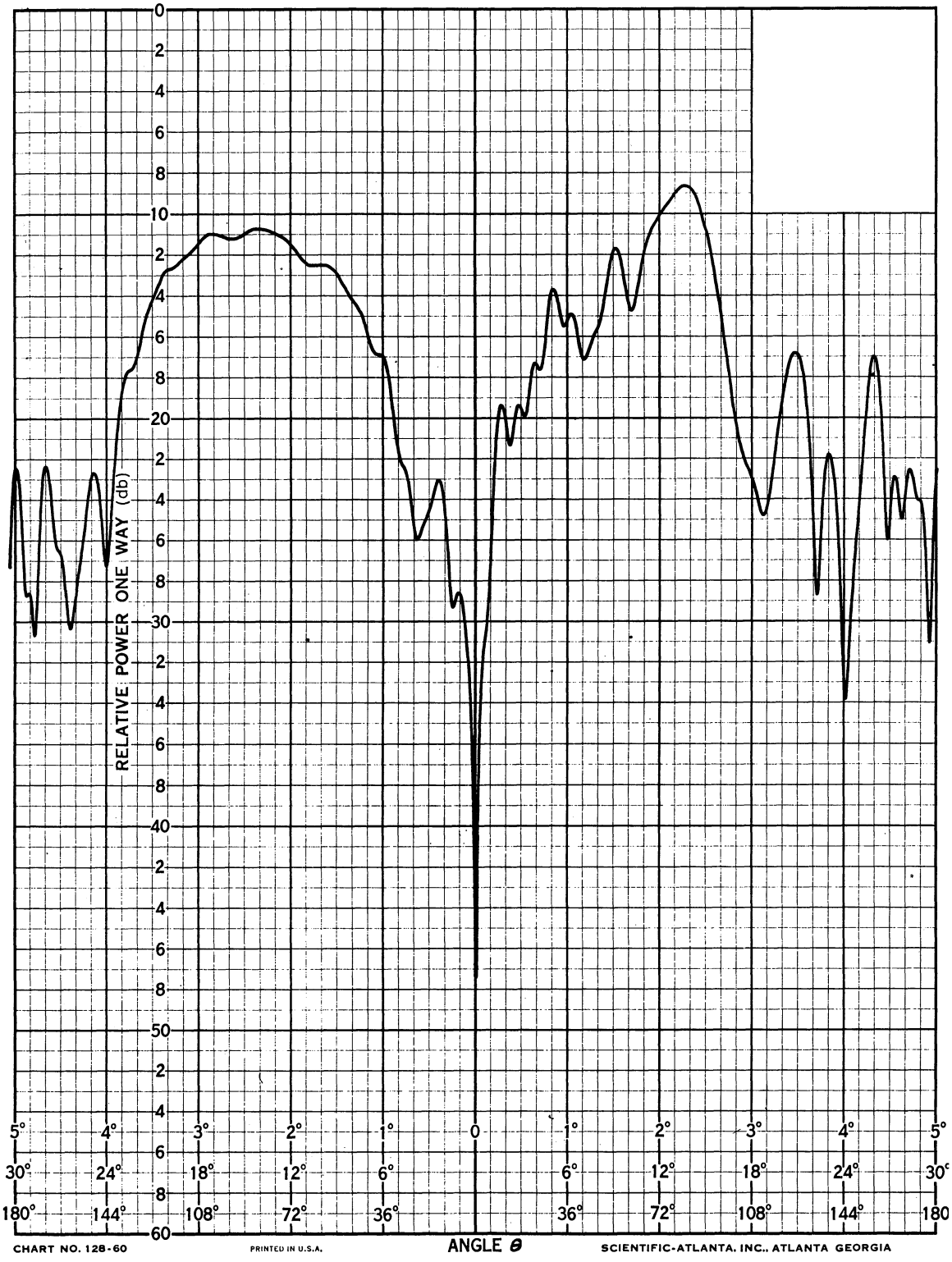

ϕ = 30° and 210°

FIG. 47: $\lambda/4$ MONOPOLE, 2.4 GHz, PRECISION T-33

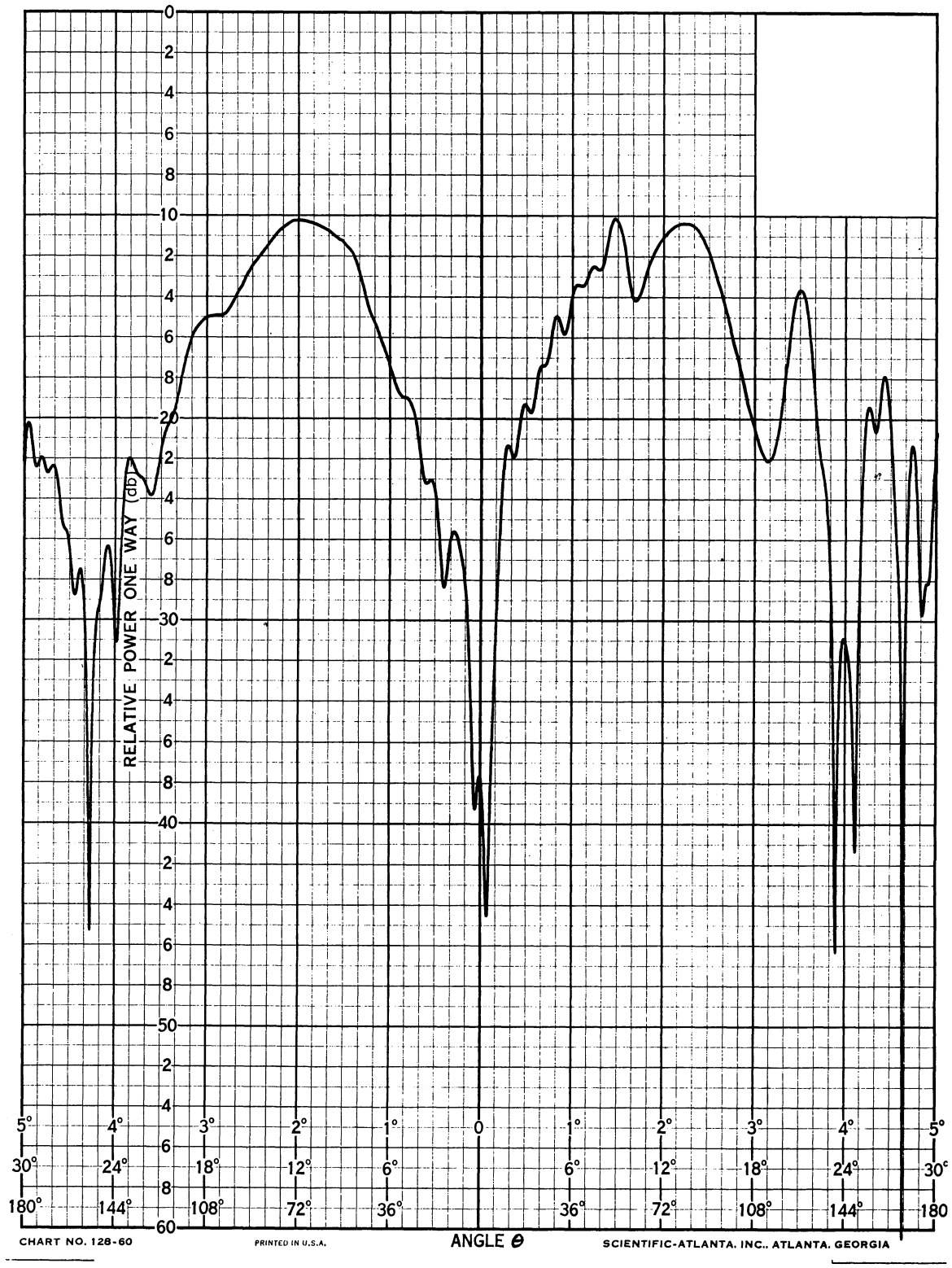

$\phi = 30^{o}$ and 210^{o}

FIG. 48: $\lambda/4$ MONOPOLE, 2.4 GHz, SIMPLIFIED T-33

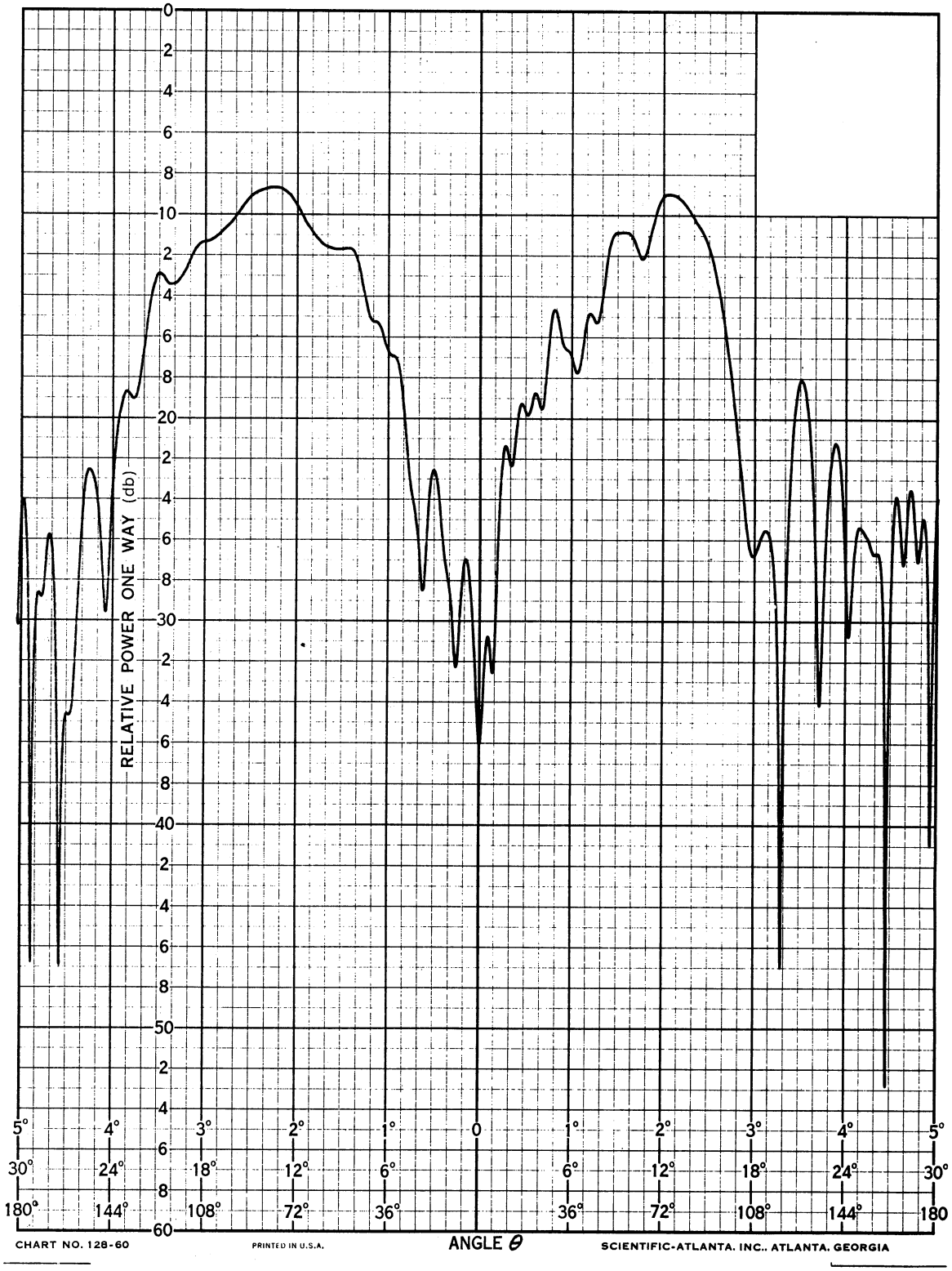

$\phi = 20^{o}$ and 200^{o}

FIG. 49: $\lambda/4$ MONOPOLE, 2.4 GHz, PRECISION T-33

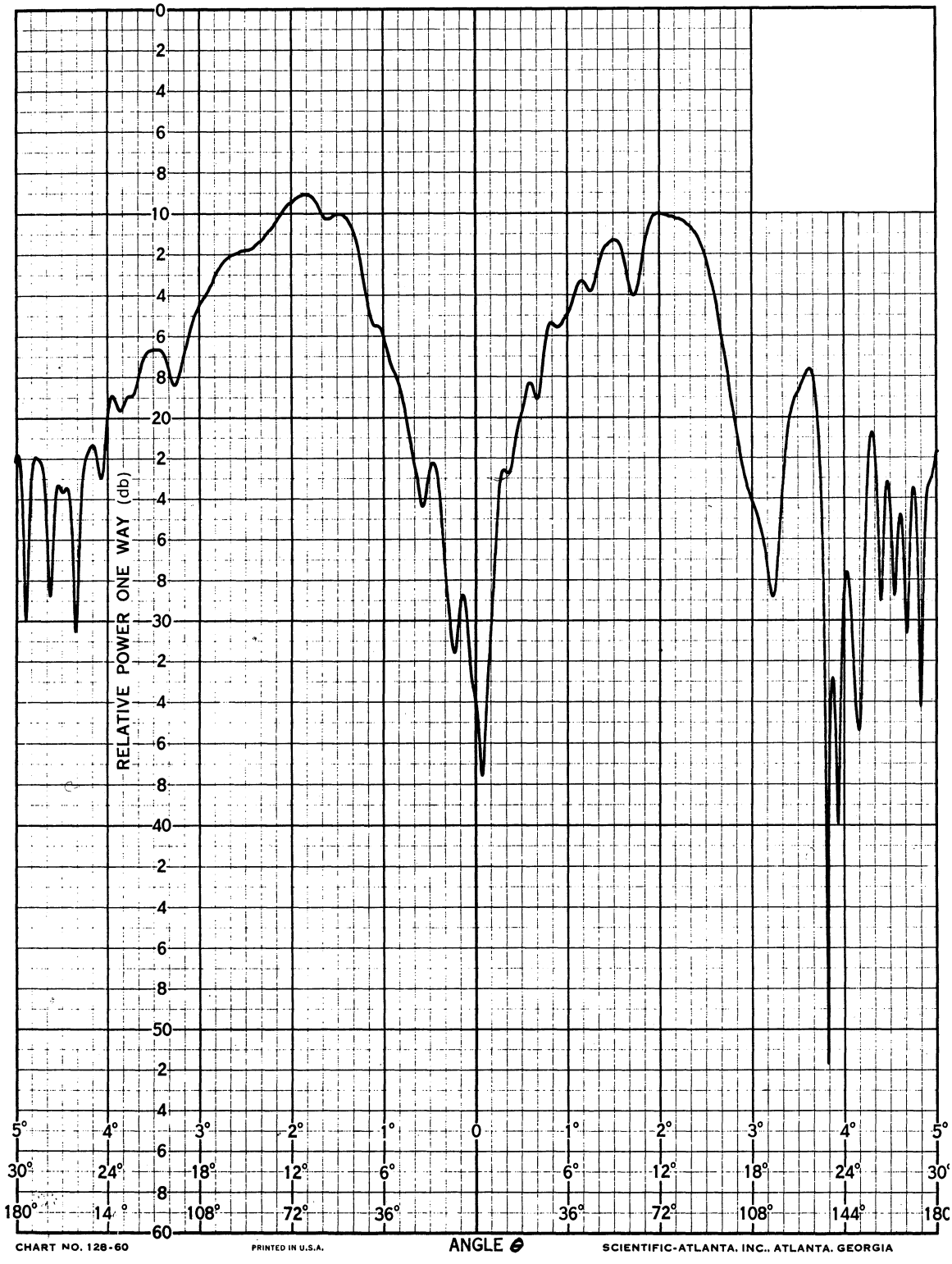

$\phi = 20^{o}$ and 200^{o}

FIG. 50 : $\lambda/4$ MONOPOLE, 2.4 GHz, SIMPLIFIED T-33

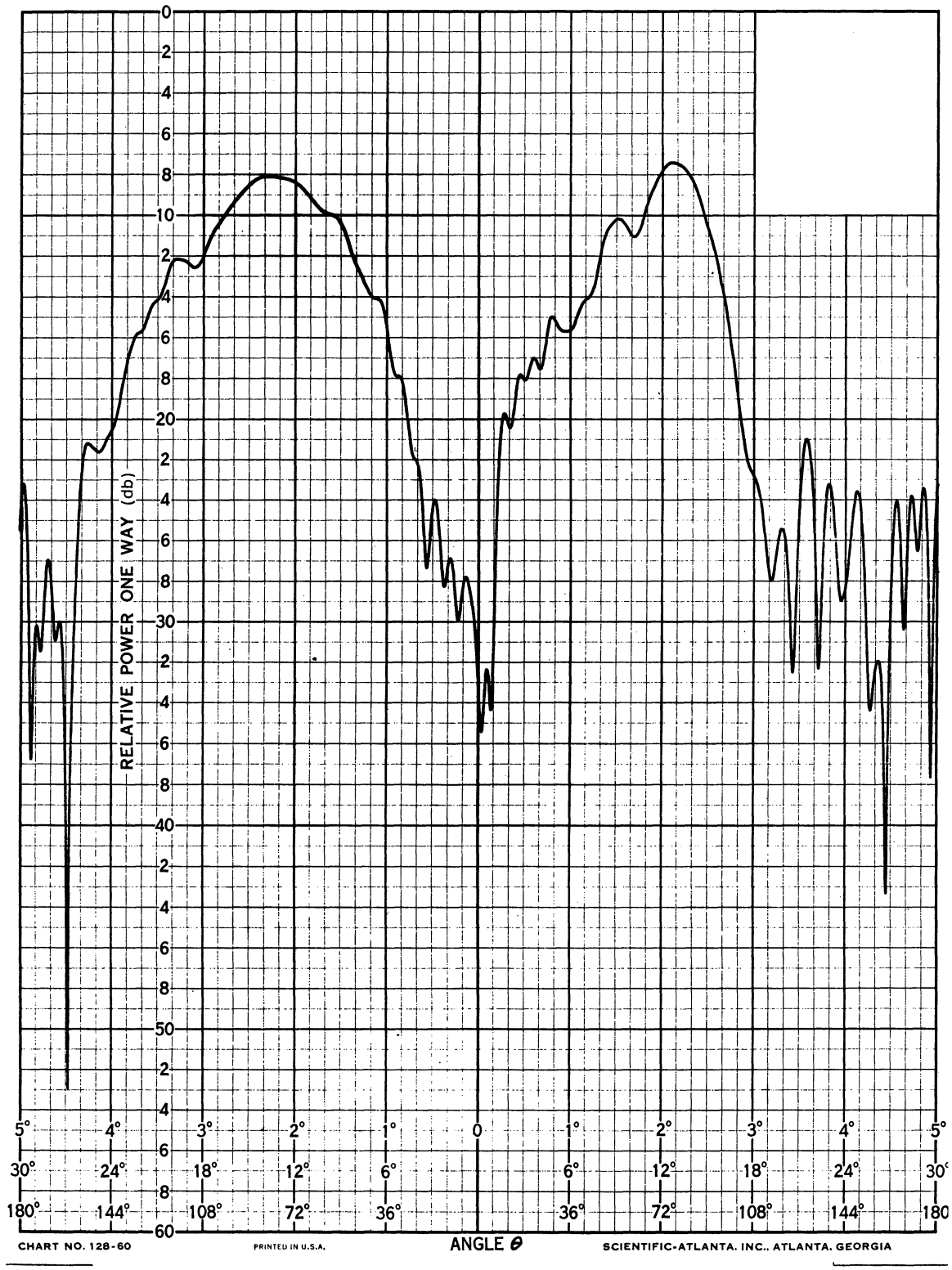

$\phi = 10^{o}$ and 190^{o}

FIG. 51: $\lambda/4$ MONOPOLE, 2.4 GHz, PRECISION T-33

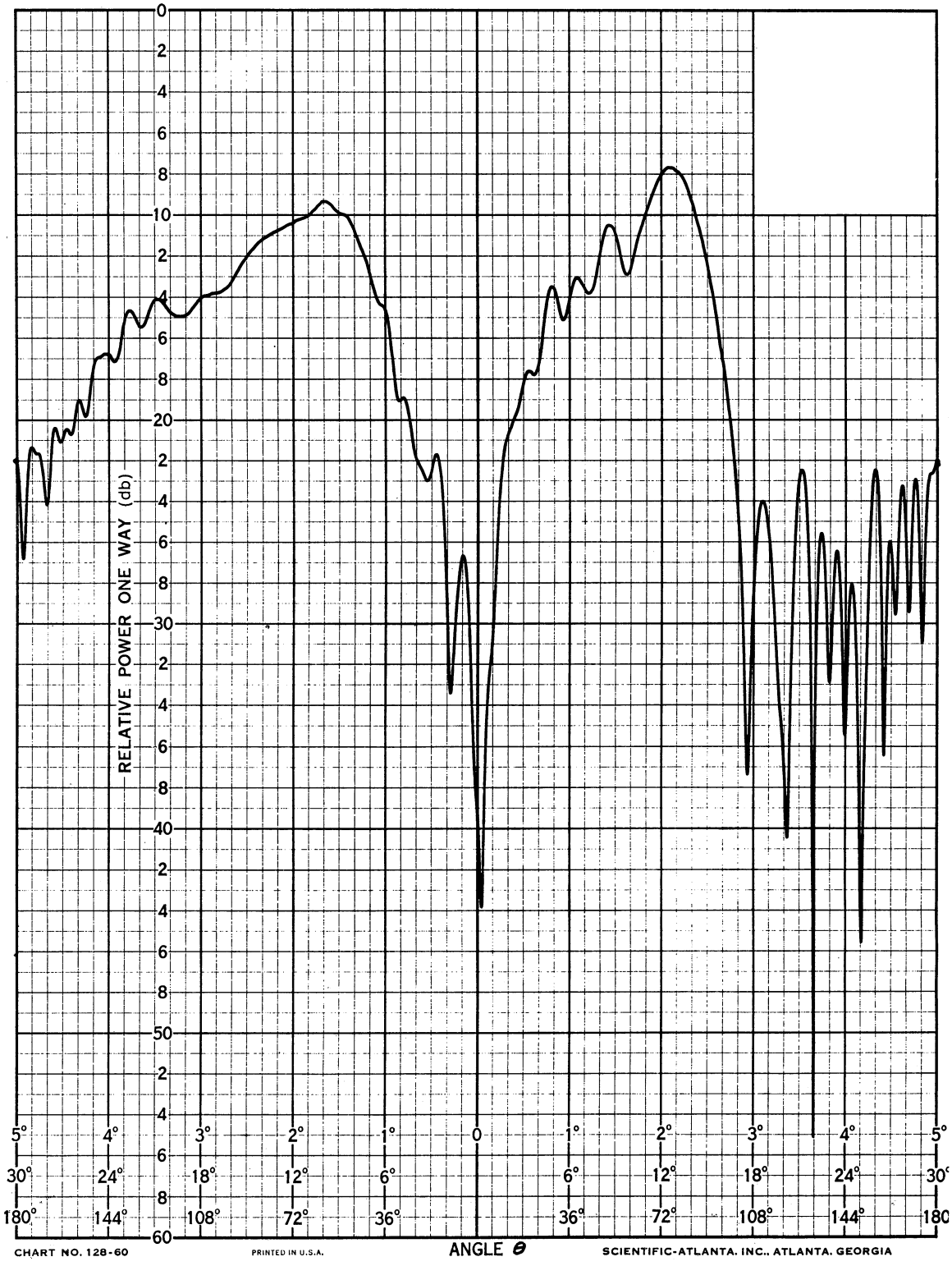

$\phi = 10^{o}$ and 190^{o}

FIG. 52: $\lambda/4$ MONOPOLE, 2.4 GHz, SIMPLIFIED T-33

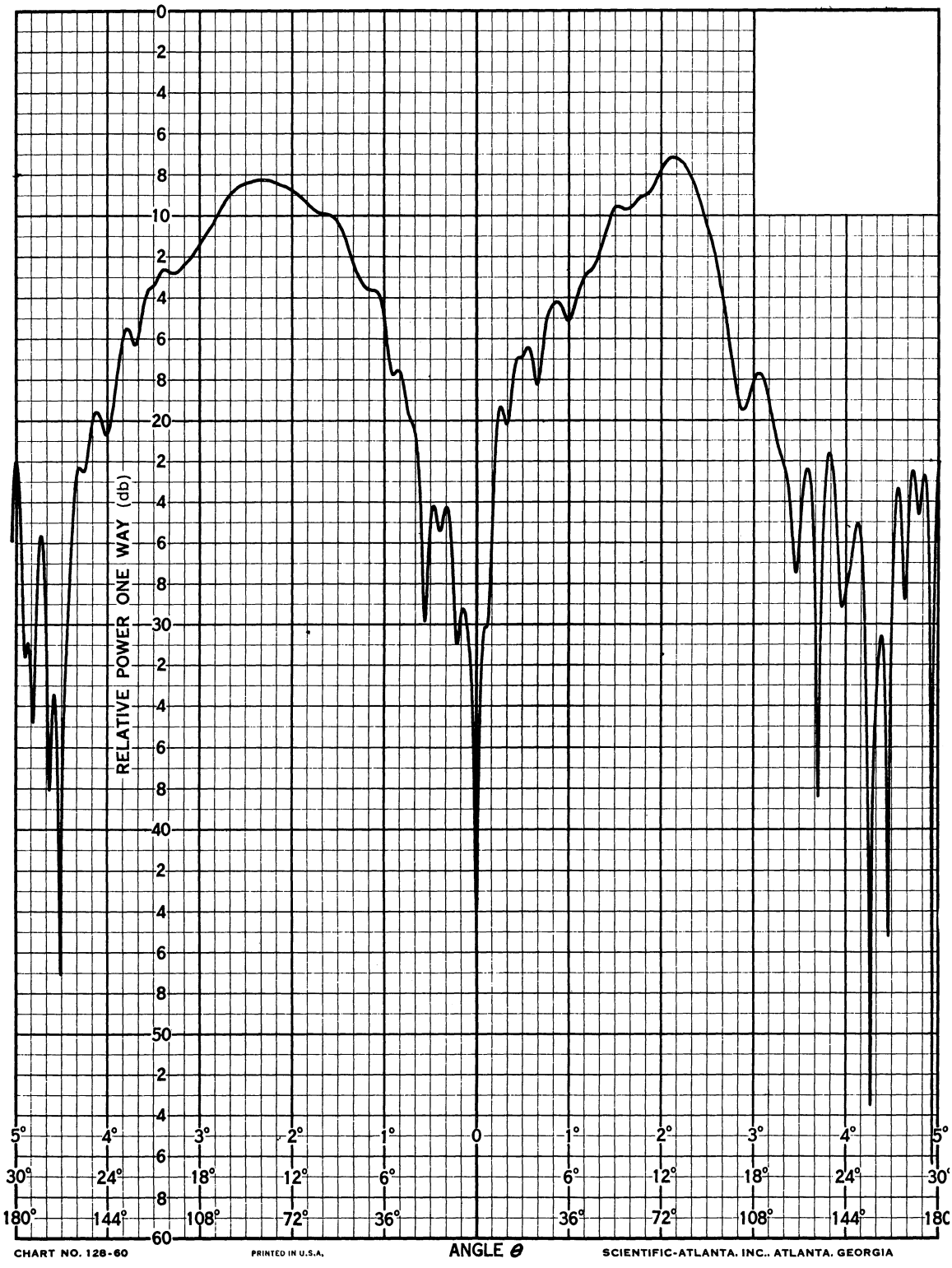

ϕ = 0° and 180°

FIG. 53: $\lambda/4$ MONOPOLE, 2.4 GHz, PRECISION T-33.

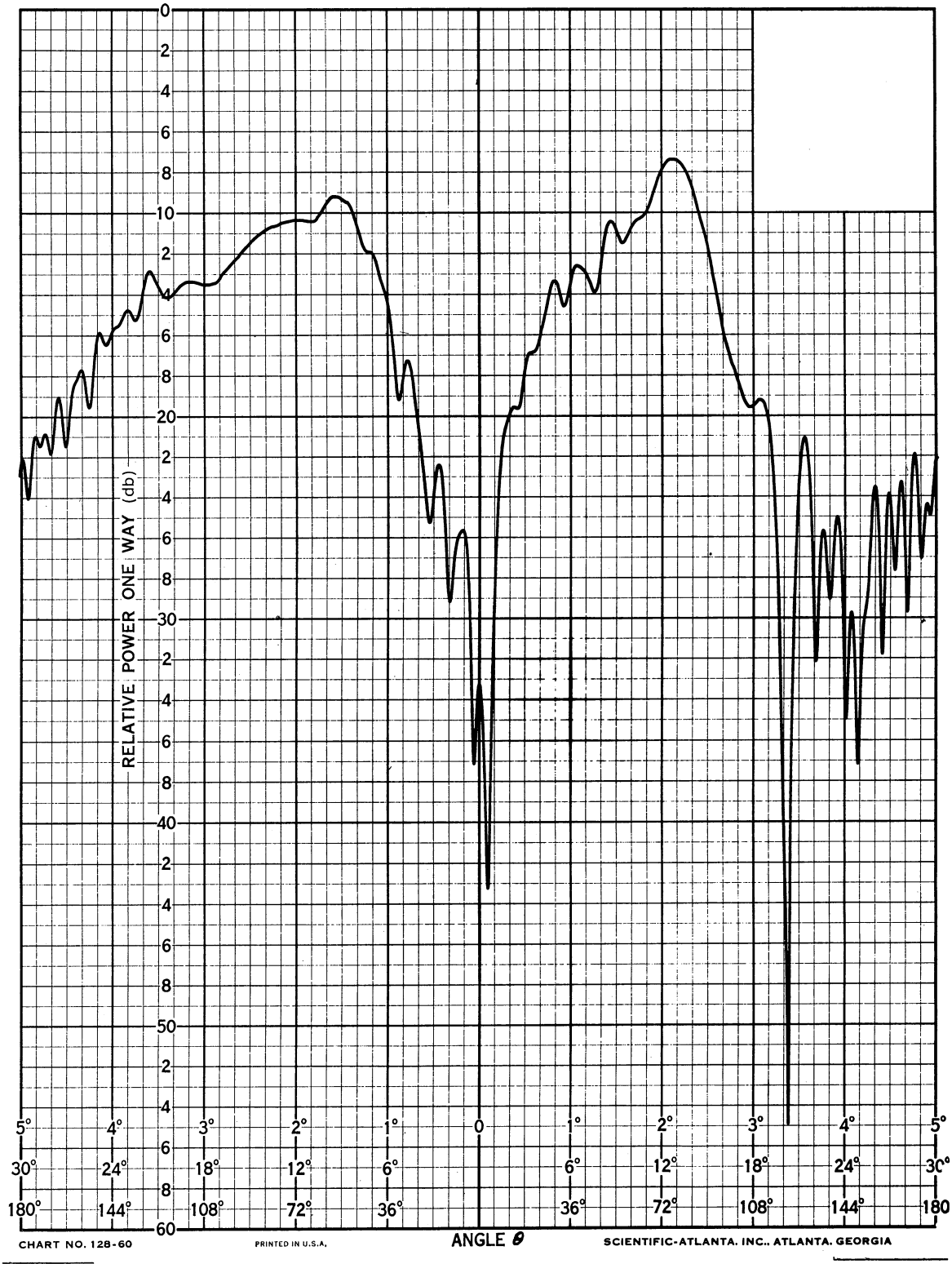

$\phi = 0^{o}$ and 180^{o}

FIG. 54: $\lambda/4$ MONOPOLE, 2.4 GHz, SIMPLIFIED T-33.

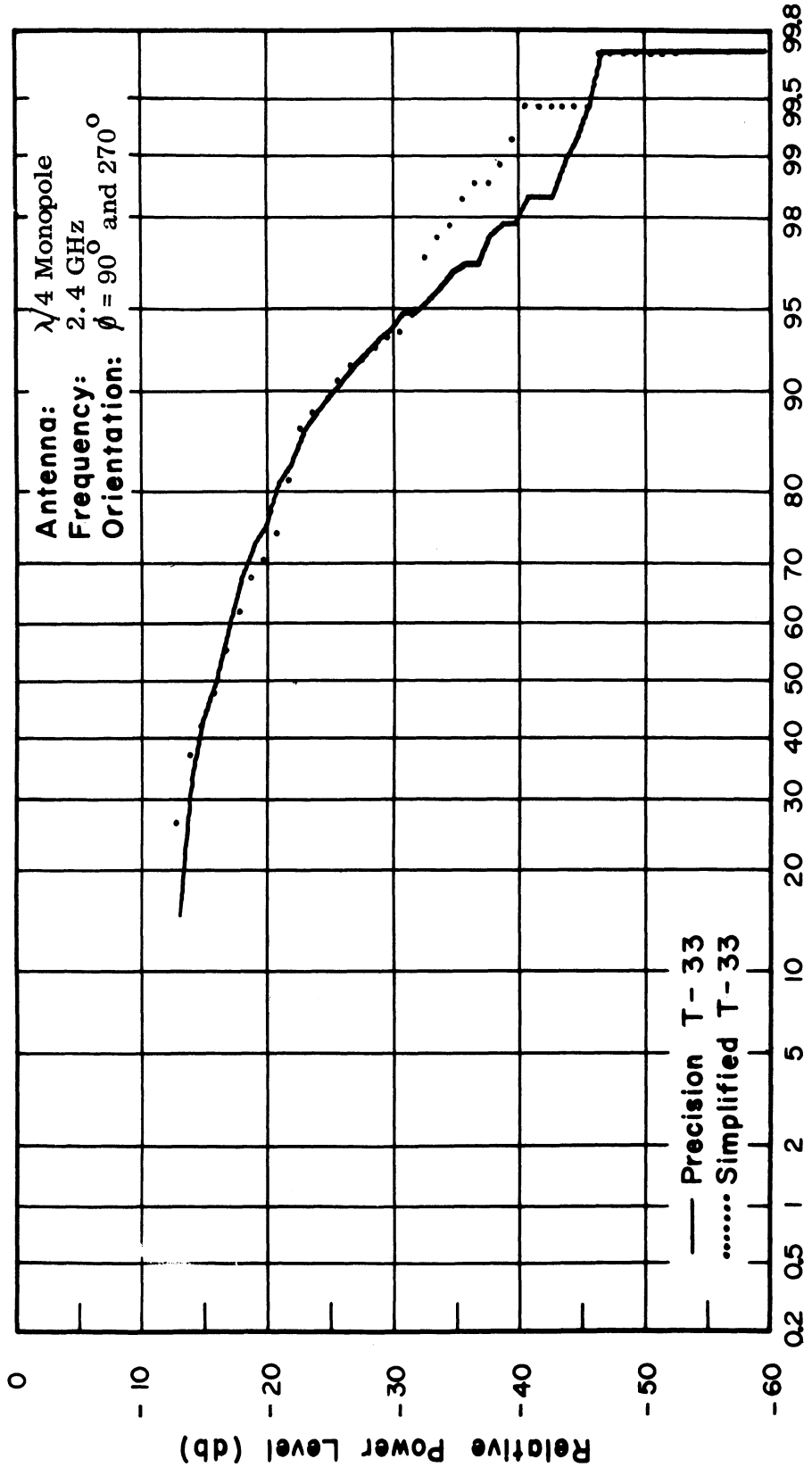

FIG. 55: CUMULATIVE GAIN DISTRIBUTIONS OF PRECISION AND SIMPLIFIED MODELS

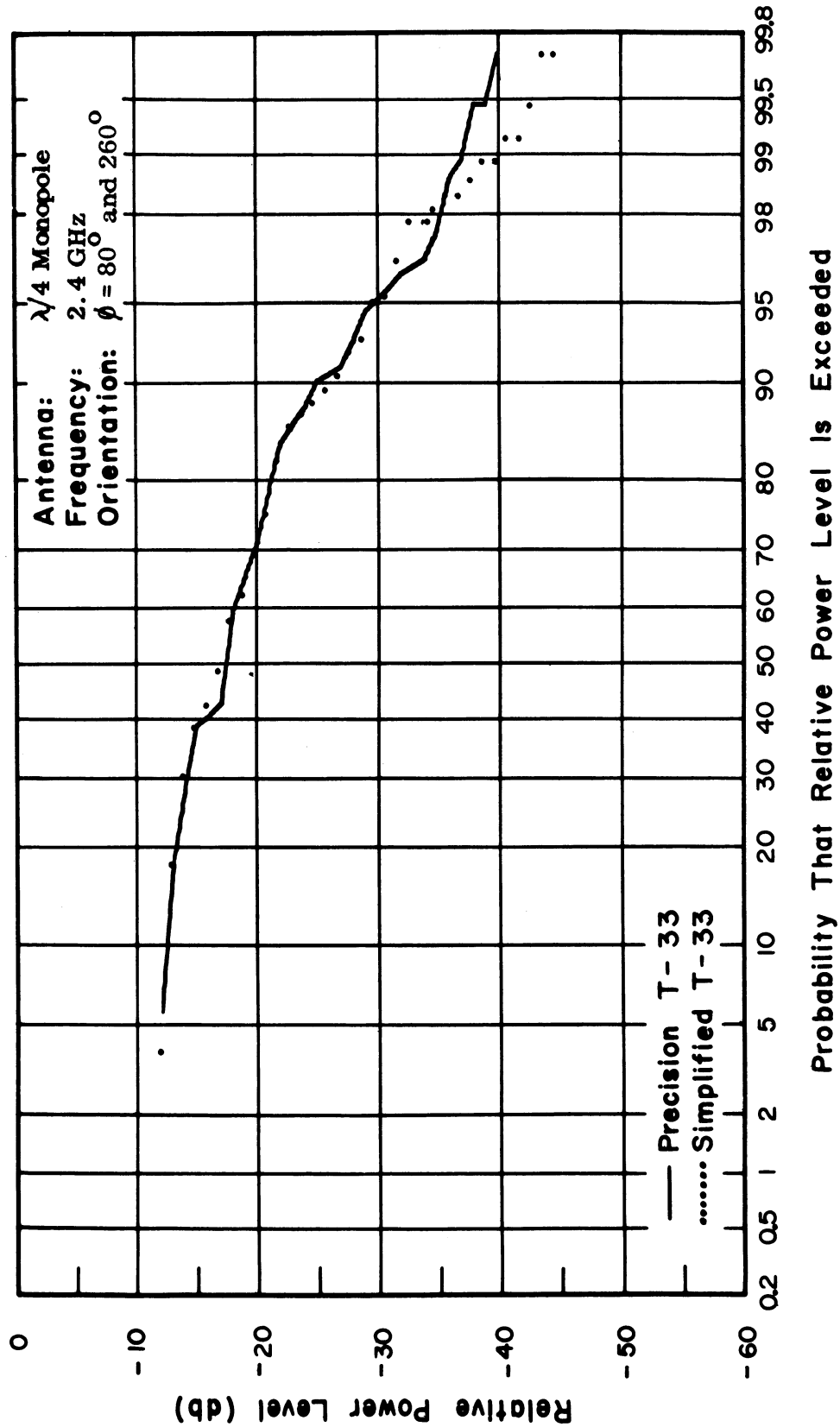

FIG. 56: CUMULATIVE GAIN DISTRIBUTIONS OF PRECISION AND SIMPLIFIED MODELS

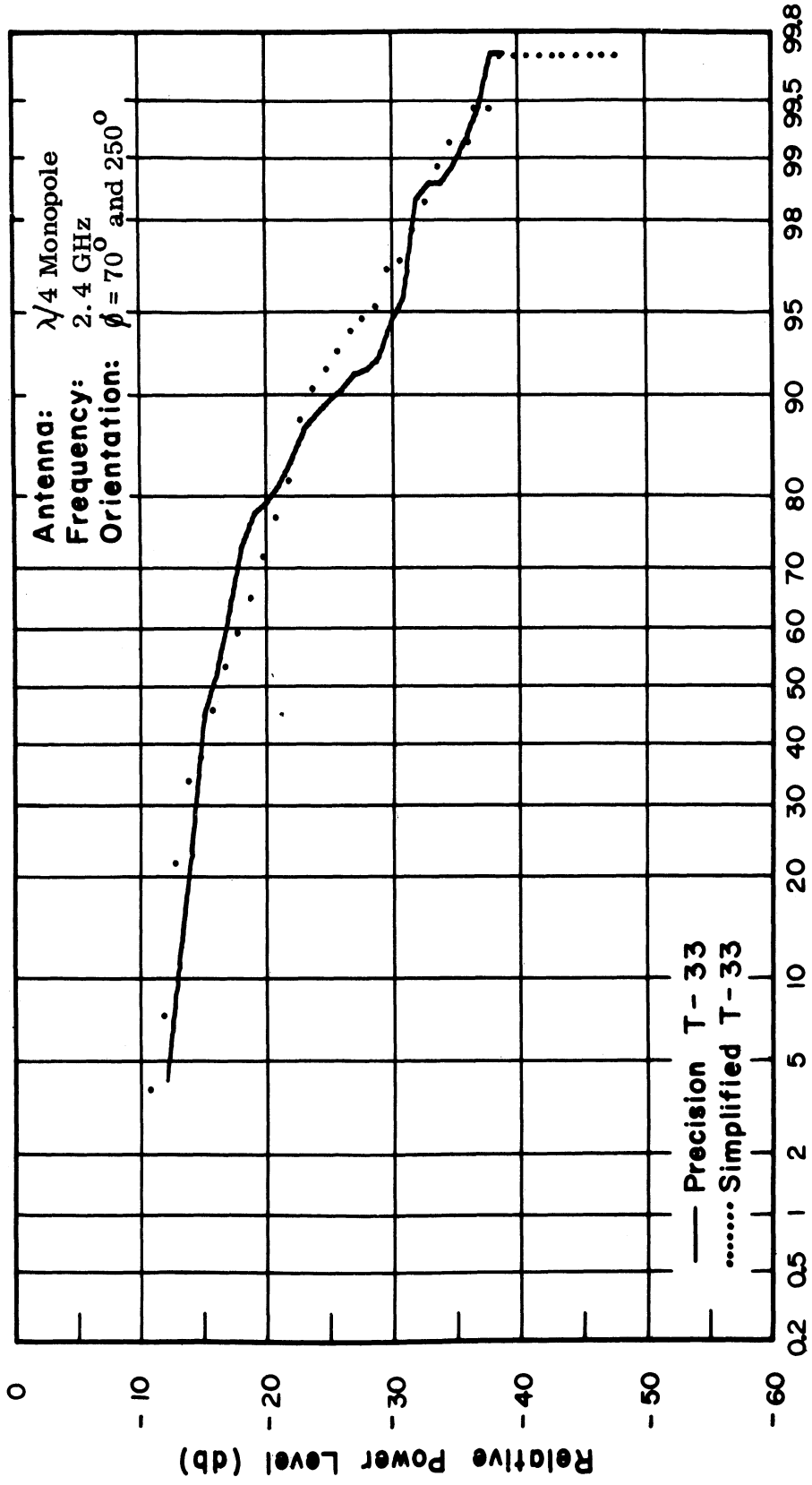

FIG. 57: CUMULATIVE GAIN DISTRIBUTIONS OF PRECISION AND SIMPLIFIED MODELS

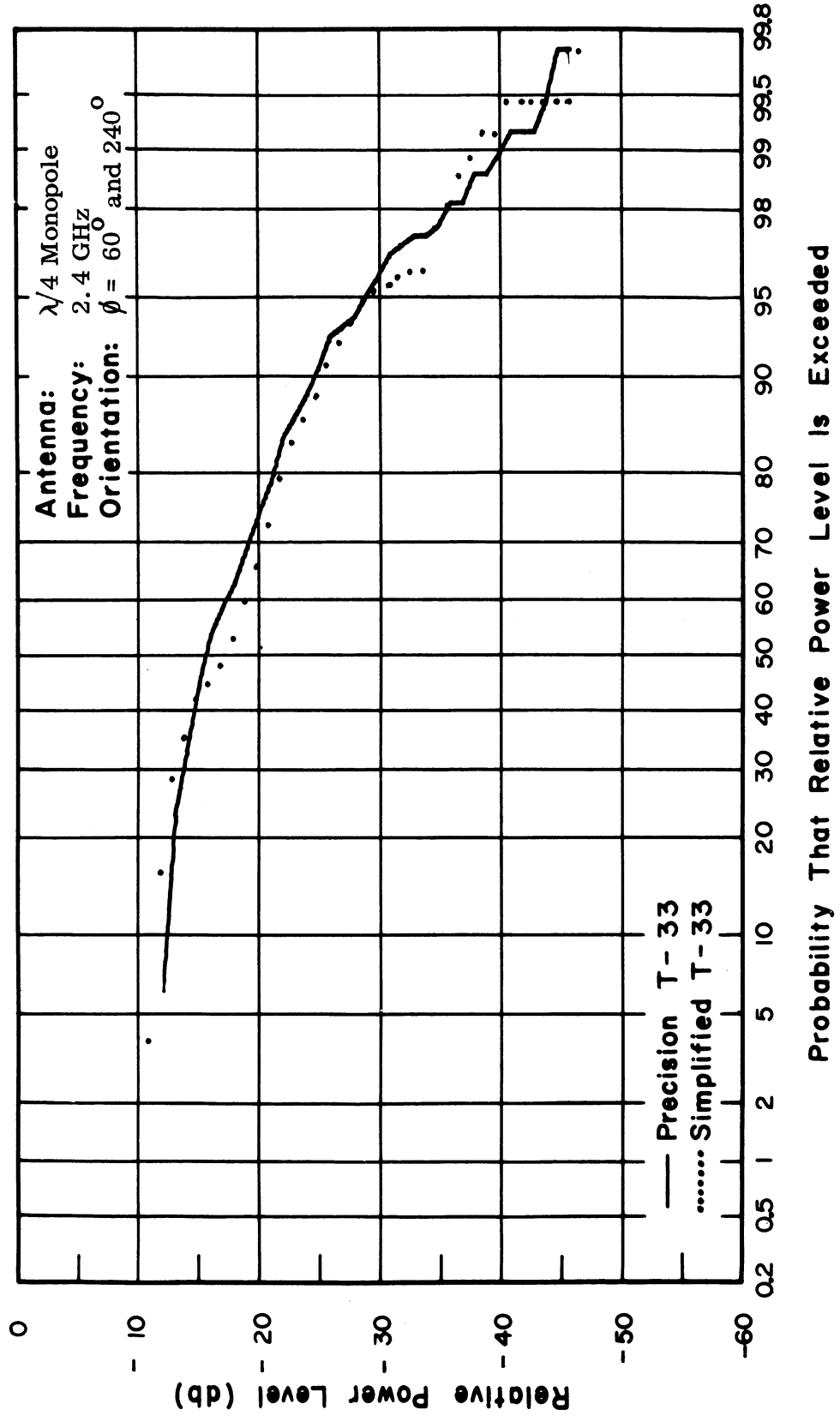

FIG. 58: CUMULATIVE GAIN DISTRIBUTIONS OF PRECISION AND SIMPLIFIED MODELS

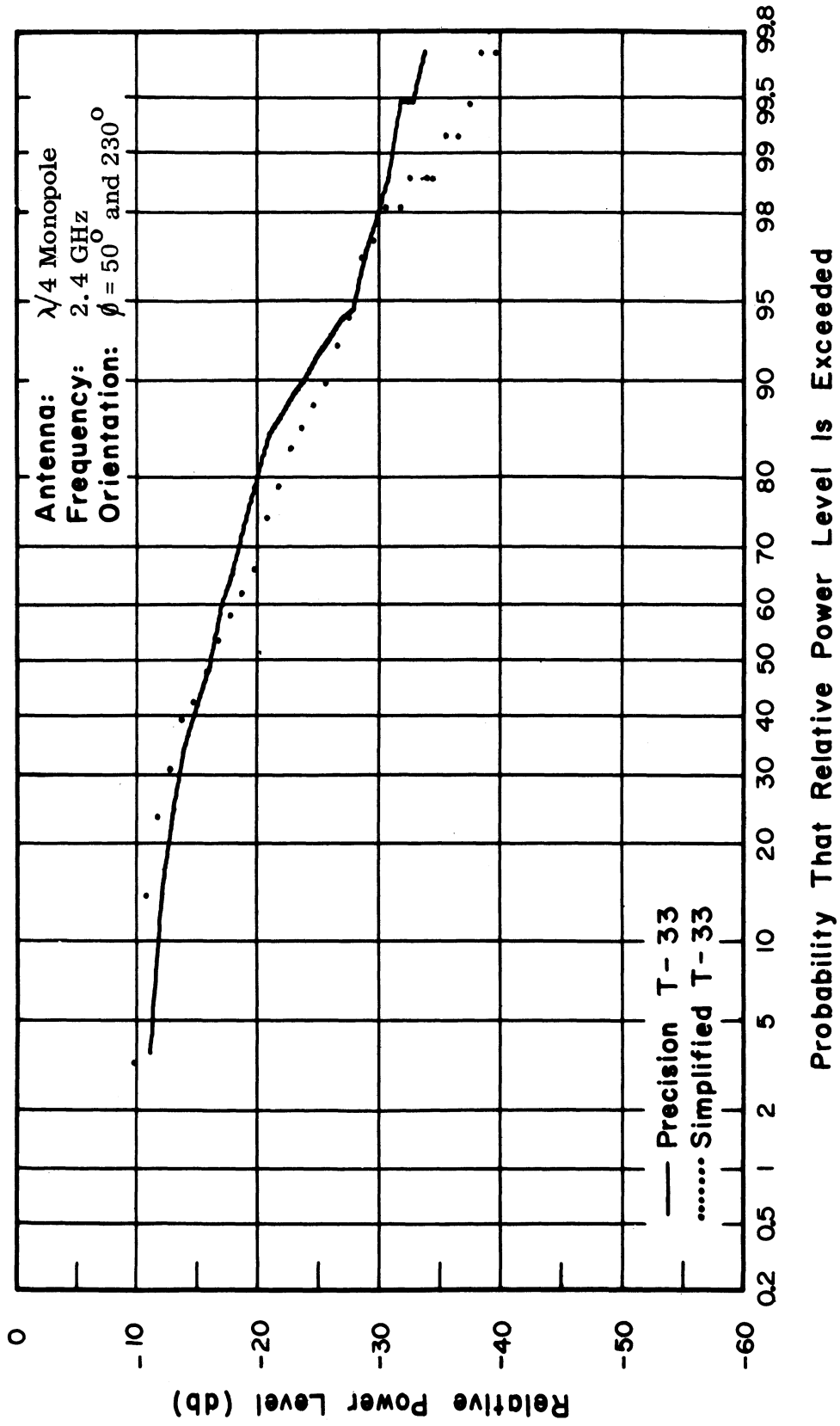

FIG. 59: CUMULATIVE GAIN DISTRIBUTIONS OF PRECISION AND SIMPLIFIED MODELS

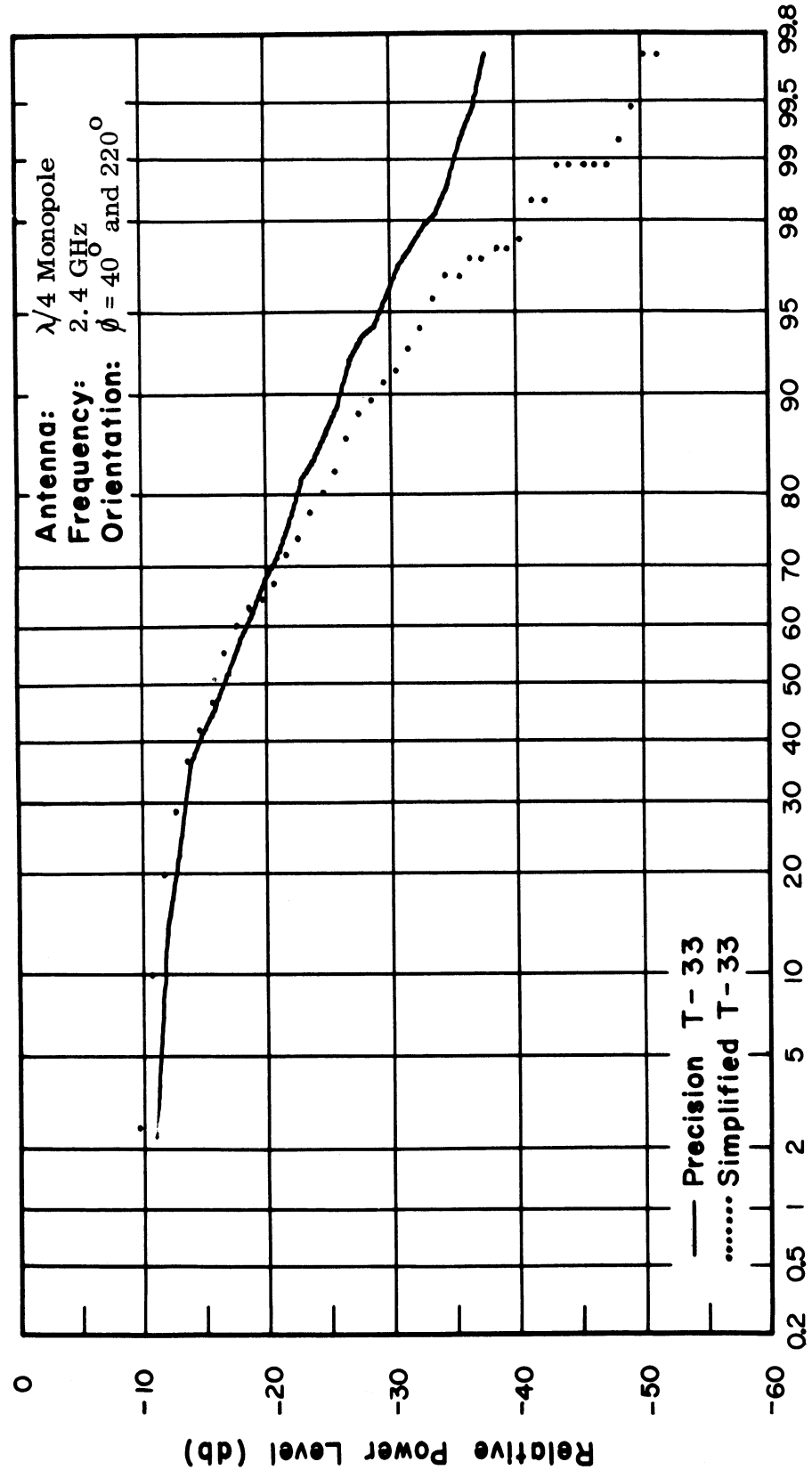

FIG. 60: CUMULATIVE GAIN DISTRIBUTIONS OF PRECISION AND SIMPLIFIED MODELS

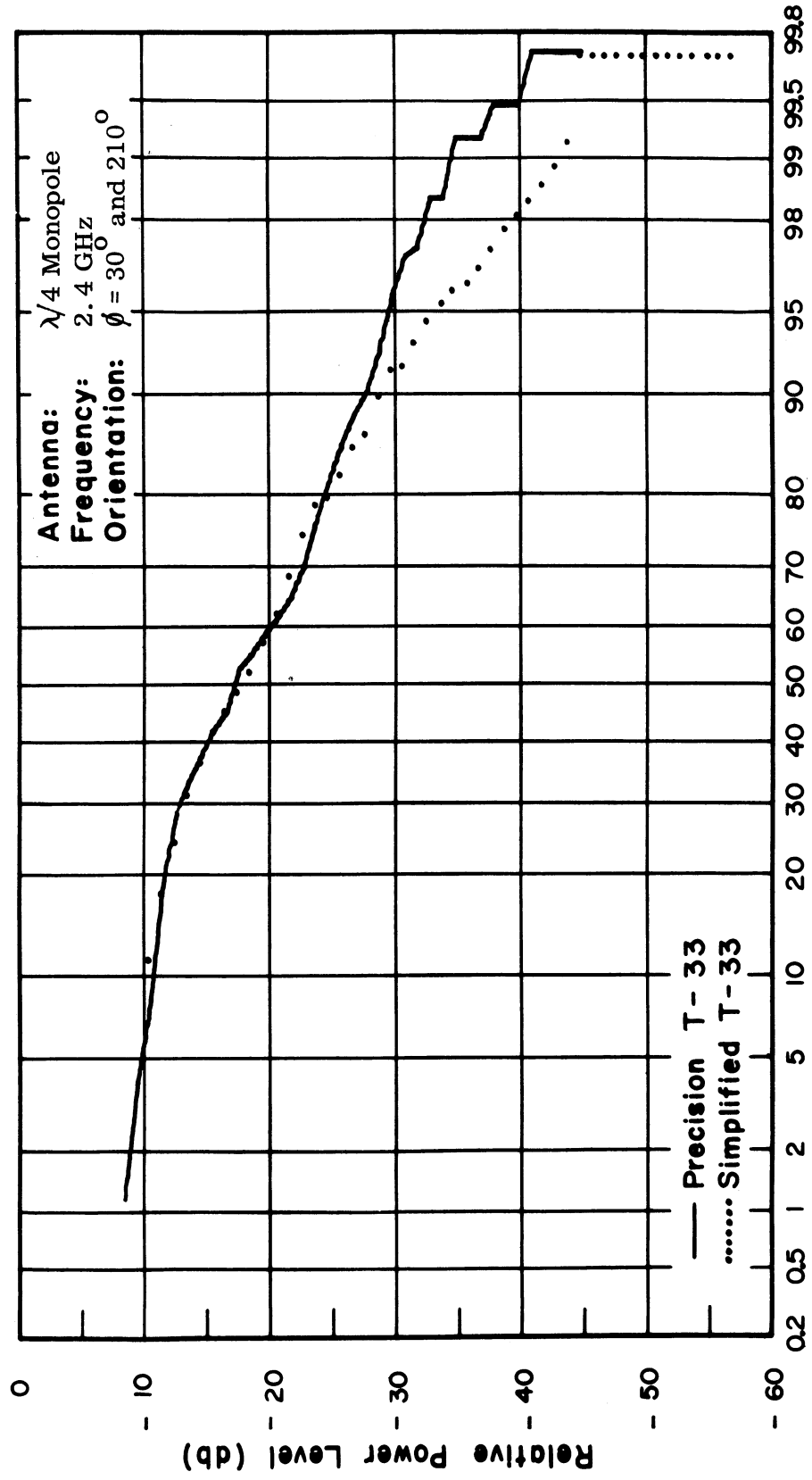

FIG. 61: CUMULATIVE GAIN DISTRIBUTIONS OF PRECISION AND SIMPLIFIED MODELS

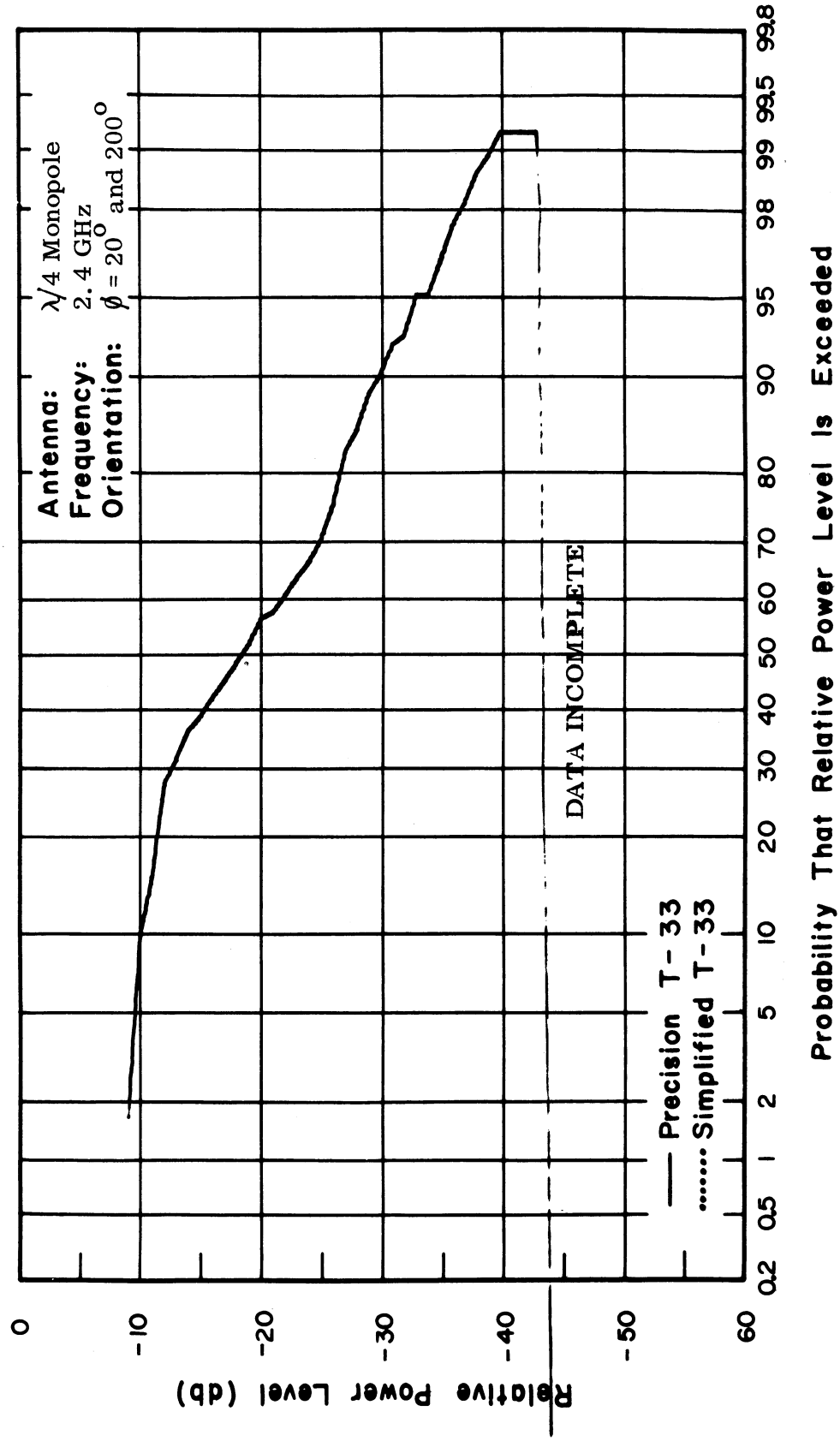

FIG. 62: CUMULATIVE GAIN DISTRIBUTIONS OF PRECISION AND SIMPLIFIED MODELS

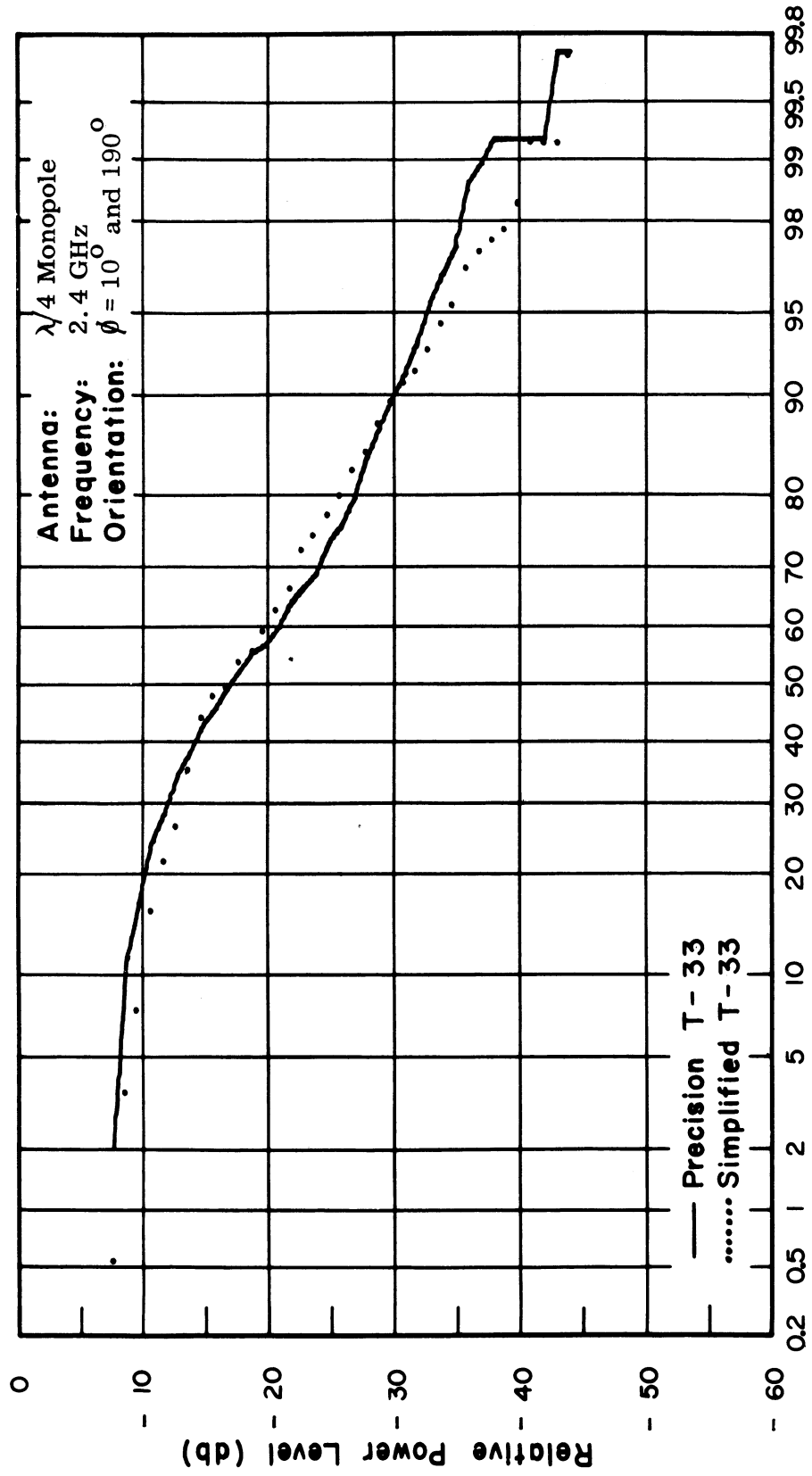

FIG. 63: CUMULATIVE GAIN DISTRIBUTIONS OF PRECISION AND SIMPLIFIED MODELS

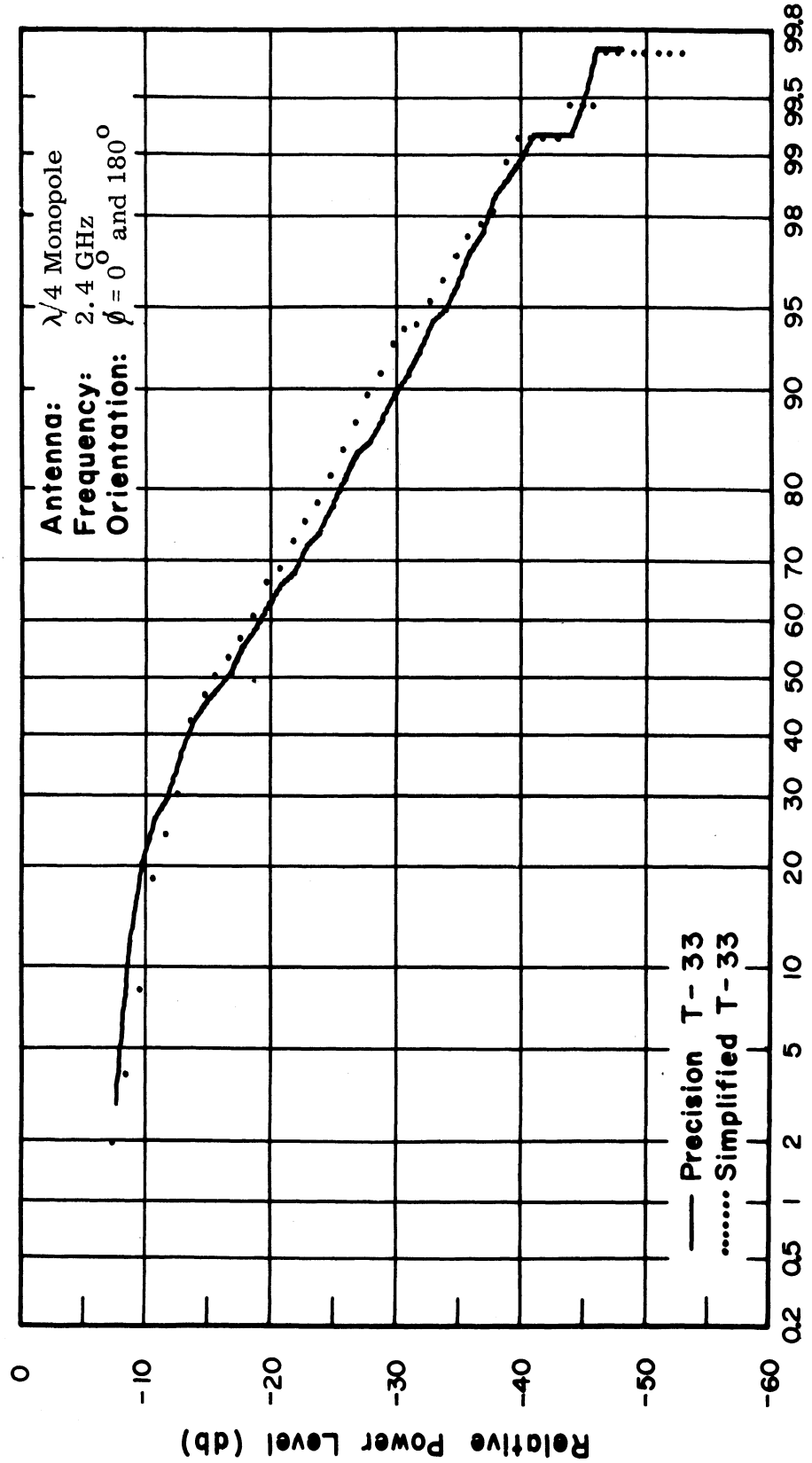

FIG. 64: CUMULATIVE GAIN DISTRIBUTIONS OF PRECISION AND SIMPLIFIED MODELS

2.4 Slot Antenna

The two previous antenna types discussed were an omnidirectional split-beam configuration. It is also of interest to examine a unilobe structure similar to antenna configurations used in the UHF frequency band for airborne systems. To simulate such an antenna, an open-ended section (Figs. 65-66) of waveguide was employed. This antenna was used to simulate typical antenna types that operate in the 1 GHz frequency range. Therefore, the scale frequency was 8.0 GHz. Signature data was collected at the fundamental and four harmonic frequencies to compare the simplified versus the precision modeling technique. The proper waveguide transitions were used between waveguide bands to minimize the probability of higher order modes being excited in the waveguide. A typical set of pattern data obtained at the fundamental through the fifth harmonic is shown in Figs. 67-76. There are some slight discrepancies in the patterns. However, good agreement is bound to occur in the statistical data shown in Figs. 77-81. It is to be noted that all data was collected using the U of M digital recording system to facilitate the reduction of the data into the proper format for final analysis.

2.5 Concluding Remarks to the Simplified Model

Three antenna configurations have been considered using the simplified modeling technique to obtain antenna spectrum signature data that can be forwarded to ECAC for further interference analysis purposes. Further, it will be noted that one simplified modeling configuration was employed during this study. In the event that more accurate statistical data is required, it is felt that the simplified modeling technique could be modified and still retain its simplicity and low-cost features. For example, in the case of the jet aircraft, one might consider the feasibility of modeling the nose region by a conic section that could easily be turned on a lathe. The fuselage might remain a cylinder and the tail section could be another conic section. The three parts could then be glued or pinned together. Also, extra care may be required in fitting of wings into the fuselage to minimize discontinuities. However,

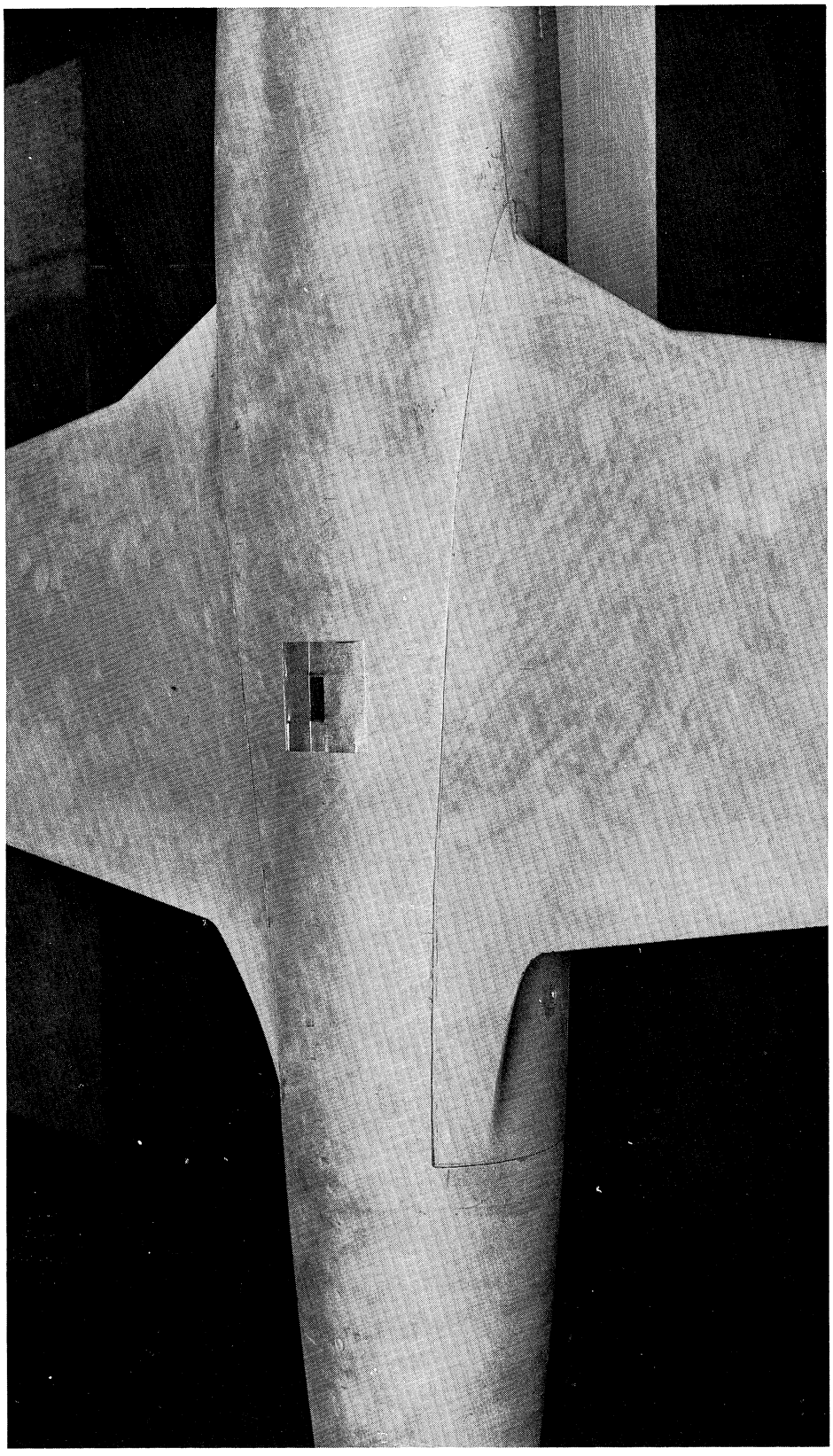

FIG. 65: SLOT ANTENNA ON PRECISION MODEL T-33

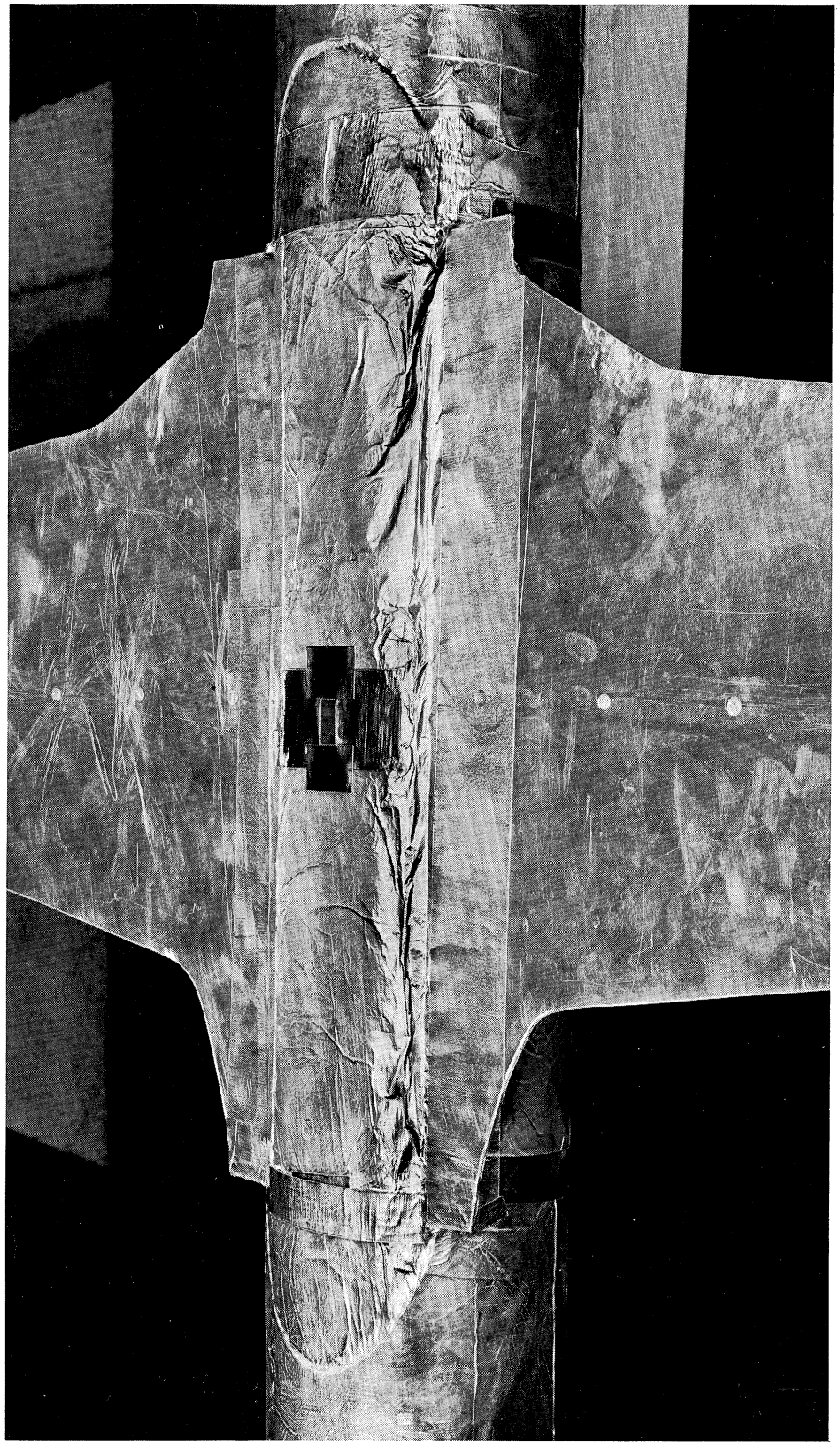

FIG. 66: SLOT ANTENNA ON SIMPLIFIED MODEL T-33

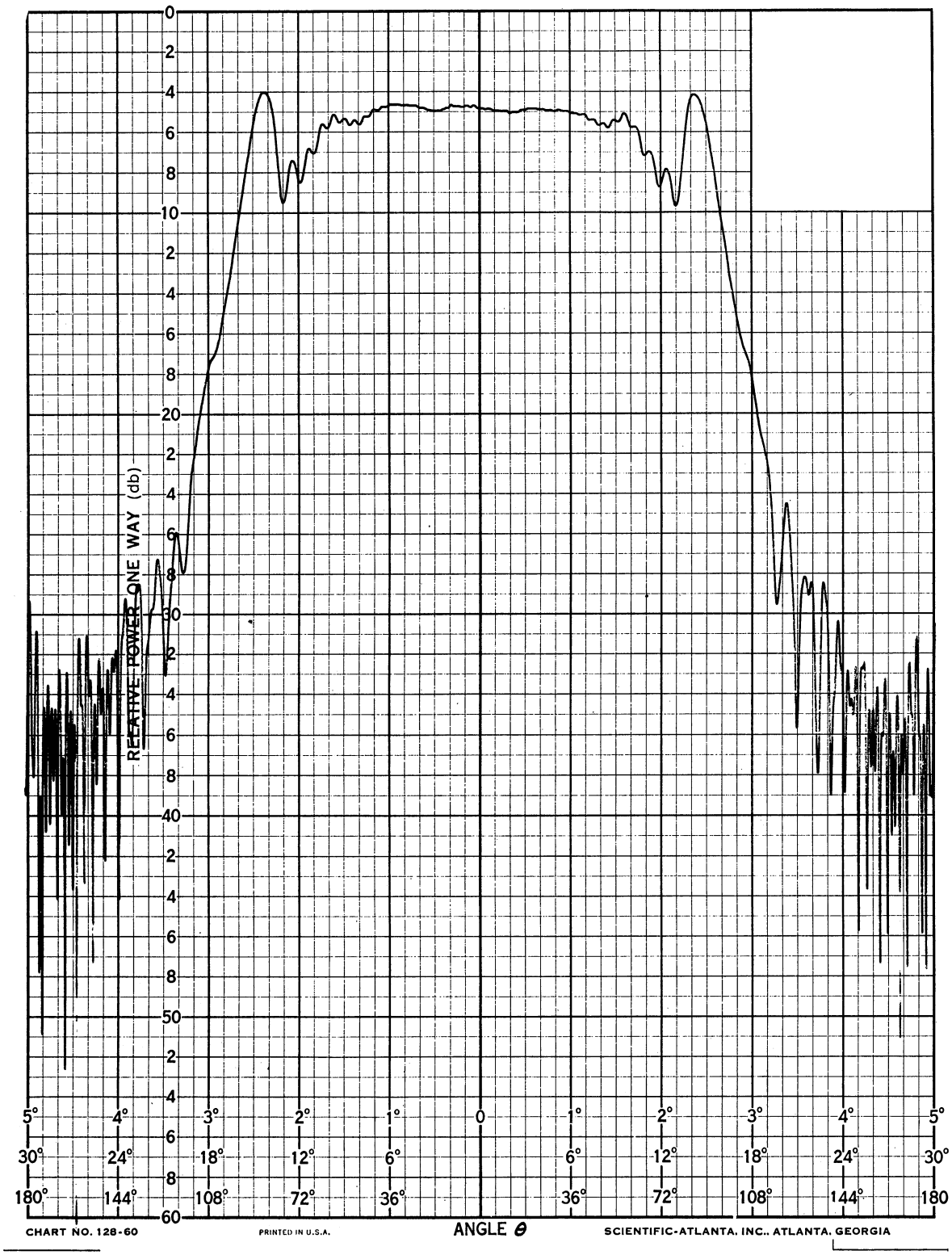

FIG. 67: X-BAND SLOT, 8.0 GHz, PRECISION T-33, $\phi = 90^{o}$ and 270^{o}

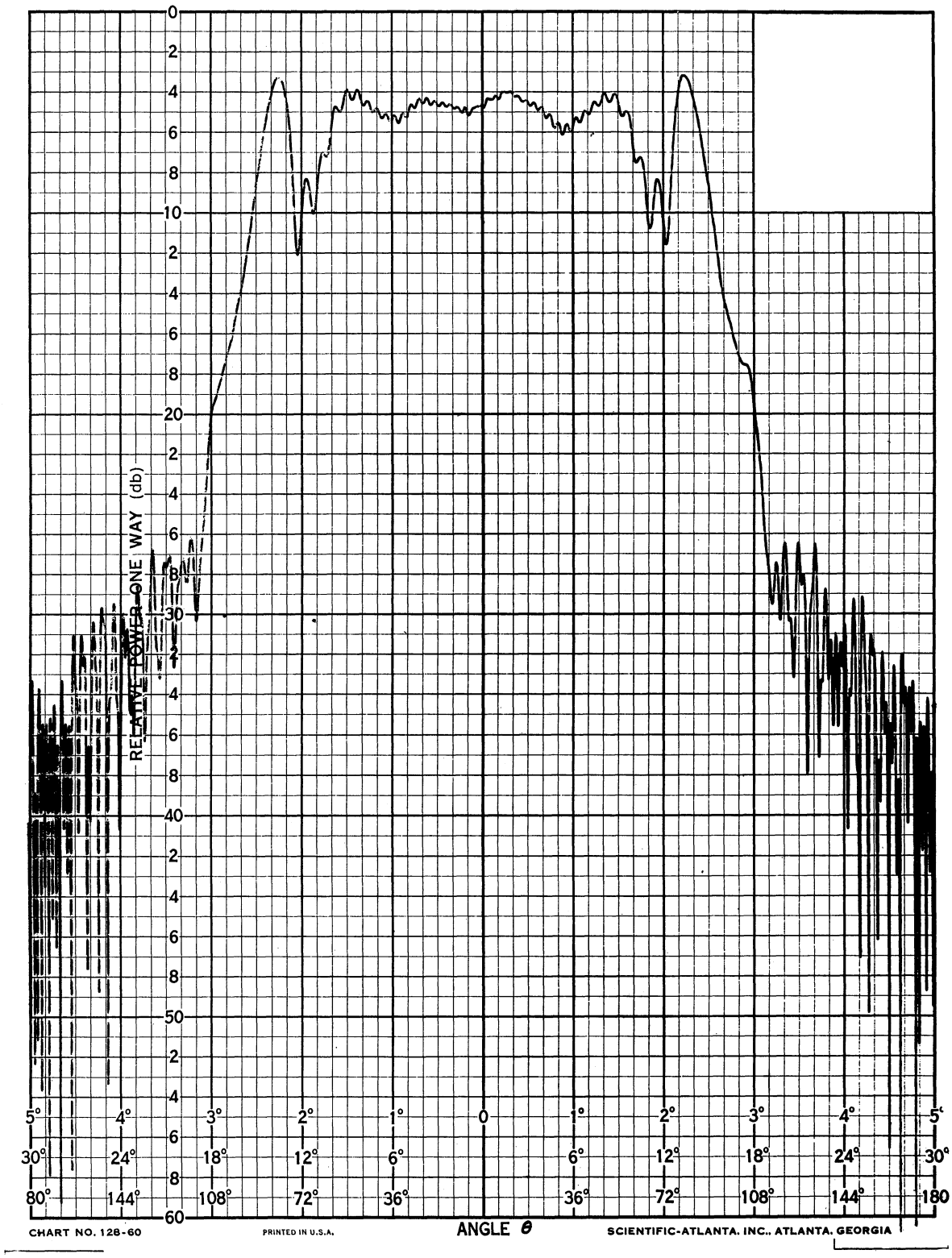

FIG. 68: X-BAND SLOT, 8.0 GHz, SIMPLIFIED T-33, $\phi = 90^{o}$ and 270^{o}

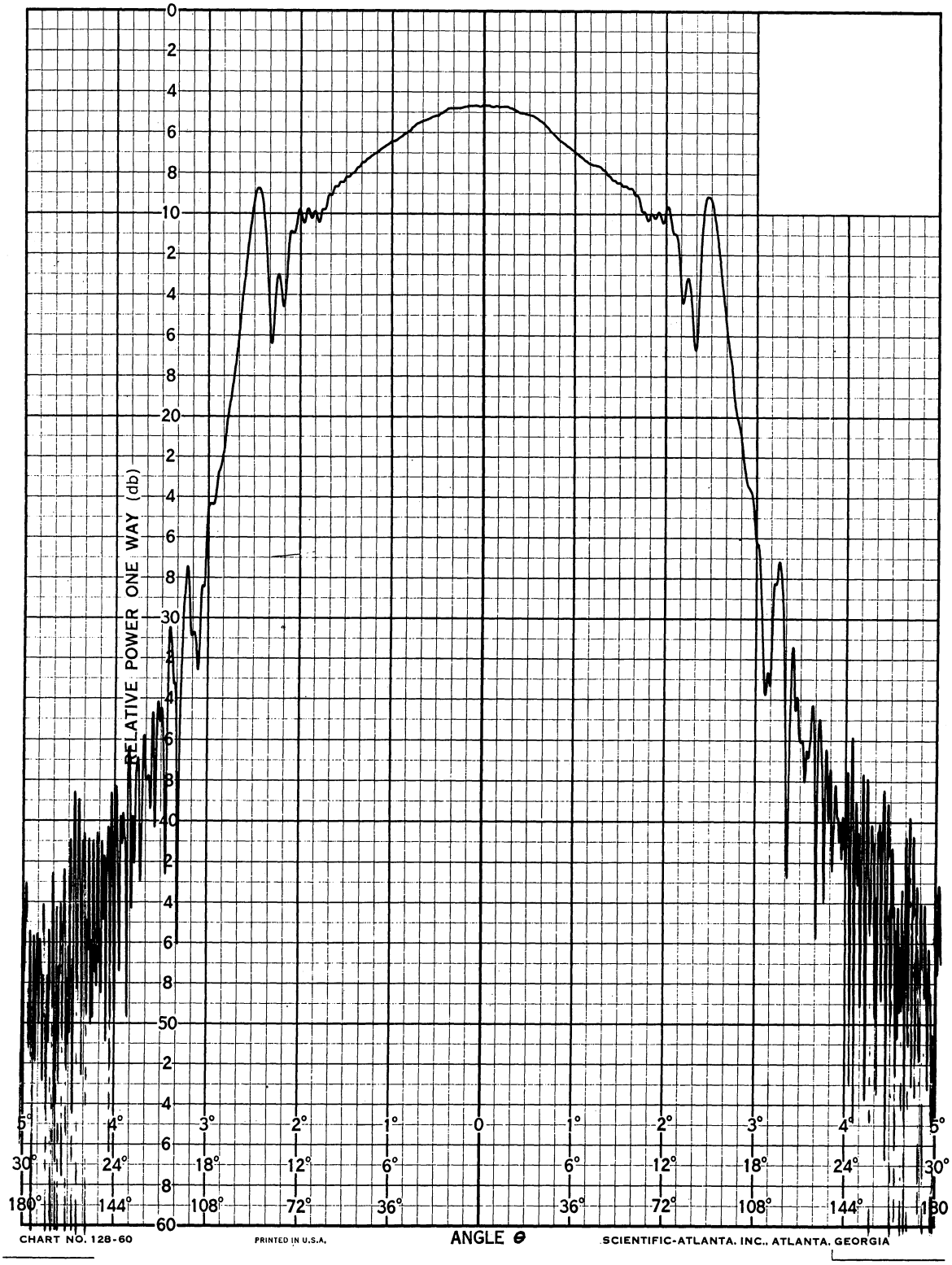

FIG. 69: X-BAND SLOT, 16.0 GHz, PRECISION T-33, $\phi = 90^{o}$ and 270^{o}

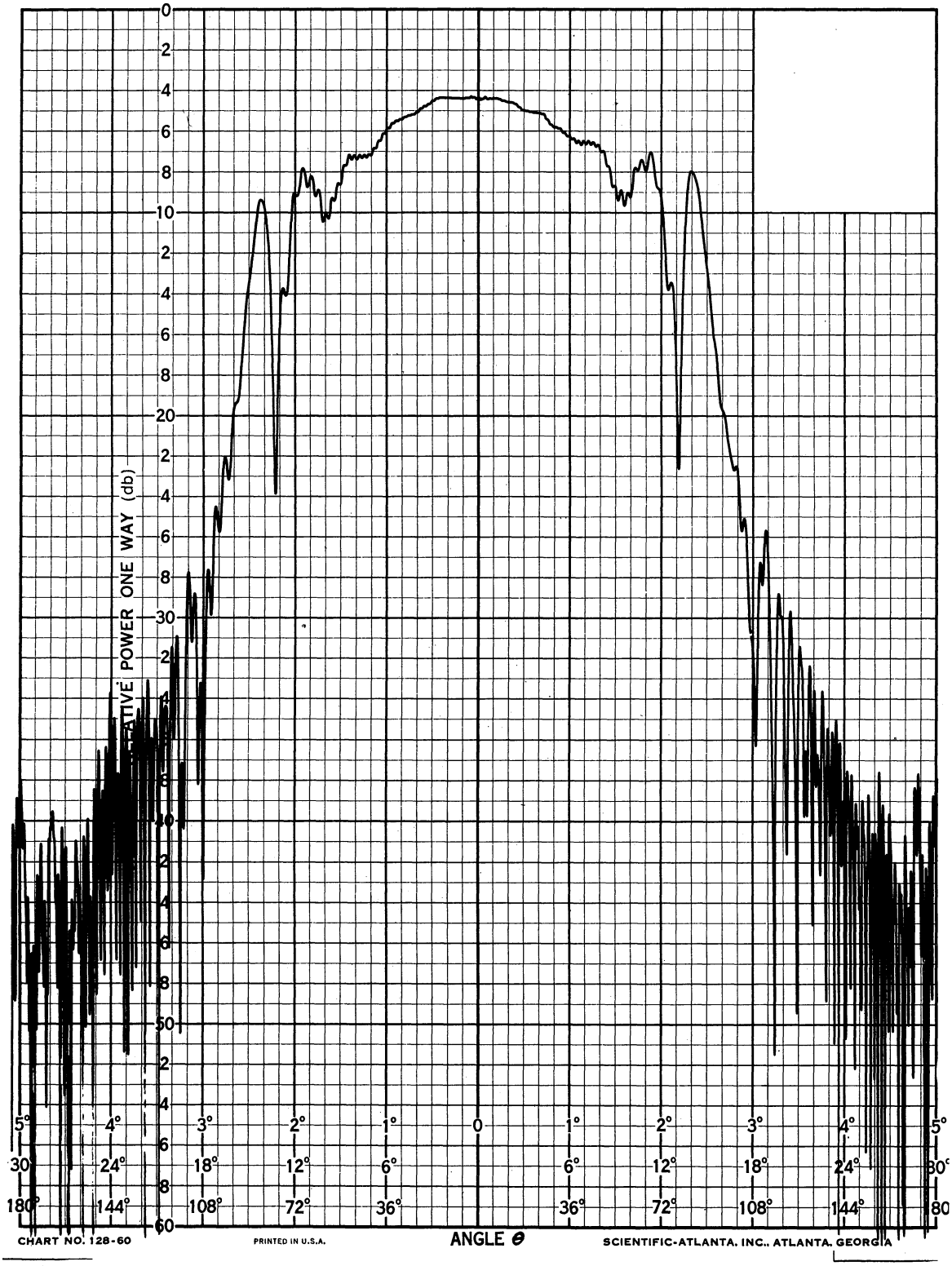

FIG. 70: X-BAND SLOT, 16.0 GHz, $\phi = 90^{o}$ and 270^{o},, SIMPLIFIED T-33

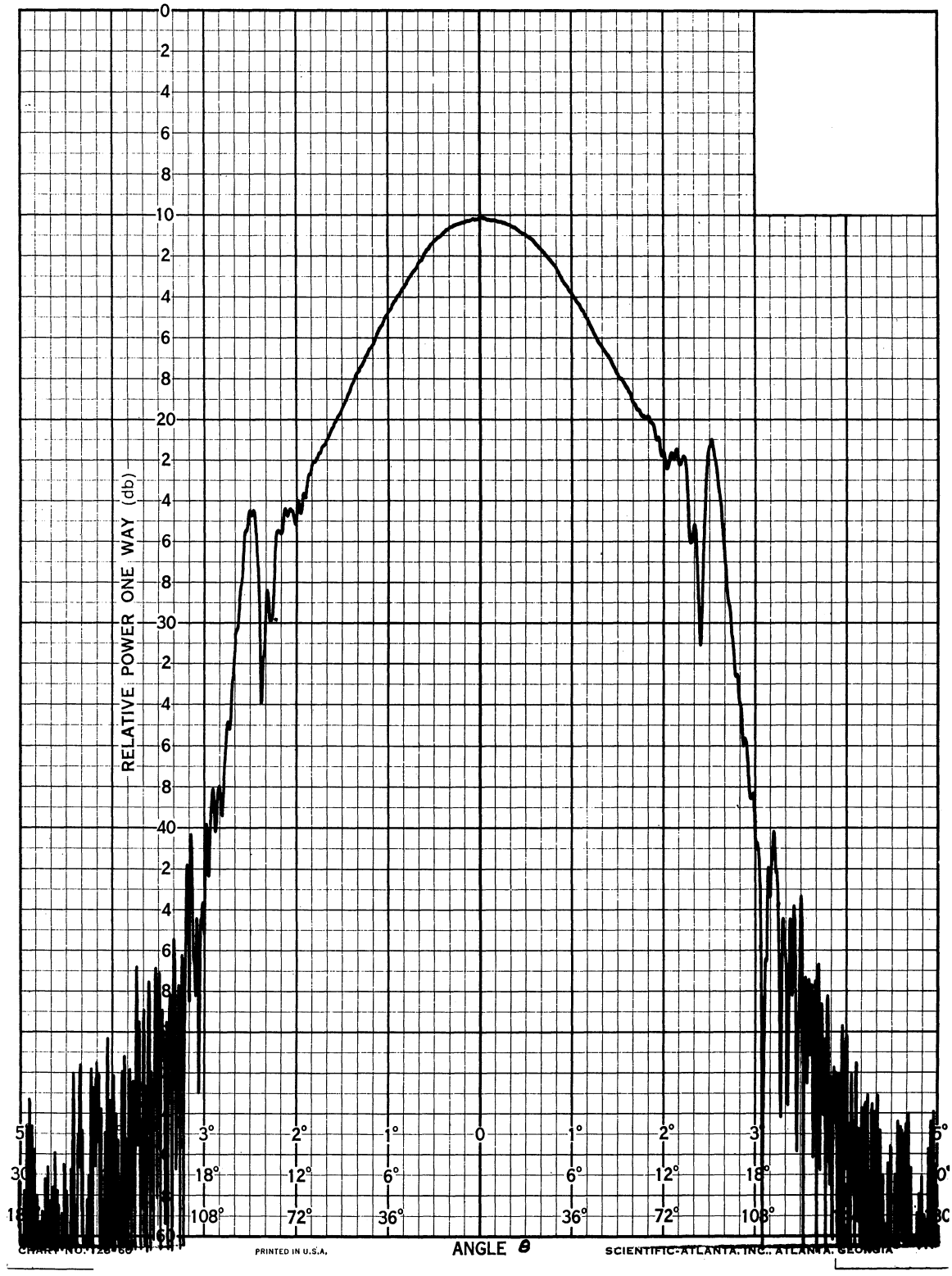

FIG. 71: X-BAND SLOT, 24. GHz, PRECISION T-33, $\phi = 90^{o}$ and 270^{o}

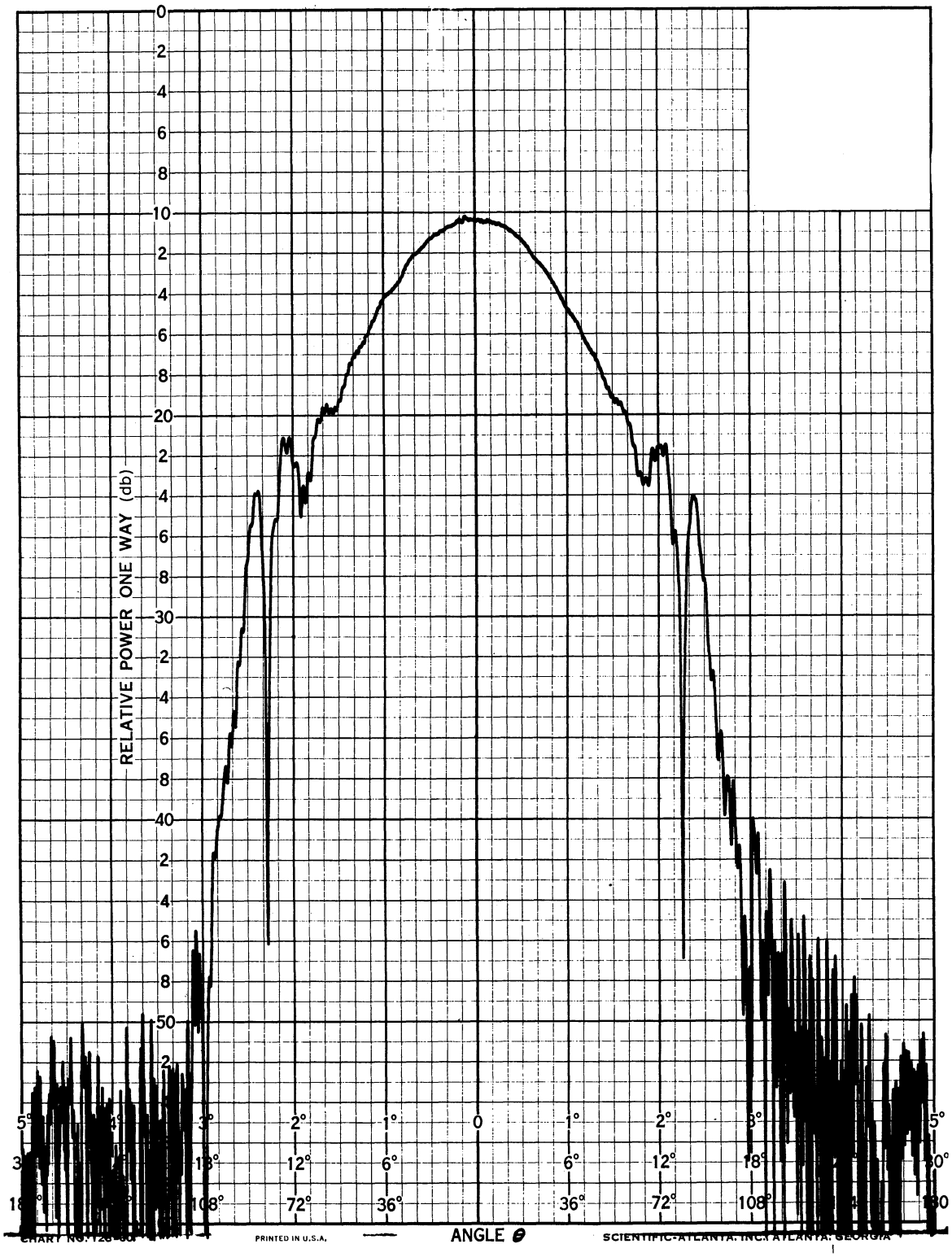

FIG. 72: X-BAND SLOT, 24.0 GHz, SIMPLIFIED T-33, $\phi = 90^{o}$ and 270^{o}

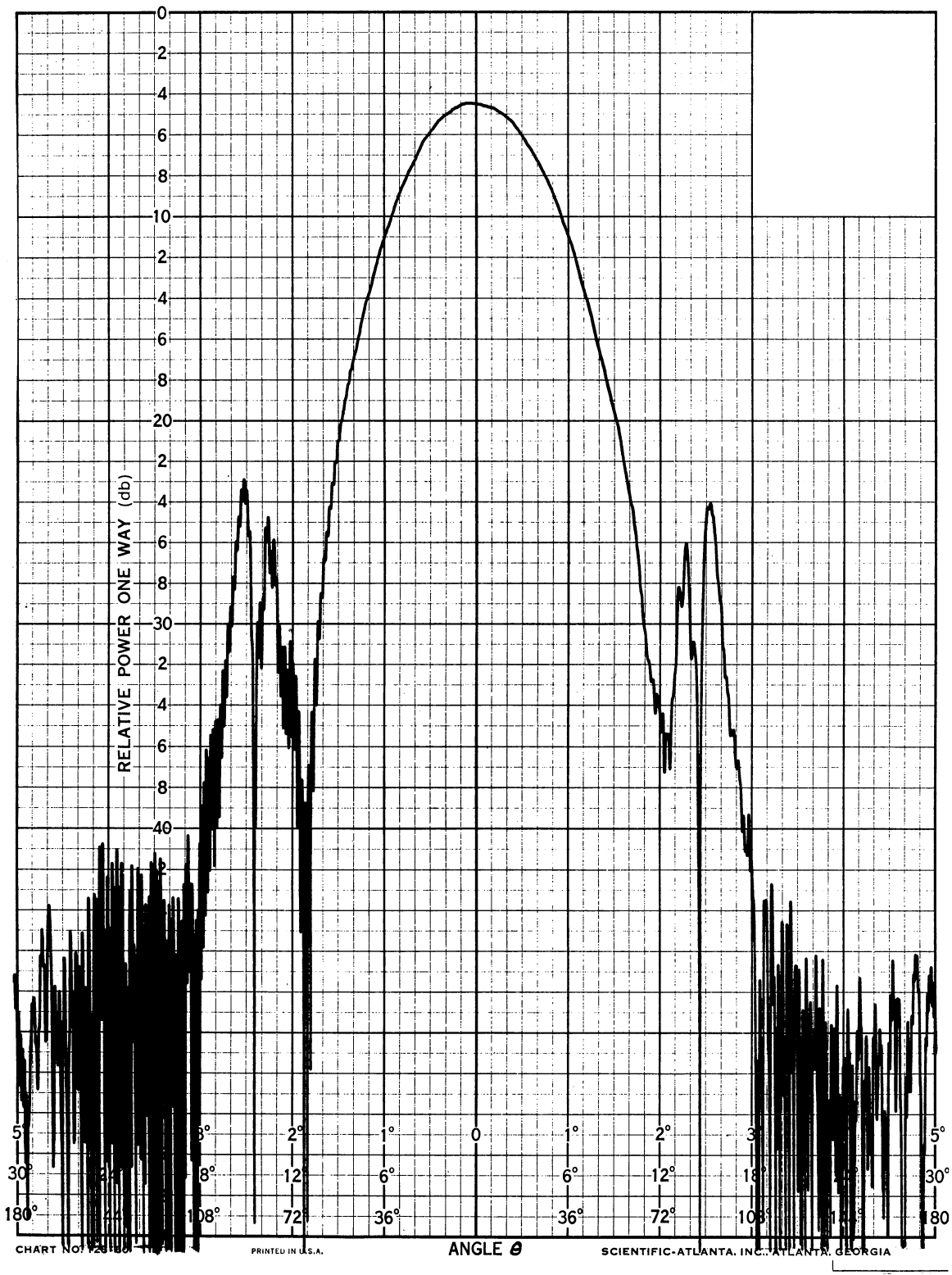

FIG. 73: X-BAND SLOT, 32.0 GHz, PRECISION T-33, $\phi = 90^{o}$ and 270^{o}

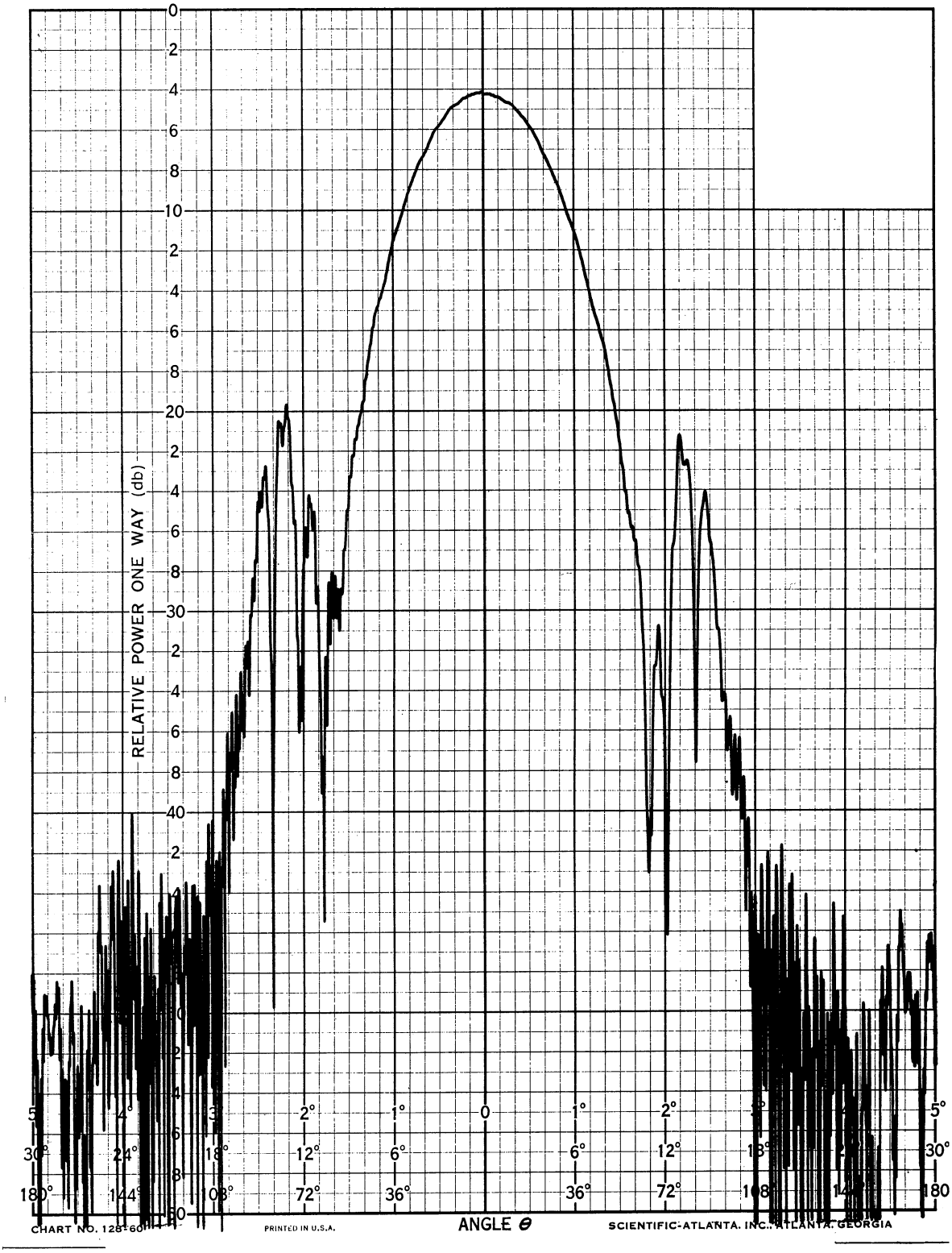

FIG. 74: X-BAND SLOT, 32.0 GHz, SIMPLIFIED T-33, $\phi = 90^{o}$ and 270^{o}

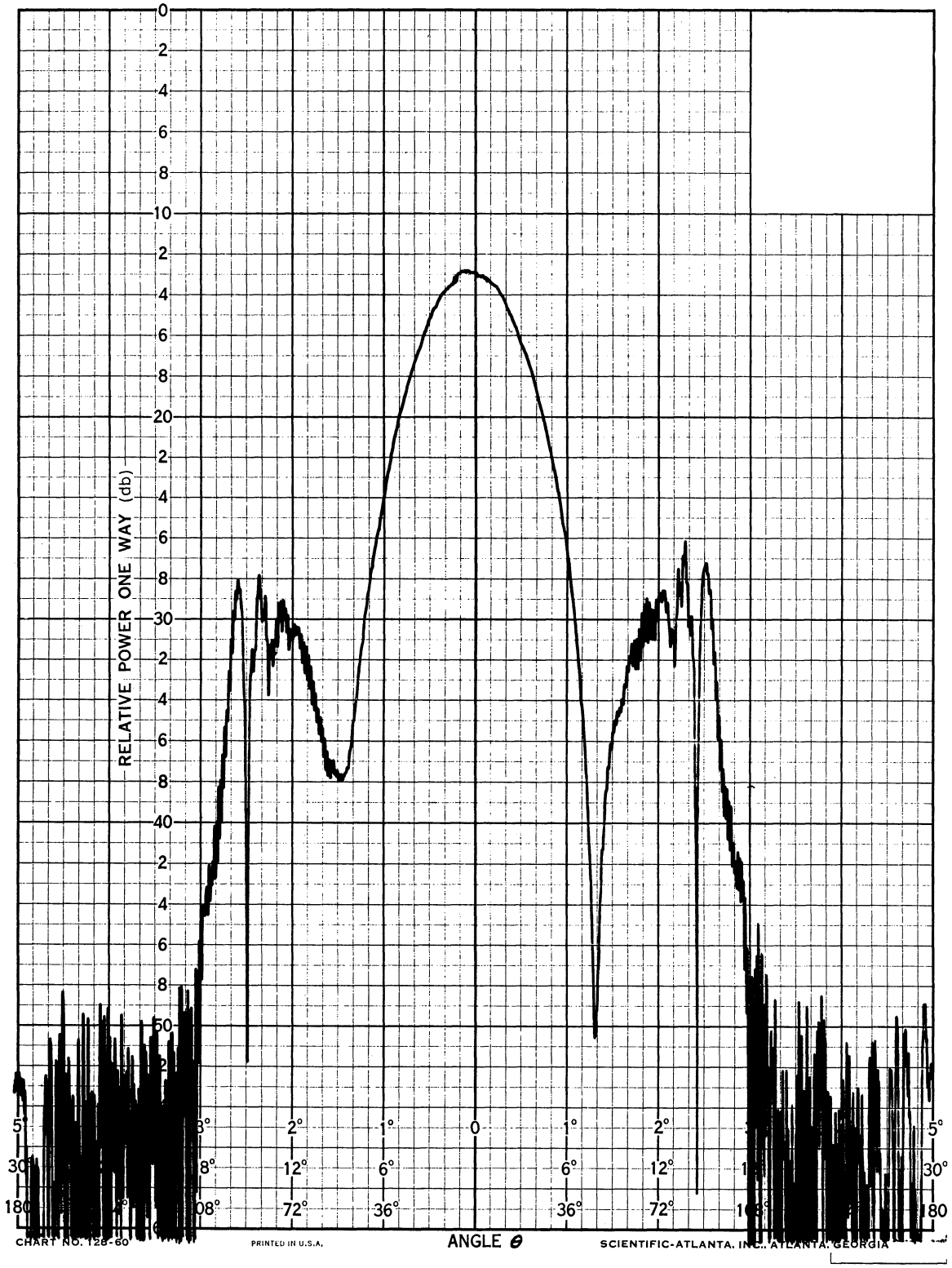

FIG. 75: X-BAND SLOT, 40.0 GHz, PRECISION T-33, ϕ = 90° and 270°

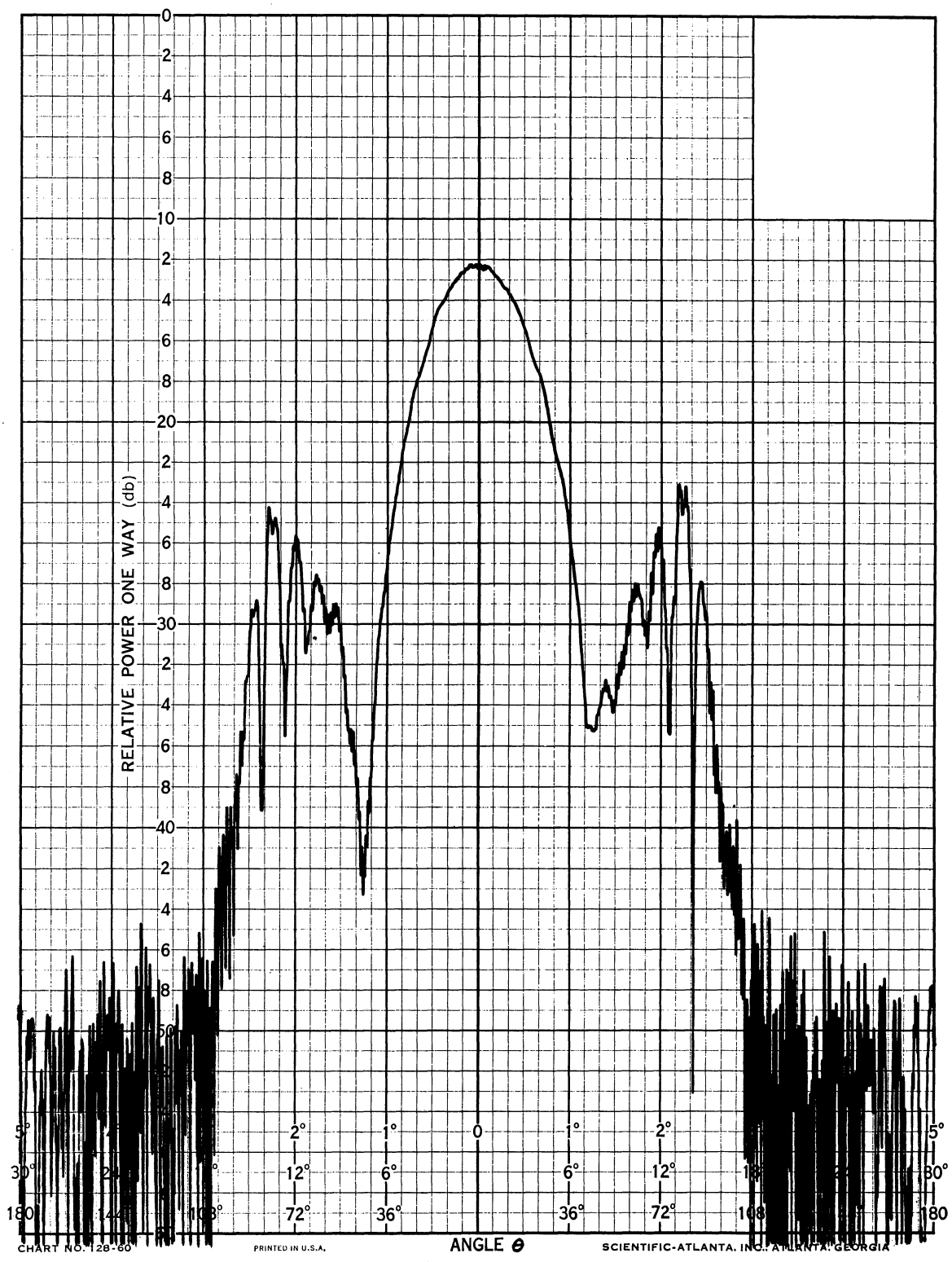

FIG. 76: X-BAND SLOT, 40.0 GHz, SIMPLIFIED T-33 $\phi = 90^{o}$ and 270^{o}

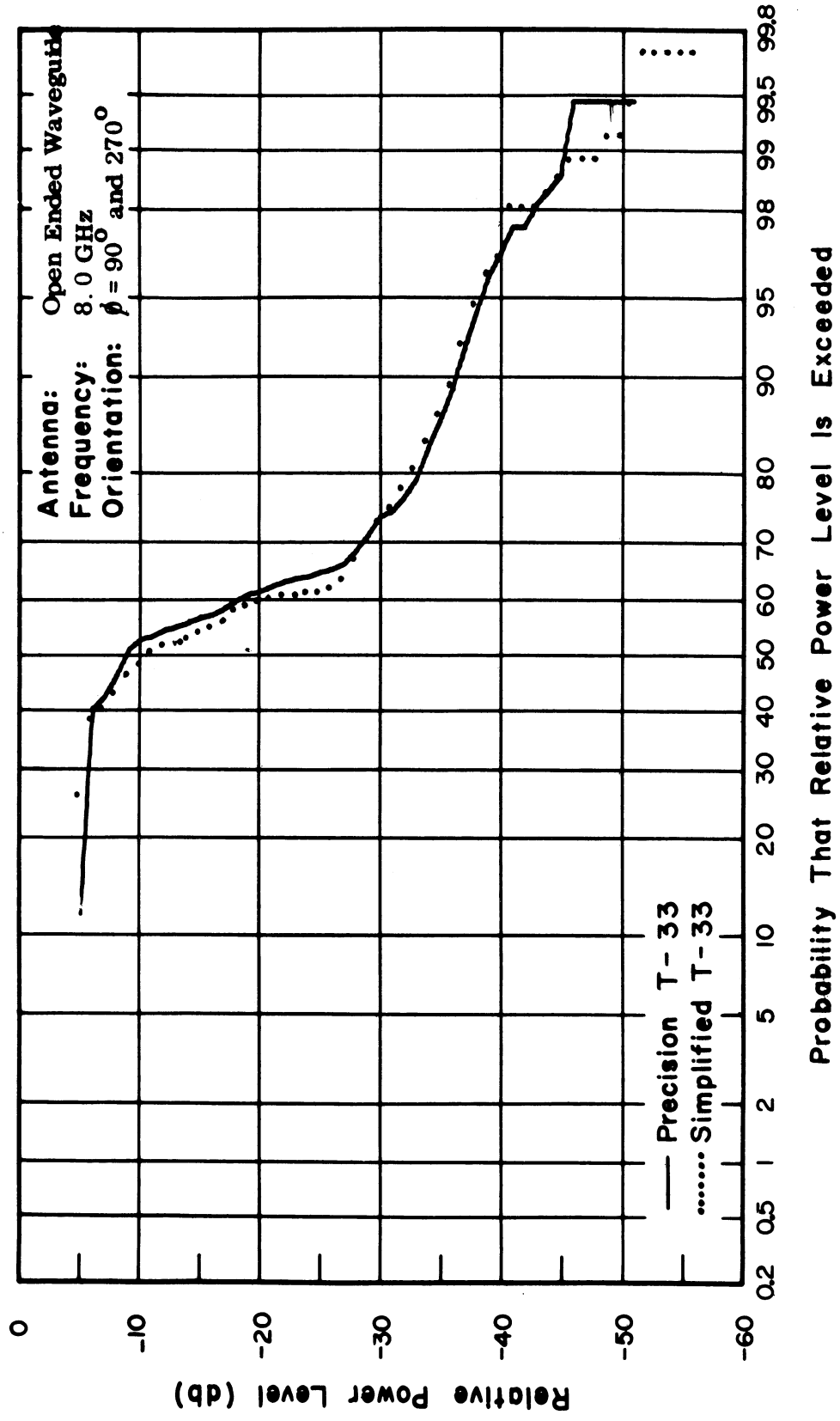

FIG. 77: CUMULATIVE GAIN DISTRIBUTIONS OF PRECISION AND SIMPLIFIED MODELS

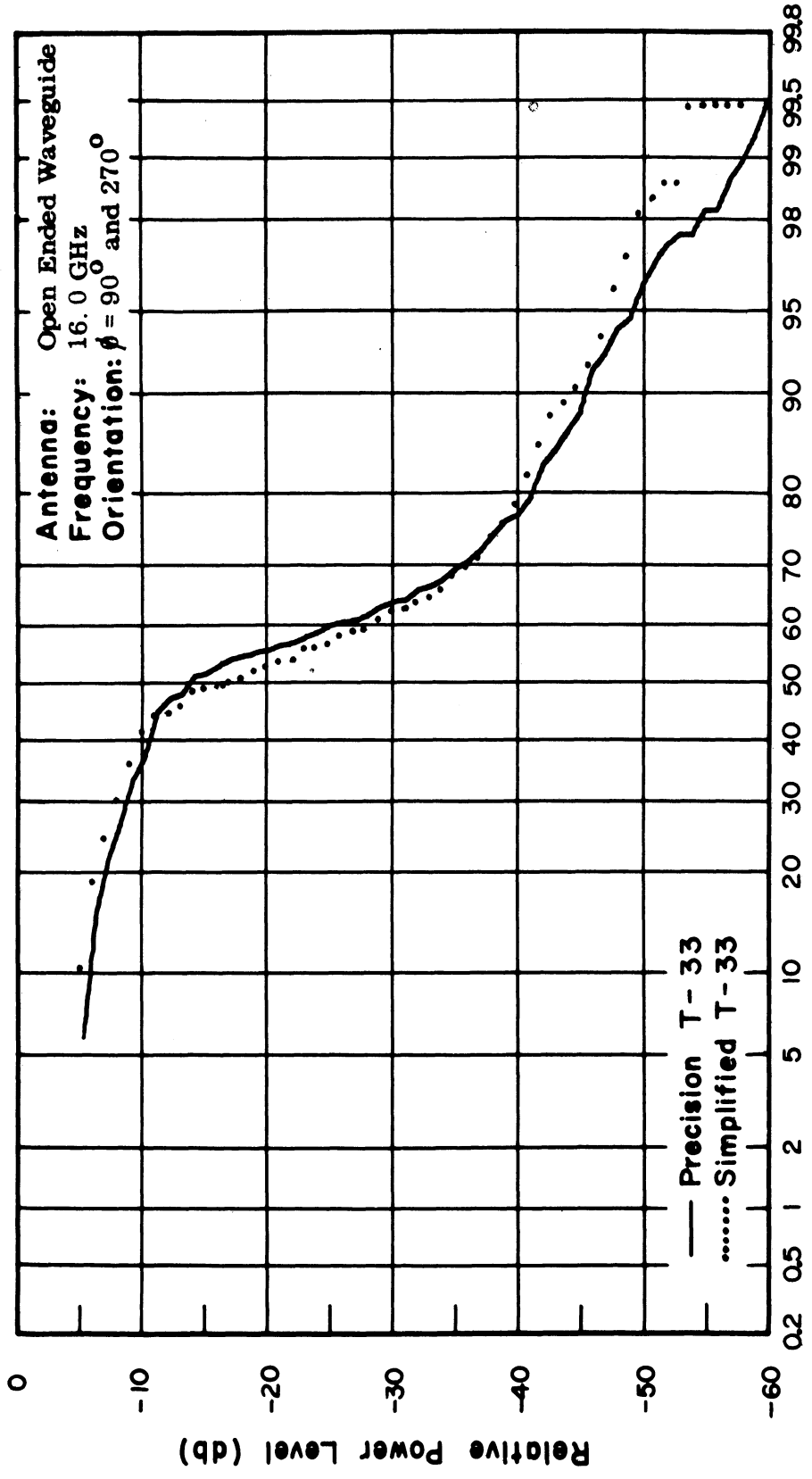

FIG. 78: CUMULATIVE GAIN DISTRIBUTIONS OF PRECISION AND SIMPLIFIED MODELS

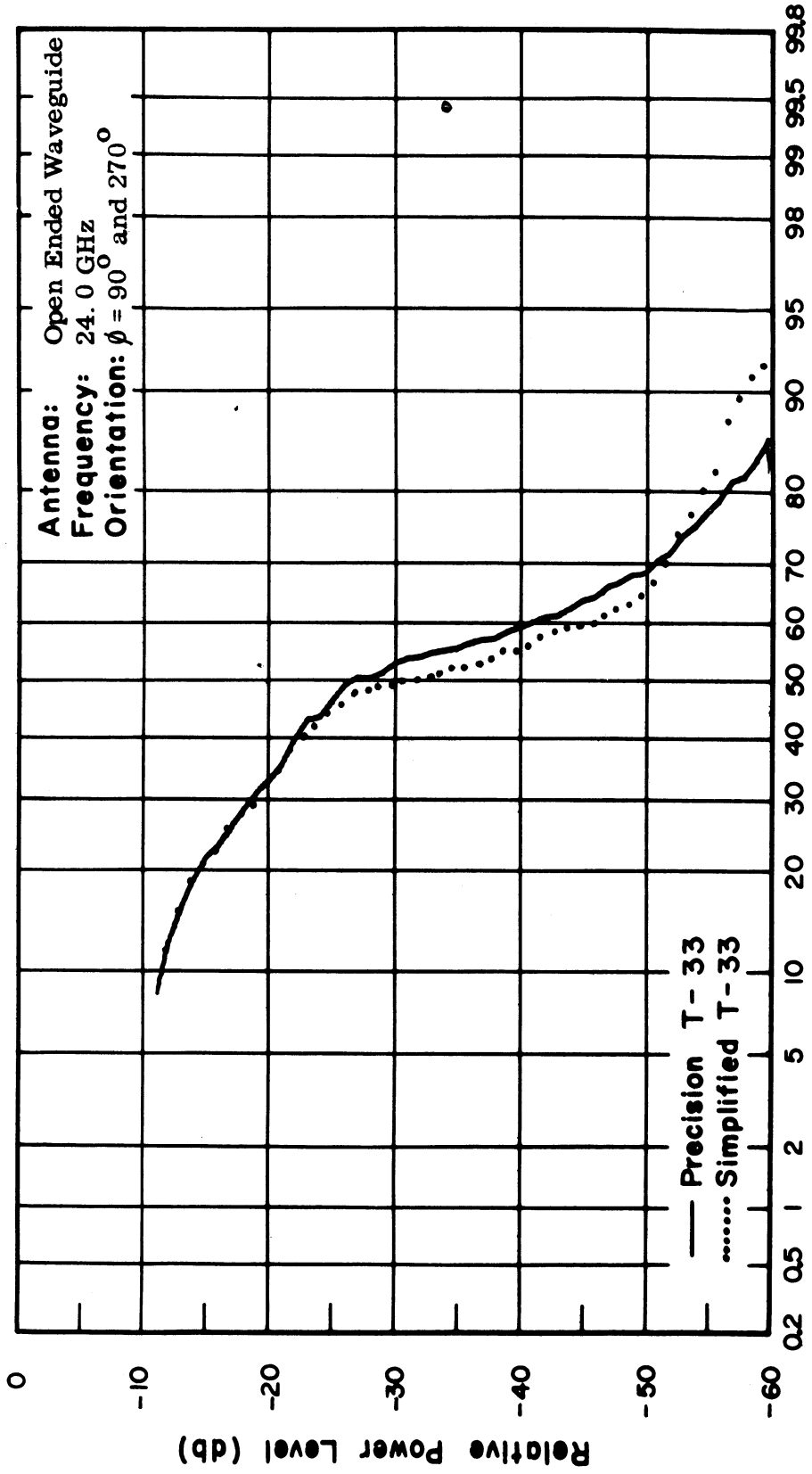

FIG. 79: CUMULATIVE GAIN DISTRIBUTIONS OF PRECISION AND SIMPLIFIED MODELS

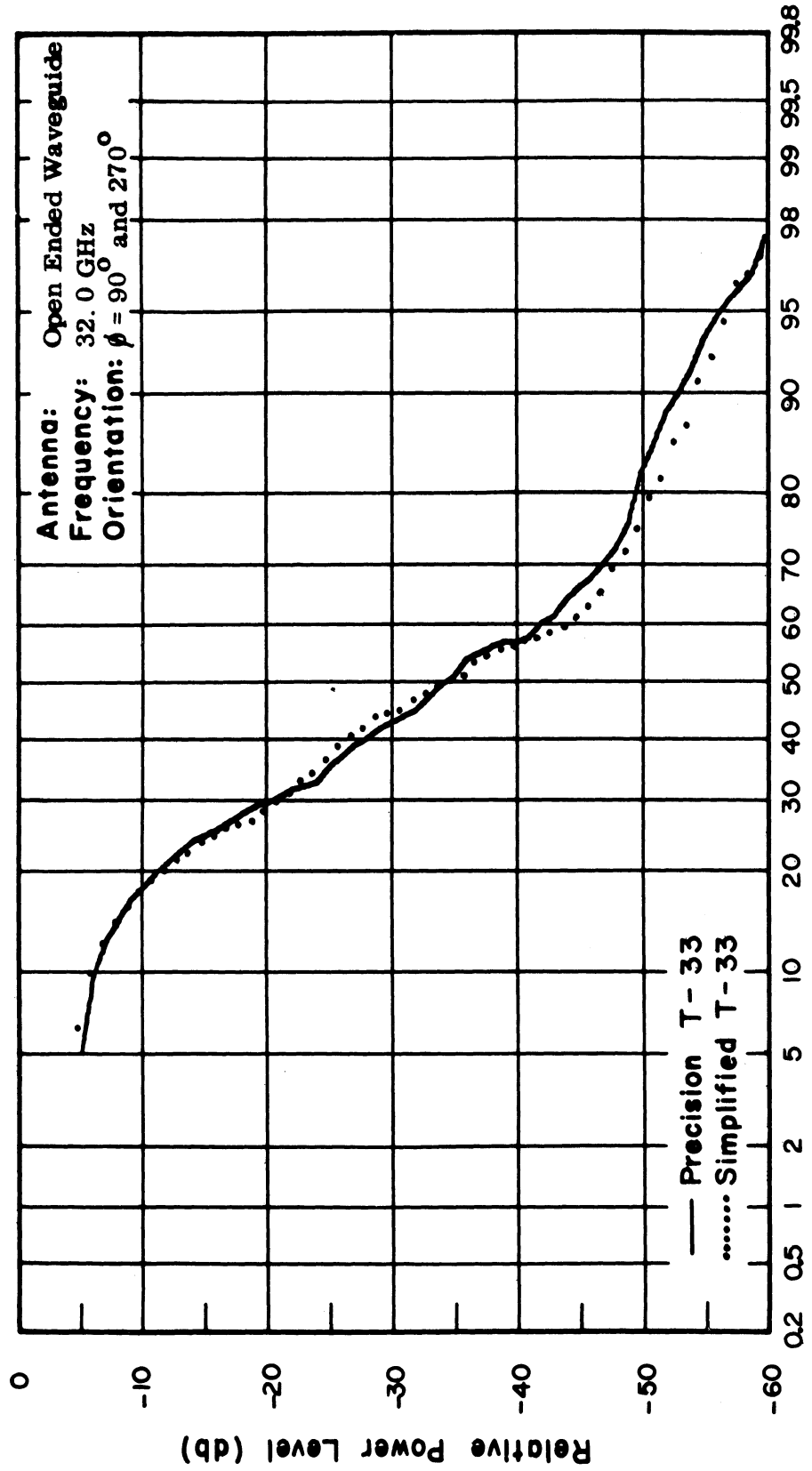

FIG. 80: CUMULATIVE GAIN DISTRIBUTIONS OF PRECISION AND SIMPLIFIED MODELS

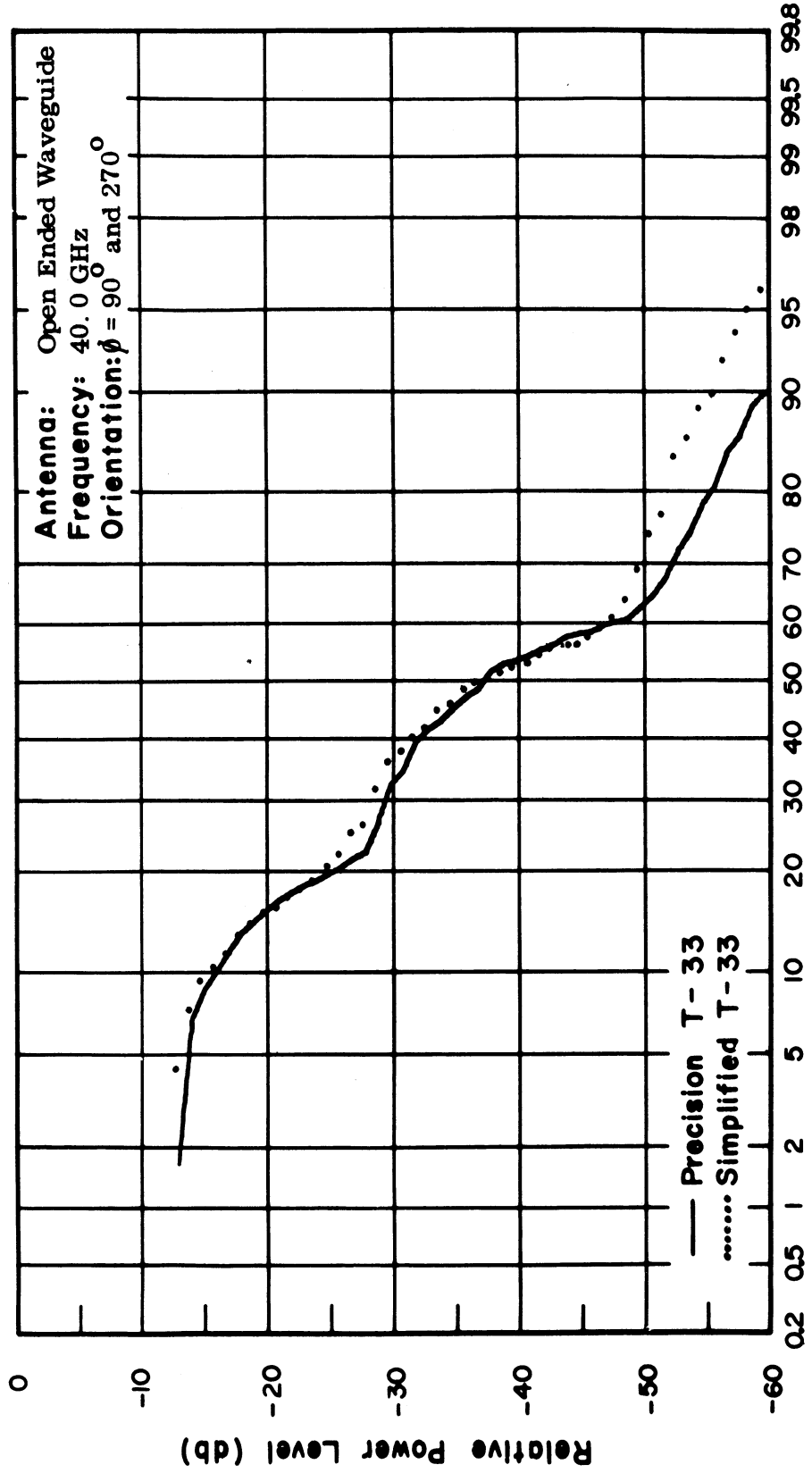

FIG. 81: CUMULATIVE GAIN DISTRIBUTIONS OF PRECISION AND SIMPLIFIED MODELS

the main purpose of this study has been to show that a relatively simple model may be used to obtain reasonably accurate signature data for interference prediction analysis. It is also feasible that further simplification of the modeling technique could be employed; e.g., rather than using surfaces of revolution, flat plane surfaces could be employed to simulate an aircraft. One such technique that has been suggested, but not investigated, is the possibility of modeling the fuselage of an aircraft with a plane surface having a silhouette outline of the fuselage.

As a result of this study, it is felt that the simplified modeling technique is justified for use in the collection of signature data for ECAC and that the next area of concern involves the techniques that may be employed to collect the data so that it can be properly transferred and stored by ECAC.

III
DATA RECORDING TECHNIQUES

A second aspect of the present contract has been an investigation of data handling techniques and procedures presenting the data obtained by the Air Force or other services to ECAC. To ensure that recommendations resulting from the techniques and procedures developed by The University of Michigan are compatible with both ECAC and the Air Force, close liaison has been maintained with these organizations.

During this study the following digital techniques were considered: 1) manual, 2) semi-automatic, and 3) automatic. In addition to investigating recording techniques, consideration has been given to the form in which the data should be collected. Therefore, a data format that has been discussed with both ECAC and the Air Force is presented as a part of this report.

3.1 ECAC Data Format

During discussions with ECAC personnel, it was learned that pattern data in the form of number-pairs is preferred. The desired number-pair consists of the antenna gain value and the associated angle (azimuth or elevation) for a given data point. Personnel of ECAC have found that it is less complicated to write the various programs required for interference predictions with the antenna pattern data in the number-pair format. This format relieves the interference program of the burden of having to search the input data to match a given gain value with its correct angle in the event data is accidentally placed in the computer in the wrong sequence. Further, if a single data format is adhered to by the Air Force and other military organizations, only one computer program will be required at ECAC to reduce antenna pattern data for statistical analysis. Therefore, costs and time will be minimized in the prediction of interference.

The medium by which data is to be stored at ECAC is IBM cards rather than magnetic tapes since cards are less susceptible to deterioration or damage. It is recommended that the antenna gain value be represented by four digits, thus enabling an amplitude to be recorded to a one-half db increment, typical of microwave measurement accuracy. It is also suggested that the angle associated with the antenna gain be represented by four digits allowing an increment of 0.5^{o} to be recorded. The one-half degree increment will enable agencies to measure high-gain, narrow-beam antennas.

Following the above format, a card will consist of nine data points and an identification code. Basically, the data will be arranged on the card as follows: nine data points will be placed on each card consuming 72 columns, and the remaining 8 columns will be used for the identification code. A total of 80 cards will be required for each antenna pattern. In addition to the data cards, it will be necessary for each set forwarded to ECAC to be accompanied with a data sheet describing the card content, i.e. antenna model, type, etc. This sheet could very well be a punched card.

3.2 Manual Digitalizing Technique

The manual procedure consists of employing an individual to examine the analog plot of the antenna pattern and record on a suitable data sheet the antenna gain, relative to the pattern maximum, at discrete angular increments. In the event the pattern is a side angle pattern configuration (half-power beamwidth $> 5^{o}$), data is recorded at 1^{o} increments for the full 360^{o} of the pattern. In those cases where the pattern has a narrow beam (half-power beamwidth $< 5^{o}$), data is recorded in increments of 0.5^{o}. The relative gain is recorded to the nearest one-half db. After the pattern data has been recorded, the data sheet is forwarded to a card punch operator, who punches both the angular position and the relative gain onto an IBM card. These cards can then be forwarded to ECAC to become a part of their data base files.

The principal disadvantage of the manual technique is the probability of human error occurring in the recording of the data. A further disadvantage is that the process is time consuming and costly.

3.3 Semi-Automatic Digitalizing Technique

A semi-automatic procedure has been considered that requires manual sampling of an analog antenna pattern. An operator manipulates a pair of cursors on a machine on which pattern data is placed. The machine is manually directed to sample the analog waveform at any selected point and supply only the magnitude of the sample value to an analog-to-digital converter unit (no provision is made to include angle information). The converter unit digitalizes the data and feeds a card punch unit which automatically punches the data onto cards (thus negating the need for one operator). Figure 82 shows the equipment used in this procedure. The analog-to-digital converter unit is seen at the left in the photo. The sampling machine "Oscar" is shown in the center and the card punch unit on the right.

This semi-automatic procedure has several drawbacks not found in the completely automatic system to be described in the following section. First, it is doubtful that it is feasible to use this system to punch the digitalized data onto IBM cards in the format suggested above, as no angle data is available. Second, the analog waveform must be sampled manually by an operator. Our investigation has shown that when the equipment is operated by an individual unfamiliar with antenna problems, there is a high probability of errors appearing in the final data. These errors are usually difficult to locate and costly to correct. Third, the curve sampling procedure is tiring to an operator's eyes and this also increases the probability of errors in the data.

We have investigated the use of untrained personnel (such as may be employed if the data were sent to a commercial facility) and also antenna trained personnel to reduce analog data into digital form using the above semi-automatic procedure. The

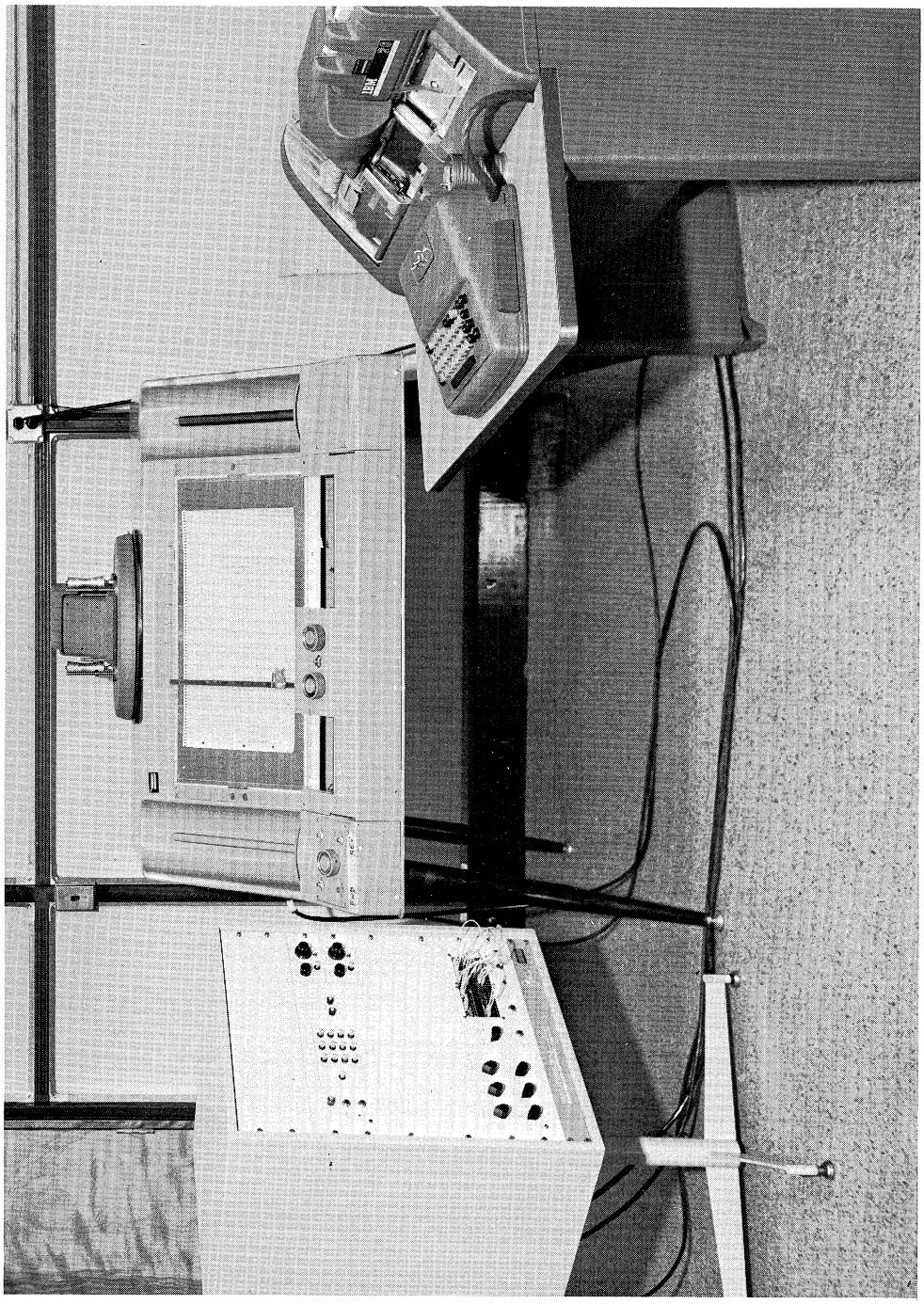

FIG. 82: SEMI-AUTOMATIC DIGITAL RECORDING EQUIPMENT

errors introduced into the data by the operator were found to be much higher when using untrained personnel. Because of these problems it is recommended that the semi-automatic procedure be avoided if at all possible and in lieu of it employ the automatic procedure discussed next.

3.4 Automatic Digitalizing Technique

An automatic digital recording technique has been developed by The University of Michigan. Figure 83 is a block diagram of that system. A high-gain receiver is employed to measure the antenna radiation characteristics and an antenna pattern recorder plots the characteristics in analog form on standard chart paper. Simultaneously, the analog waveform is sampled at 1^{o} intervals (for 360^{o} coverage) by an analog-to-digital converter and the magnitude of the sampled values are recorded on a general purpose tape recorder in the form of binary coded numbers. Figure 84 shows the wide-range high-gain receiving system which incorporates the analog recorder and the analog-to-digital converter. Figure 85 is a close-up view of the U of M analog-to-digital converter. The basic operation of the analog to digital converter is discussed in Supplement I (Dute et al 1966). Figure 86 shows the general purpose tape recorder which places the digital data on quarter-inch magnetic tape. Upon completion of the antenna measurements the general purpose tape recorder is transferred to another analog-to-digital converter facility. Here the quarter-inch magnetic tape is played back into a converter unit which transfers the data onto half-inch magnetic tape in a format which is compatible with the U of M IBM 7090 computer. The equipment used to effect the data transfer is shown in Fig. 87.

The antenna data now on tape is subsequently transferred to the punch card form by employing IBM processing equipment. A computer program, which is required to direct the processing, is read into an IBM 1401 processing unit along with the antenna data on magnetic tape. The digital data is processed and automatically

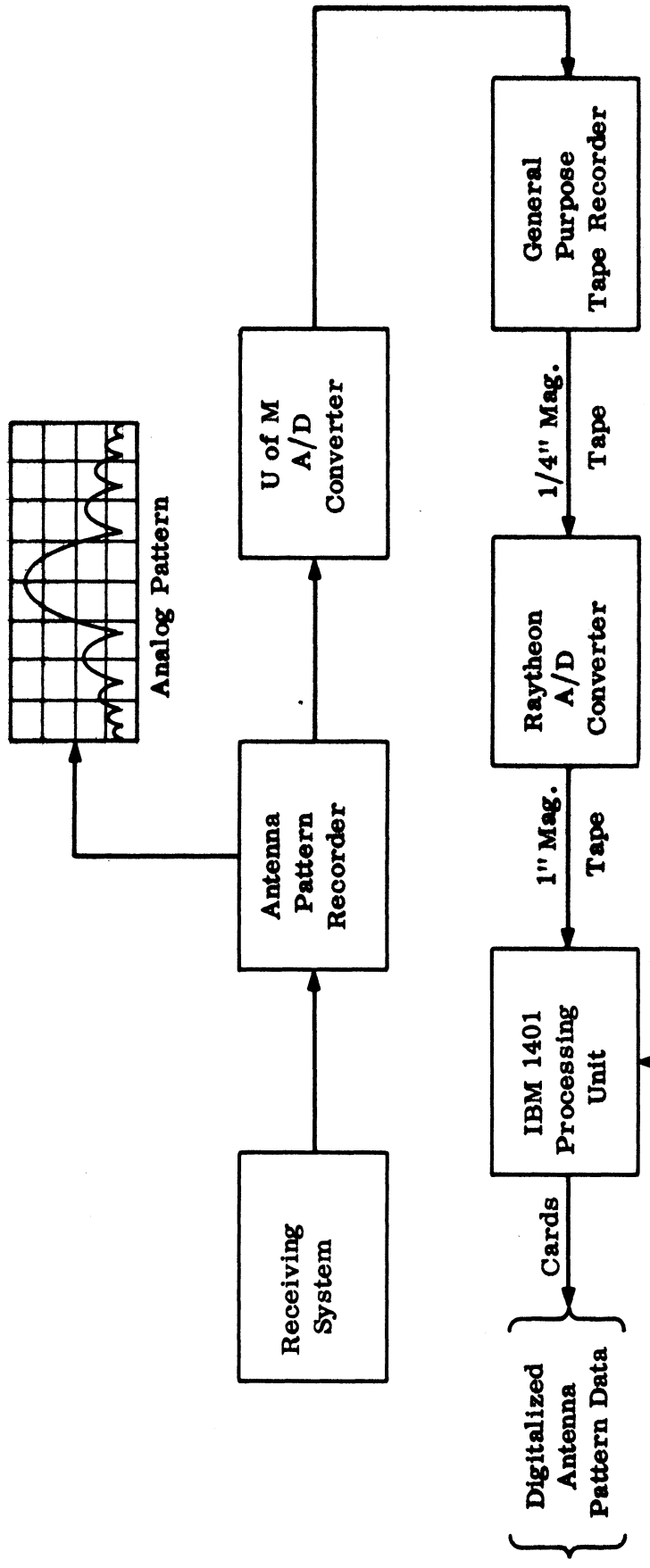

FIG. 83: AUTOMATIC DIGITAL RECORDING SYSTEM.

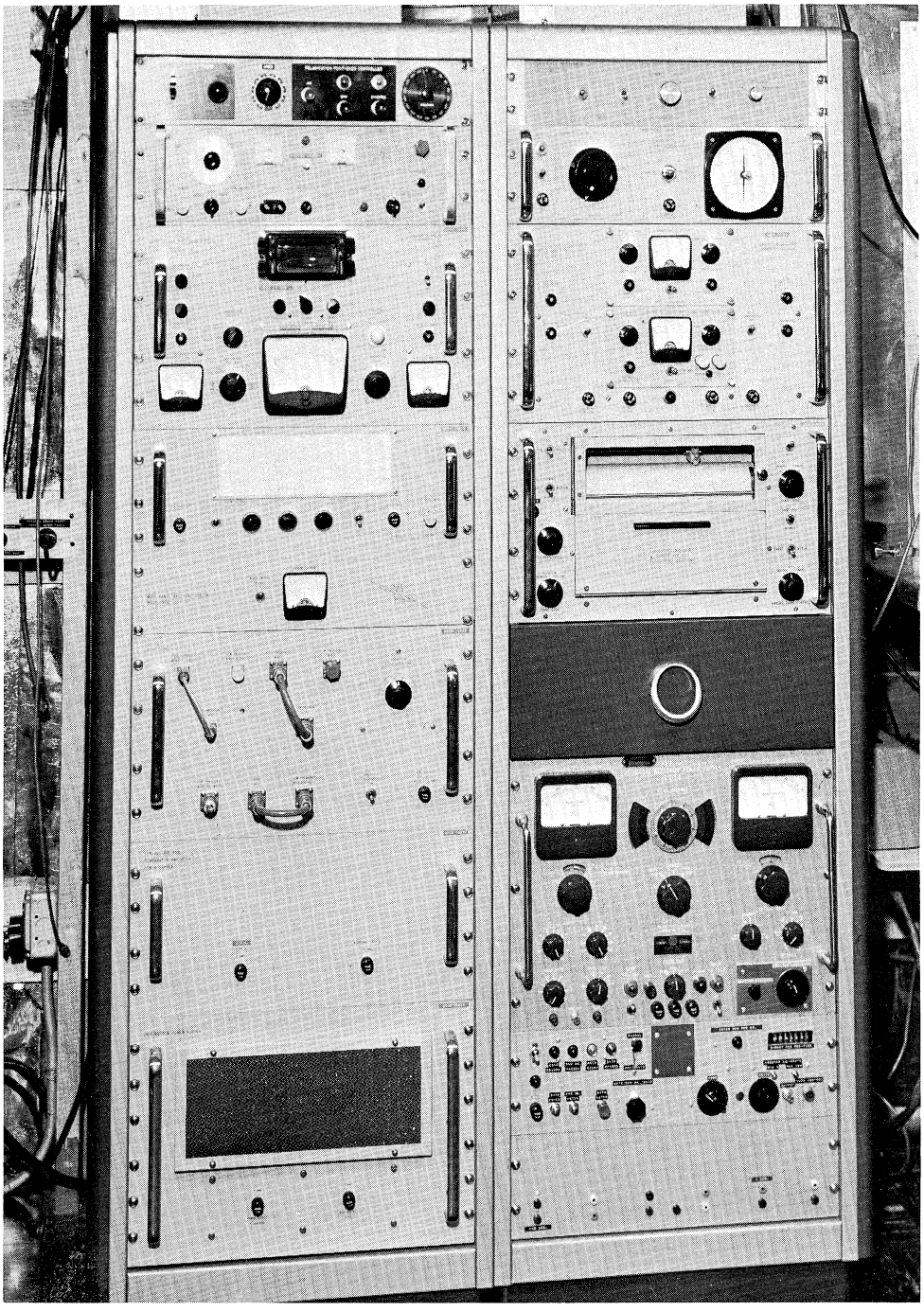

FIG. 84: WIDE-RANGE, HIGH-GAIN RECEIVING SYSTEM

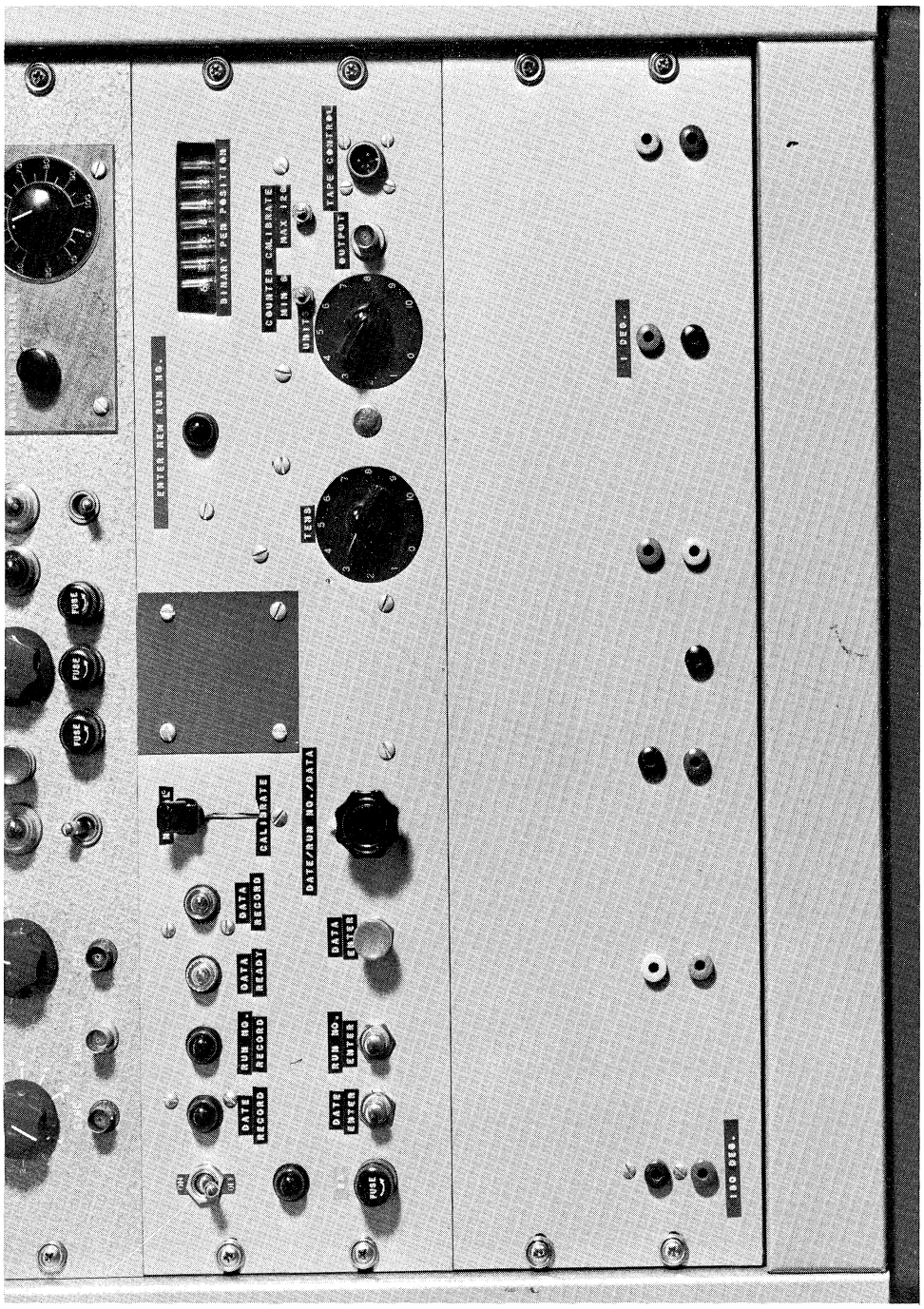

FIG. 85: U OF M ANALOG-TO-DIGITAL CONVERTER

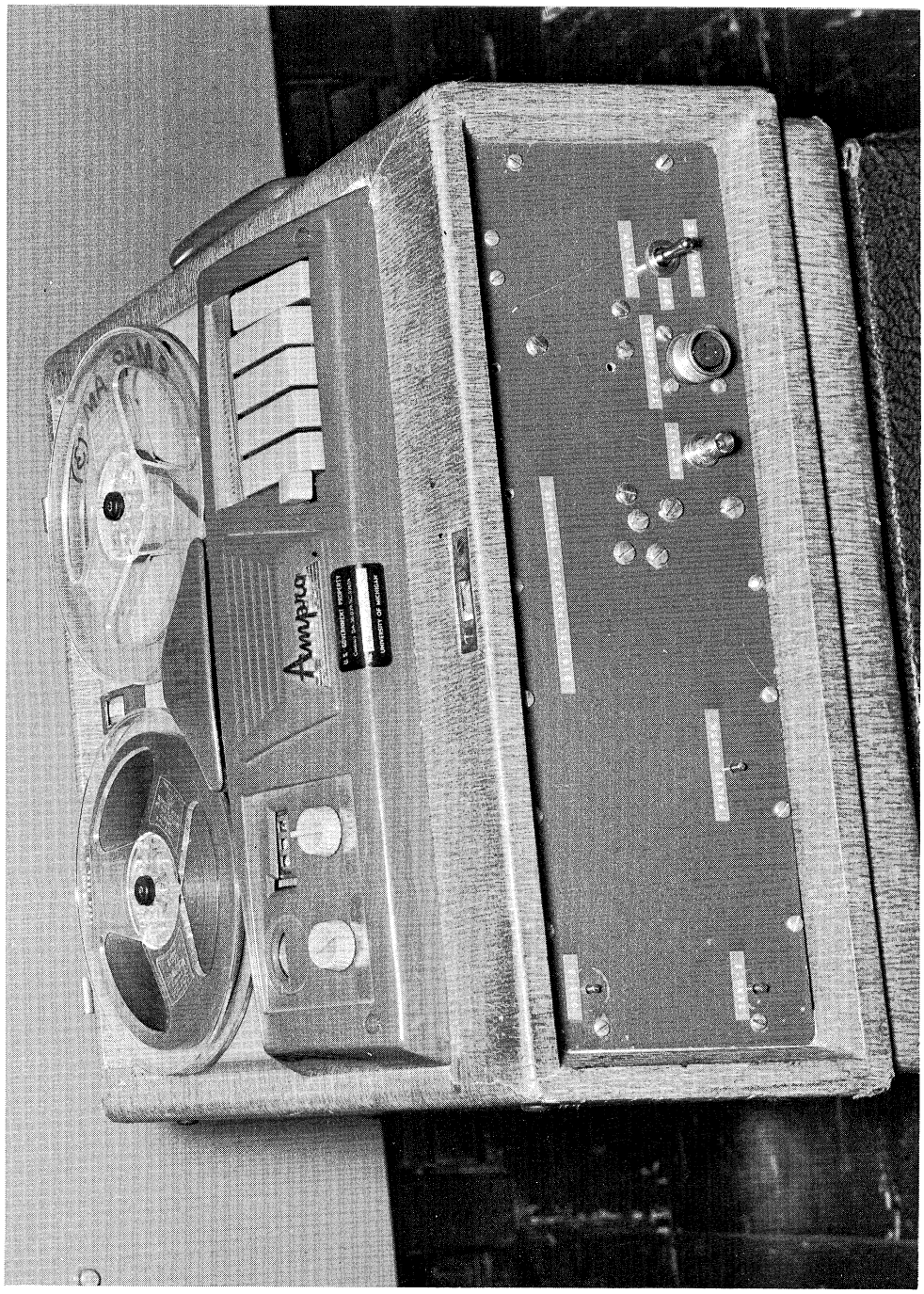

FIG. 86: GENERAL PURPOSE TAPE RECORDER

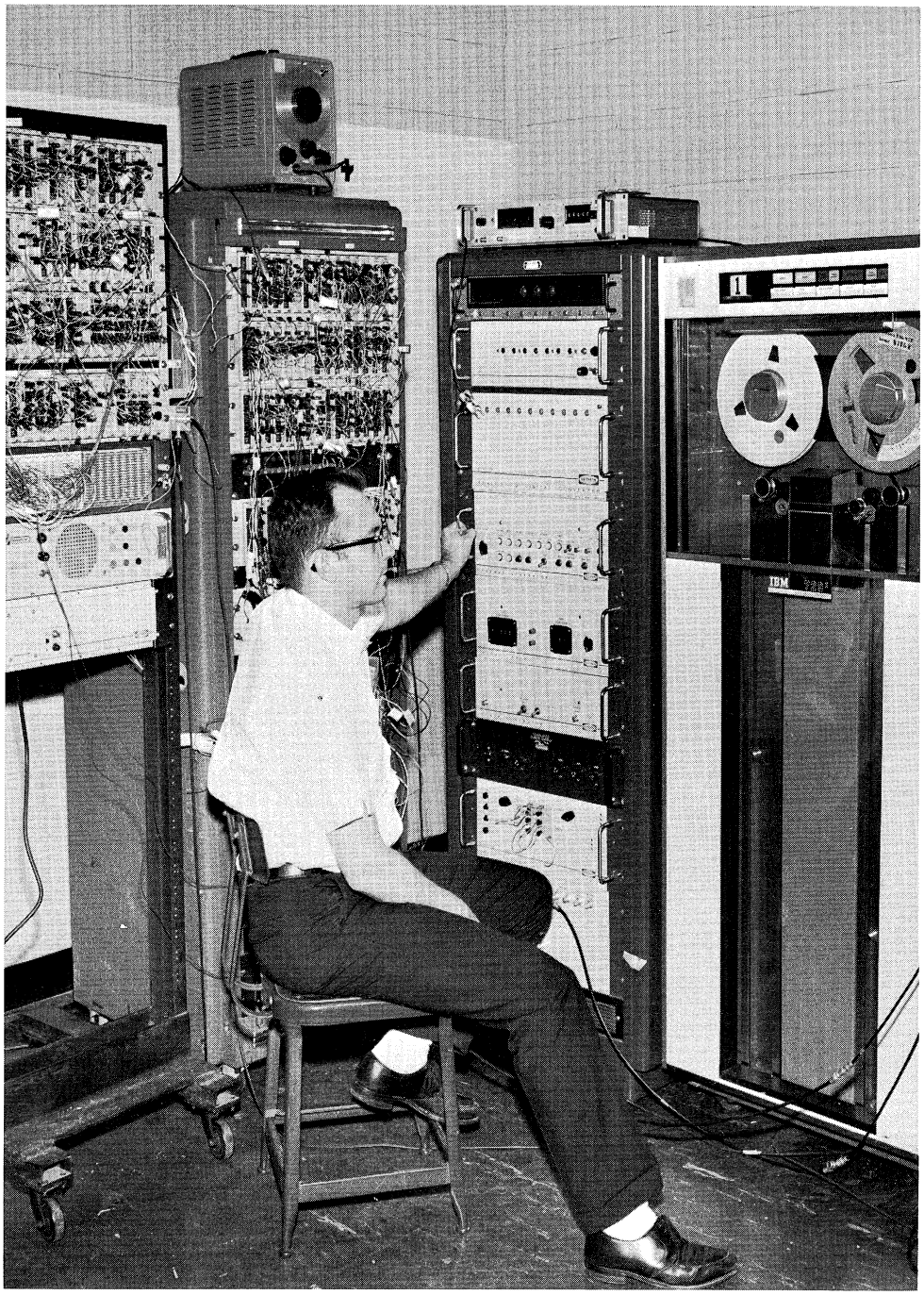

FIG. 87: RAYTHEON ANALOG-DIGITAL CONVERTER AND ASSOCIATED LOGIC RACKS (NORTH CAMPUS)

punched onto IBM cards for storage at ECAC.

Although the above procedure may appear lengthy and cumbersome, it was developed to demonstrate the feasibility of recording antenna patterns in both analog and digital form simultaneously, and the subsequent transfer of digital data to punched cards for storage. In spite of the complexity of the procedure, it was found to provide a high degree of accuracy in a shorter period than either the manual or semi-automatic procedure. This accuracy is illustrated by Figs. 88-89 which are typical analog patterns selected at random from pattern sets. Plotted as circles on these analog patterns are the digital data as read from the punched IBM cards after completion of the digitalizing procedure. Only 60 of the total 361 values sampled by the digital converter are shown on each pattern to avoid the clutter of too many points.

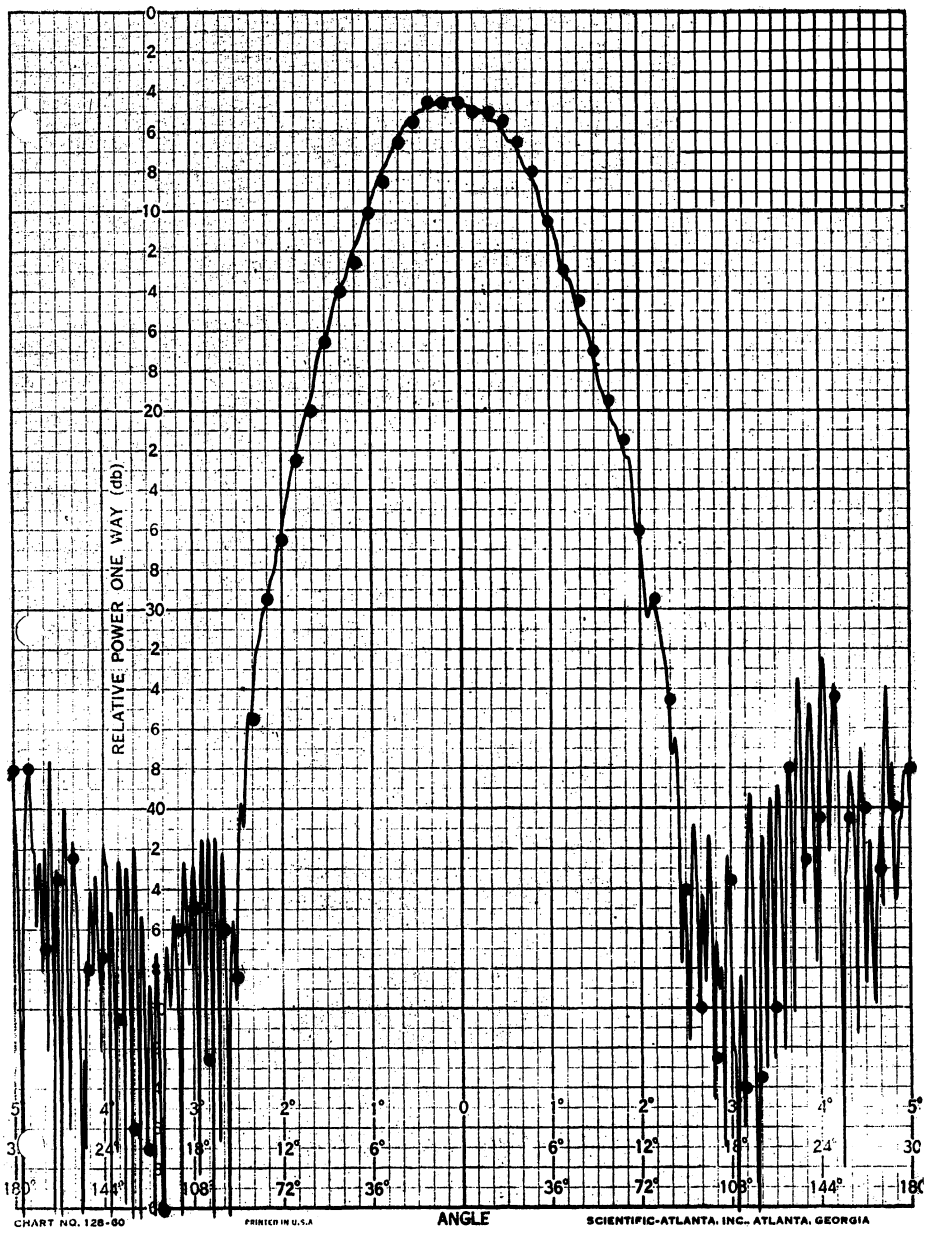

FIG. 88: X-BAND SLOT, 16.0 Gc, SIMPLIFIED T-33

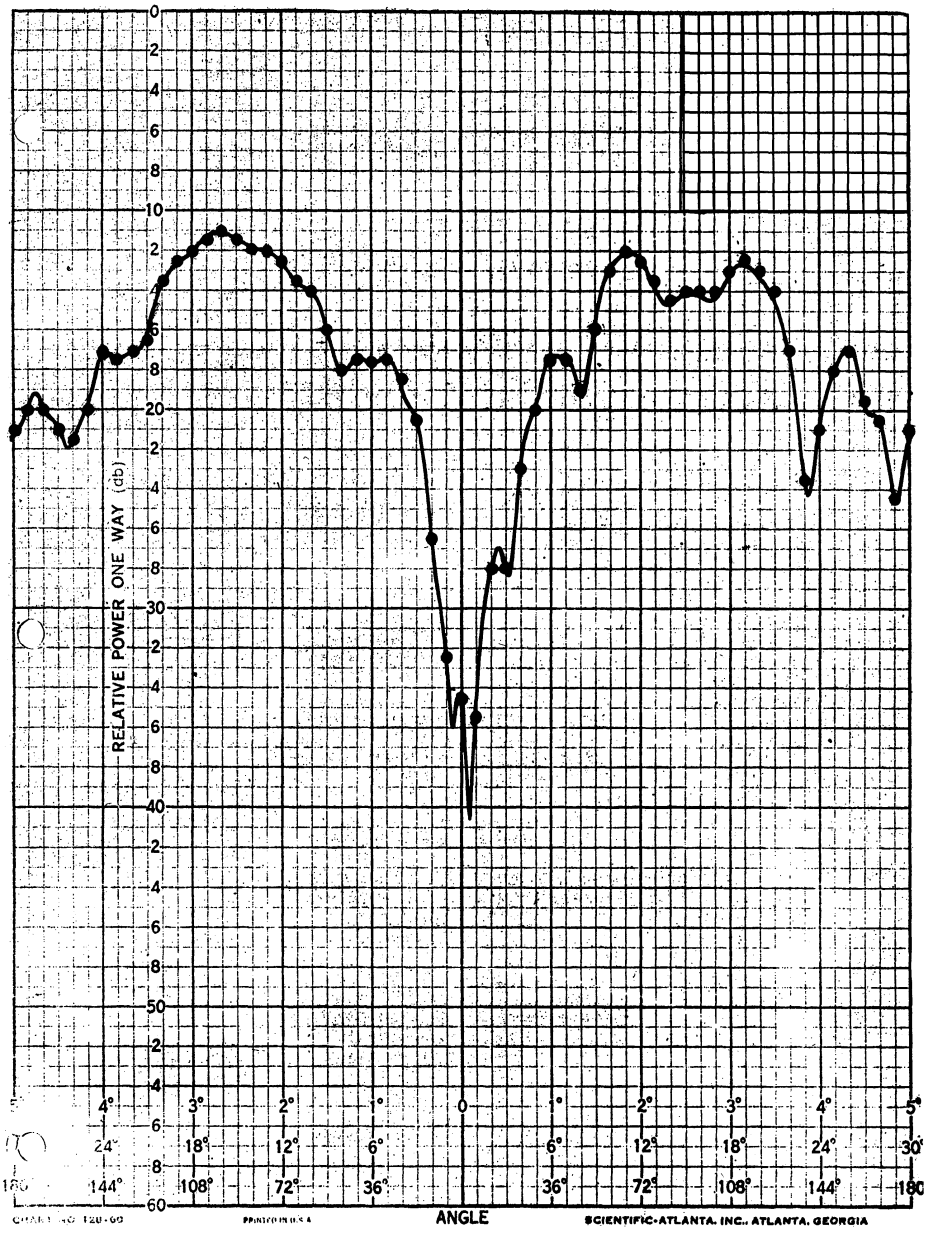

FIG. 89: λ/4 MONOPOLE, 2.4 Gc, PRECISION T-33

IV
TRANSMITTER OUTPUT CHARACTERISTICS

A third aspect of the present contract is the consideration of the overall system. Here, one must determine what data is to be collected by the military (Air Force, etc.), and supplied to ECAC for interference predictions. Since there are many types of systems in use today, the systems study has been initially limited to one of the more popular and less complicated systems. As our knowledge of this system increases, the techniques developed will be refined so that they can be employed with more complicated systems. The system initially under consideration is a communication system that functions in the VHF and UHF frequency range and employs coaxial cables as the transmission lines.

To further simplify the study, only the transmitter associated with the communication system will be evaluated. With an antenna connected to the transmitter it is necessary to show how to calculate the power available to the antenna. To aid in this study, it has been broken into three parts: 1) the multiple generator problem, 2) power transfer considerations, and 3) source impedance measurements. Each of these will be discussed in the following sections.

4.1 A Multiple Generator Model for Spurious and Harmonic Frequencies

An elementary generator can be modeled as a voltage source connected in series with an internal impedance as in Fig. 90. Such an equivalent circuit can represent a transmitter.

For the electromagnetic compatibility study, one must understand that transmitters produce spurious and harmonic outputs in addition to the fundamental. Therefore, the elementary generator is inadequate and a multiple generator model is required. Such a model is depicted in Fig. 91. For the multiple generator model, each spurious (or harmonic) frequency is represented by its own generator and internal impedance.

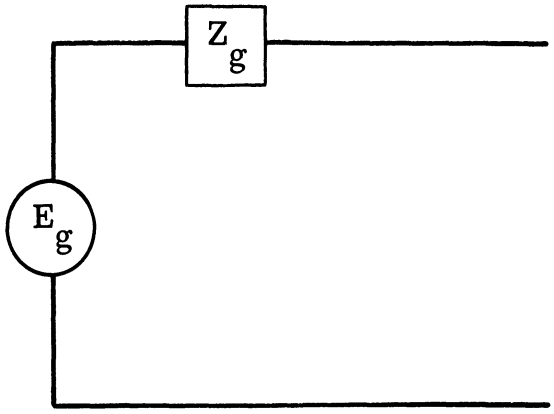

FIG. 90: ELEMENTARY GENERATOR

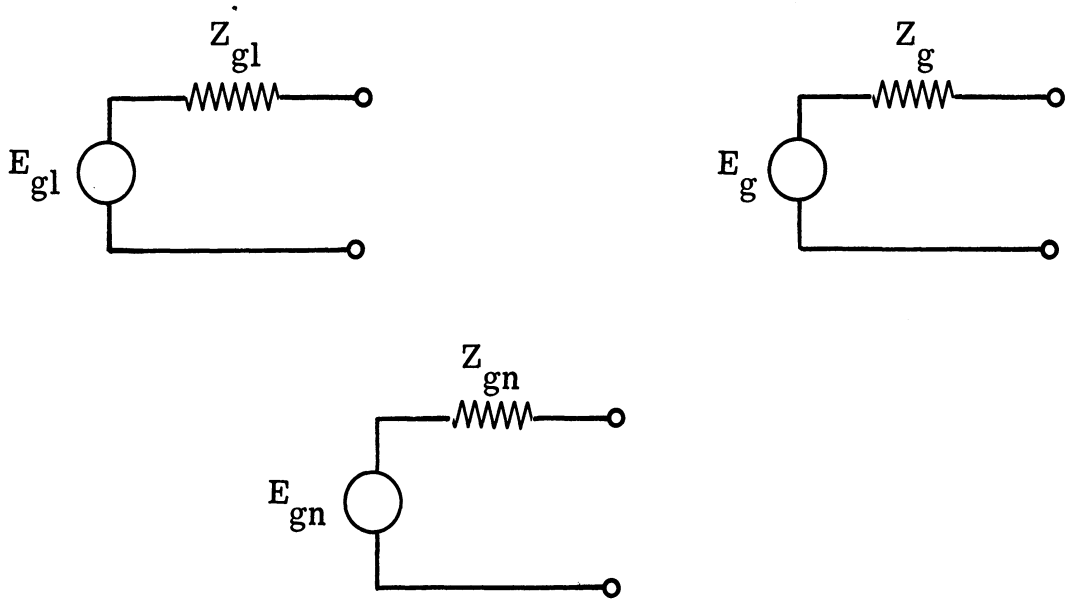

FIG. 91: MULTIPLE GENERATOR MODEL FOR A TRANSMITTER

A key consideration is the aspect of interactions between the elementary generators, which are the components of the multiple generator model. By interactions we mean the following. Suppose a load Z_{lk} is attached to generator (E_{gk}, Z_{gk}). Let Z_{lk} vary and observe generator (E_{gj}, Z_{gj}). If (E_{gj}, Z_{gj}) is constant as Z_{lk} is varied, then the model is considered to be free of interaction. If the model is assumed to be free of interaction, then the computation of power absorbed by an antenna is readily made by techniques described later. If the model is not free of interaction, then a linear correction term added to E_{gk} and Z_{gk} may provide a model with sufficient accuracy for ECAC purposes. It is necessary to gather experimental evidence to determine the extent of interaction for a real transmitter.

Since the elementary generator model must be completely understood before the multiple generator model can be adequately described, the multiple generator model will not be used in the following discussion. The calculation and measurement procedures described apply to elementary generators, which are the components of the multiple generator model.

4.2 Power Transfer Considerations

In the electromagnetic compatibility program there is need for a simple method for computing the power absorbed by a load (an antenna) when the antenna impedance, Z_a, transmission line impedance, Z_o, and source impedance, Z_g, are far from equal. A general method is desired for computing the maximum and minimum power for a given Z_a, Z_o and Z_g, if the transmission line length is varied. For some purposes, a method is necessary for determining the probability that the power absorbed by Z_a will exceed a stated power if a random length of transmission line is used. It will be assumed that the transmission line is lossless, hence $Z_o = R_o$. The general situation is as shown in Fig. 92. For a precise formulation of the problem, more dimensions should be added to Fig. 92, as shown in Fig. 93,

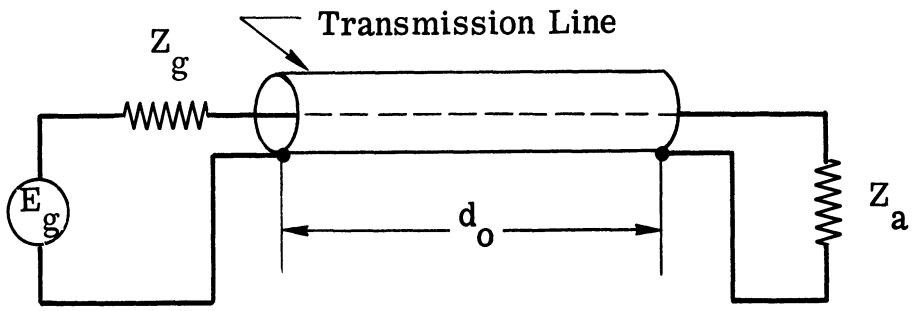

FIG. 92: GENERAL TRANSMISSION LINE PROBLEM

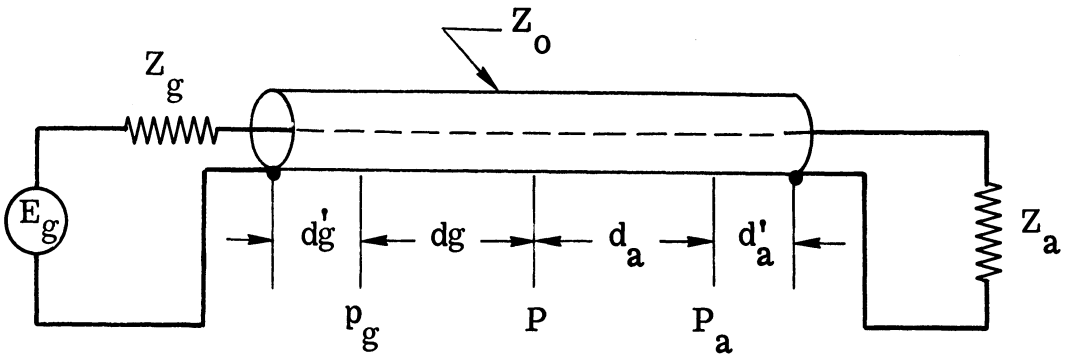

FIG. 93: MODIFIED TRANSMISSION LINE PROBLEM

where the distance d_o has been broken up into four distances d_g', d_g, d_a, and d_a' such that

$$d_g' + d_g + d_a + d_a' = d_o . \qquad (1)$$

The two distances d_g' and d_a' have been chosen in the following manner. Consider first d_g'. The antenna impedance Z_a will produce a standing wave on the transmission line; the point P_a is chosen at one of the minima of this standing wave. Then d_a' is the distance from the antenna to this point P_a. At P_a the antenna load impedance Z_a will be transformed to an impedance $Z_a' = R_a'$ and $R_a' < R_o$. The distance d_g' to point P_g is determined in the same manner but using Z_s as the terminating impedance.

Now we can write equations for the impedance seen at points P, Z_g' and Z_a'. Z_s' is the impedance at P seen looking toward the source, and Z_a' is the impedance at P seen looking toward the antenna. From these equations, an expression for the ratio of the power available at the antenna (P) to the maximum power available from the transmitter (P_{max}) may be derived as shown in the Appendix as

$$\frac{P}{P_{max}} = \frac{1}{\alpha^2 \cos^2 kd_a + \sin^2 kd_a} \qquad (2)$$

Figure 94 is a set of universal curves calculated from the above equation showing the variation of power delivered to the antenna as a function of the transmission line length, d_a. From these curves, it is a simple matter to determine the probability that, with a particular transmitter and antenna, the power radiated by the antenna will exceed some arbitrary power level when the exact length of the transmission line is not known. This information may be obtained from three measurements: 1) the antenna standing wave ratio, 2) the transmitter standing wave

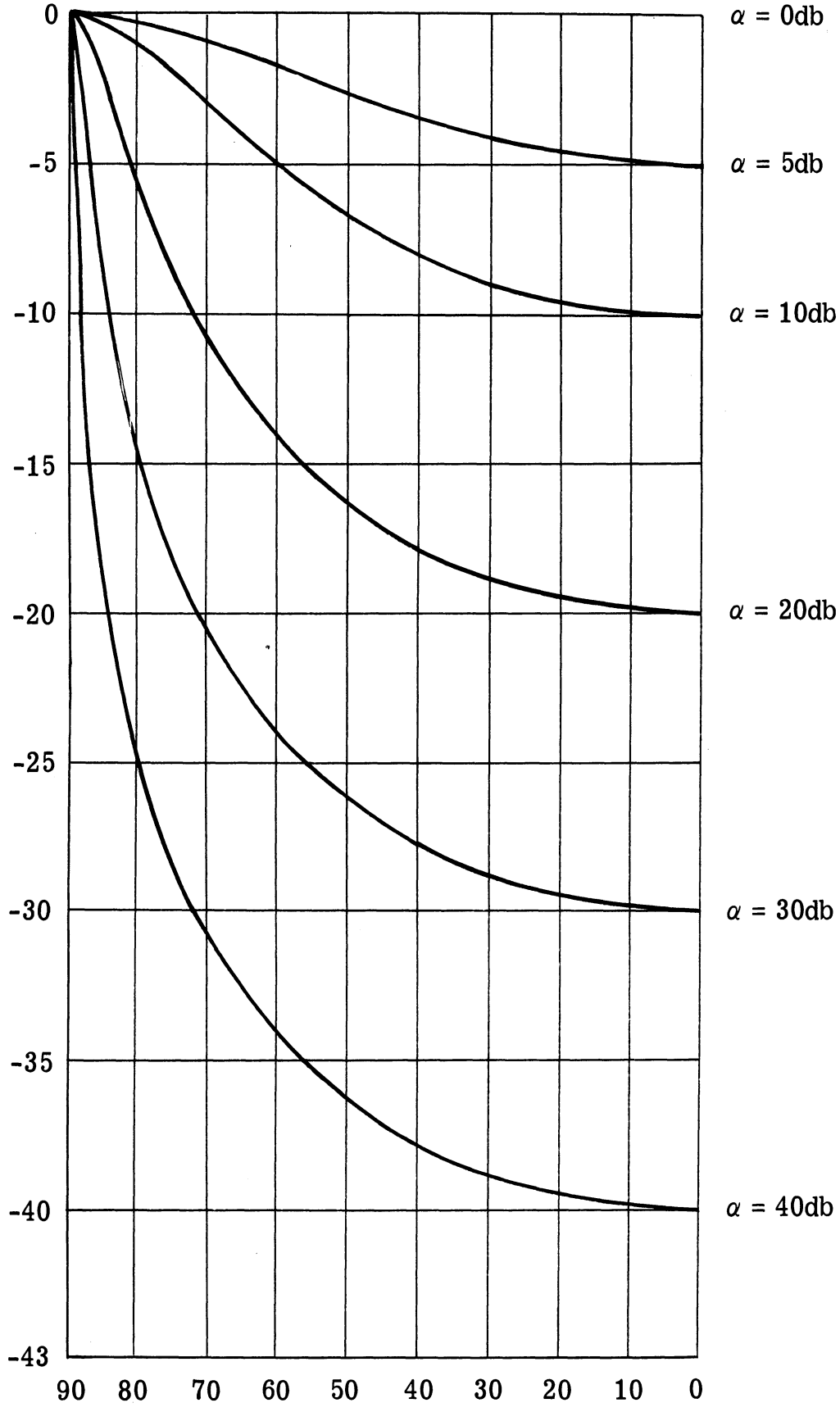

FIG. 94: POWER TRANSFER AS A FUNCTION OF TRANSMISSION LINE LENGTH

ratio, and 3) the maximum power available from the transmitter. These three measurements should be made at a point on the transmission line near the antenna to minimize the effects of transmission line losses. Techniques for the first and third measurements are relatively simple, but the measurement of the transmitter standing wave ratio is not well understood. Therefore, a technique of obtaining this data must be developed.

4.3 Source Impedance Measurements

Here it will be shown that, if the transmitter impedance is not a function of the termination, the impedance can be measured with a line stretcher terminated in a short circuit and a detector tuned to the frequency of interest. The measurement procedure is very similar to that for measuring a termination impedance with a slotted line.

The circuit used is shown schematically in Fig. 95. The transmitter is represented by a voltage source E_g and a series impedance Z_g. Neither E_g nor Z_g are a function of the termination. The transmitter terminals AB are connected to a transmission line of variable length, ℓ. A detector is placed across the line a fixed distance, d, from the short circuit. The exact value of d is not important but should remain fixed throughout a measurement. The largest voltage for the detector is obtained when $d = \lambda/4$, $3\lambda/4$, etc, but the effect of detector loading is most pronounced at these points. For a measurement device, $d = \lambda/8$ may be a good compromise.

The impedance Z_t seen at the input of a shorted transmission line of length ℓ and propagation constant k is given by:

$$Z_t = jX_t = jR_o \tan k\ell \qquad (3)$$

This is the impedance seen looking to the right of terminals AB of Fig. 95. The voltage V_1 across terminals AB is given by:

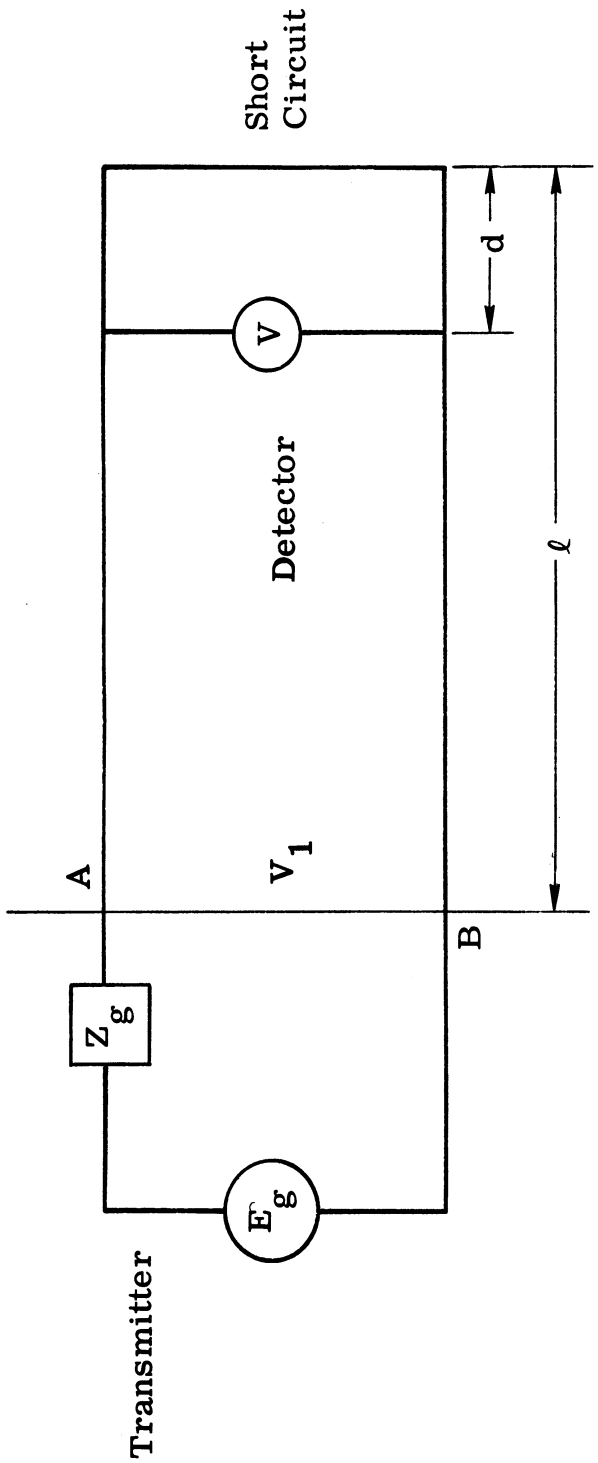

FIG. 95: GENERATOR IMPEDANCE MEASUREMENT CIRCUIT
(using a short-circuit load)

$$V_1 = \left| I_1 \, jX_t \right| \tag{4}$$

$$= \frac{E_g \, X_t}{\left| Z_g + jX_j \right|} \tag{5}$$

let $$Z_g = R_g + jX_g \tag{6}$$

then $$V_1 = \frac{E_g \left| X_t \right|}{\sqrt{R_g^2 + (X_g + X_t)^2}} \tag{7}$$

$$= \frac{E_g \, R_o \tan k\ell}{\sqrt{R_g^2 + (X_g + R_o \tan k\ell)^2}} \tag{8}$$

Because the transmission line is shorted at the far end, an infinite sinusoidal standing wave appears on the line such that

$$V_1 = V_p (\sin k\ell) . \tag{9}$$

The quantity V_p represents the peak value of the standing wave appearing at every odd number of quarter wavelengths from the short. The voltage, V, indicated by the detector will be some fixed fraction, a, of this peak voltage. Hence,

$$V = a V_p . \tag{10}$$

Combining equations (8), (9) and (10), we obtain

$$V\frac{|\sin k\ell|}{a} = \frac{E_g R_o |\tan k\ell|}{\sqrt{R_g^2 + (X_g + R_o \tan k\ell)^2}} \tag{11}$$

from which

$$V = \frac{a E_g}{\sqrt{\left[\frac{R_g}{R_o}\right]^2 \cos^2 k\ell + \left(\frac{X_g}{R_o}\cos k\ell + \sin k\ell\right)^2}} \tag{12}$$

In equation (12) the magnitude signs are no longer necessary; the positive sign is attached to the radical in the denominator.

Now let us examine equation (12) for the condition of $R_g = R_o$ and $X_g = 0$. Equation (12) becomes

$$V\Big|_{\substack{R_g = R_o \\ X_g = 0}} = \frac{a E_g}{\sqrt{\cos^2 k\ell + \sin^2 k\ell}}$$

$$= a E_s \tag{14}$$

Thus when the source impedance matches the line impedance ($Z_g = R_o$) the detector reading is independent of the line length ℓ. This condition is equivalent to the matched termination of a line that produces a flat line. The flat line counterpart for a "source standing wave" is demonstrated by equation (14).

Now what happens when $Z_g \neq R_o$, i.e., the source impedance is not matched. For this situation, let us consider, in general, the situation viewed at terminals AB but at terminals A'B' a distance ℓ_1 from the transmitter. Let us choose ℓ_1 so that the transmitter impedance Z_g is transformed to a pure resistance R_g' so that $R_g' \geq R_o$. Equation (12) then becomes

$$V = \frac{a E'_g}{\sqrt{\left[\frac{R'_g}{R_o}\right]^2 \cos^2 k(\ell - \ell_1)\, k + \sin^2 k(\ell - \ell_1)}} \tag{15}$$

Equation (15) has a maximum value when $\cos k(\ell - \ell_1) = 0$ and a minimum value when $\sin k(\ell - \ell_1) = 0$. To show this, differentiate the quantity under the radical and set it equal to zero.

$$\frac{d}{\left[d\ k(\ell - \ell_1)\right]} \left[\left[\frac{R'_g}{R_o}\right]^2 \cos^2 k(\ell - \ell_1) + \sin^2 k(\ell - \ell_1) \right]$$

$$= -2 \left[\frac{R'_g}{R_o}\right]^2 \sin k(\ell - \ell_1) \cos k(\ell - \ell_1) + 2 \sin k(\ell - \ell_1) \cos k(\ell - \ell_1) \tag{16}$$

$$= 2 \left\{ 1 - \left[\frac{R'_g}{R_o}\right]^2 \right\} \sin k(\ell - \ell_1) \cos k(\ell - \ell_1)\ . \tag{17}$$

Equation (17) is zero when

$$\sin k(\ell - \ell_1) = 0 \tag{18}$$

or

$$\cos k(\ell - \ell_1) = 0\ . \tag{19}$$

Using equation (18) in (15) we have

$$V_{min} = a E'_g \frac{R_o}{R'_g}\ . \tag{20}$$

Using equation (19) in (15) we have

$$V_{max} = a E_g' \tag{21}$$

Equation (20) gives V_{min} because $R_g' > R_o$.

Now, dividing equation (20) by equation (21) gives

$$\frac{V_{max}}{V_{min}} = \frac{R_g'}{R_o} \tag{22}$$

To determine the impedance seen looking back into the transmitter terminals, AB, we must enter the Smith Chart at

$$\frac{R_g'}{R_o} = \frac{V_{max}}{V_{min}} = \text{VSWR} \tag{23}$$

and go around the chart a distance equivalent to ℓ_1 in the direction "toward the load" indicated on the chart. This point on the chart represents the transmitter impedance Z_g.

4.3.1 Experimental Verification of the Source Impedance Measurement Using a Short Circuit Load

To experimentally verify the above analysis, a signal generator and a variable reactive load have been employed. The system block diagram is shown in Fig. 96. The slotted line was employed to determine the distance between the generator terminals and a null of the standing wave pattern (which is equivalent to finding AB/λ_g since a null occurs every $\lambda_g/2$).

The results of this experiment are shown in Fig. 97. Assuming the generator impedance Z_g is $50 + j0$ and the stub introduces an imaginary component only, one would expect the locus of points on the Smith Chart to form a circle tangent to the

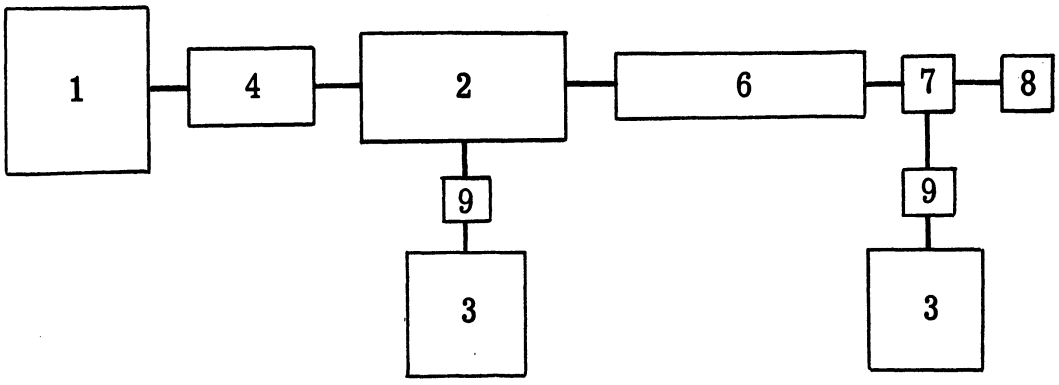

FIG. 96: EQUIPMENT ORGANIZATION FOR GENERATOR IMPEDANCE MEASUREMENT

Equipment List

1) 600 MHz Standard Laboratory Signal Generator
2) Coaxial Slotted Line
3) VSWR Detector
4) Variable Stub Tuner
5) Standard Laborator 50 OHM Coaxial Termination
6) Variable Length, Constant Impedance Coaxial Line
7) Signal Probe
8) Standard Coaxial Short Circuit Termination
9) Bolometer Detector

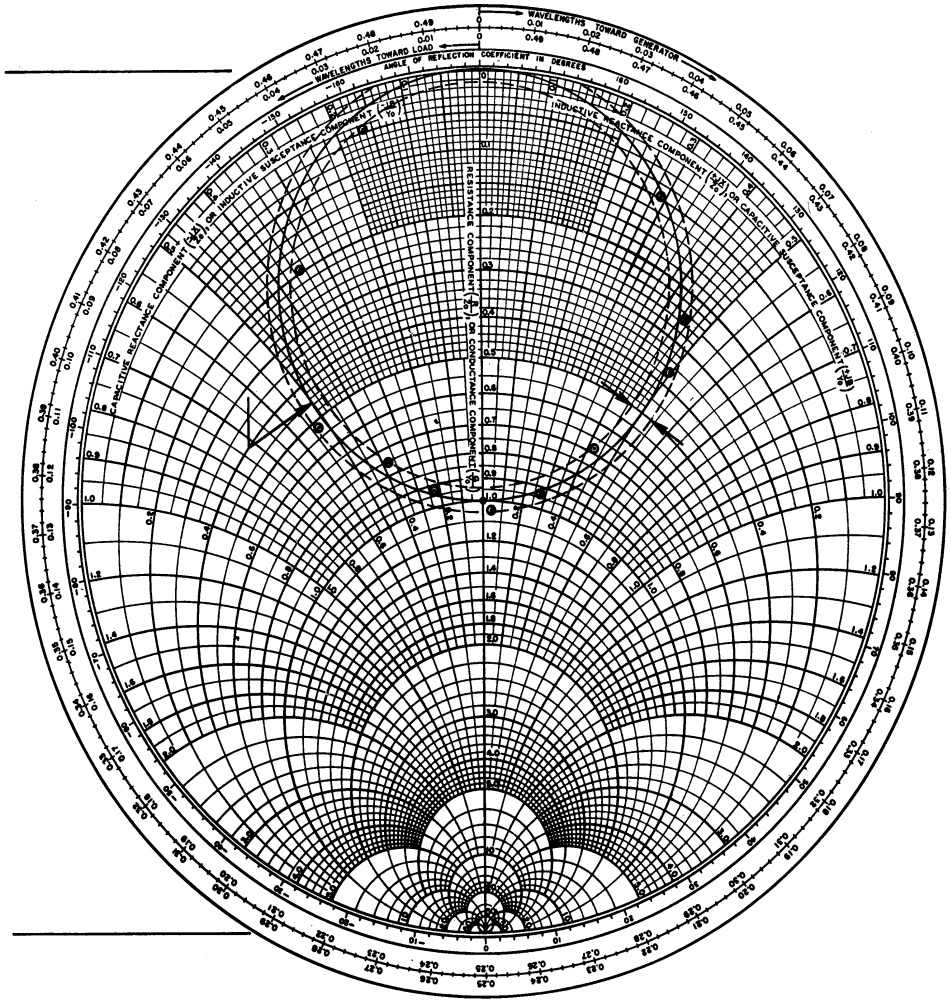

— $\frac{Z}{Z_o} = 1 + jx$ ---- Area of Uncertainty Due to Minimum VSWR>1:1

FIG. 97: IMPEDANCE OF GENERATOR IN SERIES WITH STUB TUNER (using a short-circuit load)

points $Z = 1.0 + j0$ and $Z = 0 + j0$ with the real axis including these points as the diameter. However, the minimum measurable VSWR was 1.09 and the experimental data points vary by approximately this amount from the ideal circle. No data points corresponding to large values of stub reactance appear on the generator impedance plot. The mismatch between the generator and the tuning stub was so great in this region that the energy transfer to the line is insufficient to make accurate measurements.

These results has been verified by comparing them to the impedance of the stub tuner in series with a standard laboratory 50 ohm termination. These measurements were obtained using standard slotted line techniques. The block diagram for the equipment appears in Fig. 98. The latter results were in excellent agreement with the source impedance measurements, the only difference being that data points were available for large values of stub reactance.

4.3.2 Measurement of Transmitter Impedance Using a Complex Load

A technique for measuring the impedance of a transmitter using a short circuit has been discussed above. This may be found to be impractical for many transmitters since they are generally designed to work into a well-matched load at the fundamental frequency. In this section, a similar measurement procedure will be discussed utilizing a complex load. It will be necessary for the VSWR of the load to be accurately known at the frequency of interest.

A test setup similar to that shown in Fig. 96 will be used to measure the impedance (and VSWR) of the transmitter. The only difference being that the short circuit termination is replaced by a load. The slotted line is employed to measure the load impedance, e.g., an antenna. The variable line is then adjusted to obtain both a voltage maximum, $V_{c(max)}$, and minimum, $V_{c(min)}$ With the line adjusted for a voltage minimum, a null on the slotted line is recorded. The VSWR of the source is then calculated from the following expression:

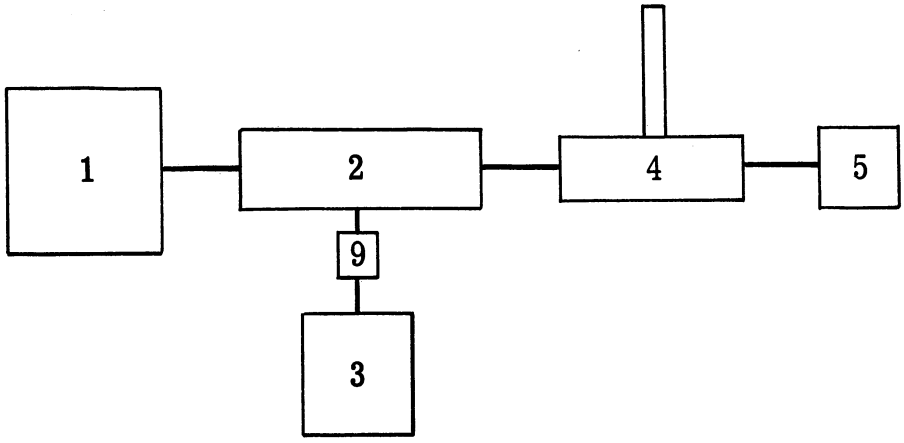

FIG. 98: EQUIPMENT ORGANIZATION FOR 50 Ω AND TUNING STUB IMPEDANCE MEASUREMENT

(See Equipment List in Fig. 96)

$$\text{VSWR} = \frac{K r_\ell - 1}{r_\ell - K}, \text{where } K \text{ is } \frac{V_c(\max)}{V_c(\min)}, \text{ and } r_\ell \text{ is the load VSWR.}$$

To determine the transmitter impedance, one must enter the Smith Chart at the top along the $R+j0$ (where $R = 1/\text{VSWR}$ such that $0 < R < 1$) line and rotate along the generator VSWR circle (from the expression above) a distance ℓ_1/λ_g toward the load. ℓ_1 is the distance from the null on the slotted line to the generator terminals when V_c is a minimum (see Fig. 100), and λ_g is the wavelength of the signal in the transmission line. The transmitter and load are shown schematically in Fig. 99. The transmitter is modeled as a voltage source E_g in series with impedance Z_g. The variable length of the constant impedance transmission line, AC, is terminated by a known load Z_1 at B. Distance BC is constant. A detector is included at C.

Let V_i be the total forward going voltage incident on the load and V_r the reflected voltage propagating from the load. At any point along the line the voltage will be given by

$$V_t = V_i + V_r . \tag{24}$$

The reflection coefficient at the load is defined as ρ.

$$\rho_1 = \frac{V_r}{V_i} . \tag{25}$$

Let V_i' be the reflected voltage incident on the generator. Further, let V_r' be the incident voltage reflected from the generator. The reflection coefficient at the generator is defined as ρ_g,

$$\rho_g = \frac{V_r'}{V_i'} . \tag{26}$$

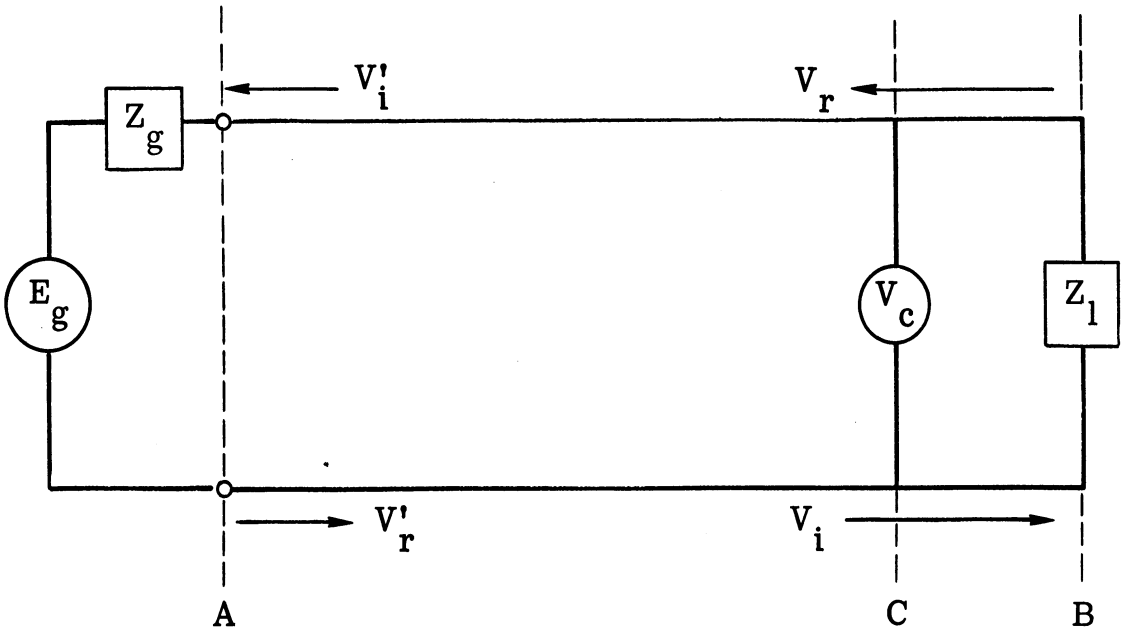

FIG. 99: GENERATOR IMPEDANCE MEASUREMENT CIRCUIT
(using a complex load)

The VSWR of the source is then equal to

$$VSWR = \left| \frac{V_i' + V_r'}{V_i' - V_r'} \right| = \frac{1 + \left| \frac{V_r'}{V_i'} \right|}{1 - \left| \frac{V_r'}{V_i'} \right|} \tag{27}$$

Substituting equation (26),

$$VSWR = \frac{1 + |\rho_g|}{1 - |\rho_g|} . \tag{28}$$

The maximum voltage measured by the detector at C as the line length AC is varied will be $V_{c(max)} = |V_i| + |V_r'|$. The minimum is

$$V_c(min) = |V_i| - |V_r'| \tag{29}$$

Consider the ratio

$$\frac{V_{c\,(max)}}{V_{c\,(min)}} = \frac{|V_i| + |V_r'|}{|V_i| - |V_r'|}$$

$$= \frac{|V_i| + |\rho_\ell|\,|\rho_g|\,|V_i|}{|V_i| - |\rho_\ell|\,|\rho_g|\,|V_i|} = \frac{1 + |\rho_\ell|\,|\rho_g|}{1 - |\rho_1|\,|\rho_g|} . \tag{30}$$

Let

$$\frac{V_{c\,(max)}}{V_{c\,(min)}} = K = \frac{1 + |\rho_\ell|\,|\rho_g|}{1 - |\rho_\ell|\,|\rho_g|} \tag{31}$$

Then,

$$K\left[1 - |\rho_\ell|\,|\rho_g|\right] = 1 + |\rho_\ell|\,|\rho_g| \tag{32}$$

$$\text{or} \quad |\rho_g| = \frac{K - 1}{|\rho_\ell| \ (K + 1)} \tag{33}$$

Substituting equation 28 into equation 33,

$$\text{VSWR (Source)} = \frac{1 + \dfrac{K - 1}{(K + 1) \ |\rho_\ell|}}{1 - \dfrac{K - 1}{(K + 1) \ |\rho_\ell|}} \tag{34a}$$

$$= \frac{K(1 + |\rho_1| \ ) - (1 - |\rho_1| \ )}{-K(1 - |\rho_1| \ ) + (1 + |\rho_\ell| \ )} \ . \tag{34b}$$

Let VSWR (Load)$= r_\ell$. Dividing equation (34a) by $(1 - |\rho_\ell| \ )$ and recalling that $\text{VSWR (Load)} = \dfrac{1 + |\rho_\ell|}{1 - |\rho_\ell|}$ one has

$$\text{VSWR (Source)} = \frac{K r_\ell - 1}{r_\ell - K} \tag{35}$$

where K is $\dfrac{V_{c\,(max)}}{V_{c\,(min)}}$ and r_ℓ is the load VSWR.

A simple determination of the source VSWR with any complex load is now possible with two voltage measurements. If the load VSWR is known, the source impedance can be determined with the aid of a Smith Chart.

Consider Fig. 100. Let ℓ_1 be the distance from the generator terminals to the point D along the transmission line AC where Z_g appears to be purely resistive when looking back toward the generator. Let this value be R_g'. Further, select ℓ_1 so that $R_g' < Z_o$, the characteristic impedance of the transmission line. If the line length AB is adjusted so that the voltage measured at B is a minimum, a null

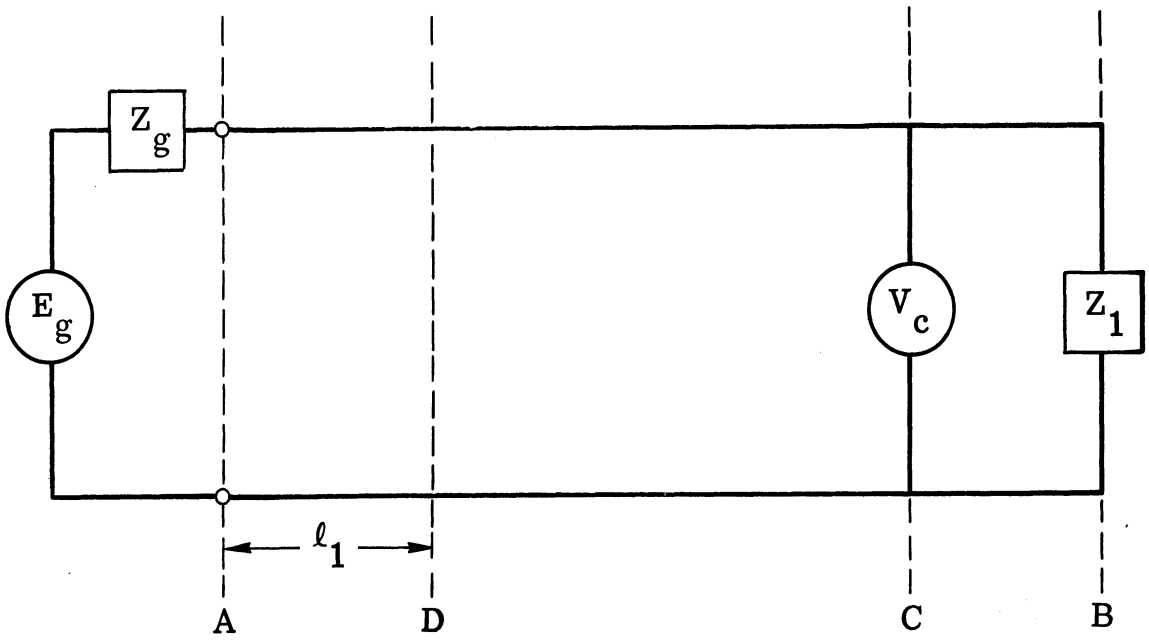

FIG. 100: CIRCUIT FOR THE DETERMINATION OF ℓ_1

in the standing wave along the line due to the load will occur precisely at D. Suppose the generator impedance is R_g' and the generator terminals are located at D. Further, represent the load and line length DB by a variable impedance Z_ℓ' at D, as in Fig. 101. Clearly, the voltage V' across Z_1' will be a minimum when Z_1' is a minimum. This is exactly analogous to the case discussed above. Thus the voltage V at C will be a minimum when the length AC is adjusted so that a null occurs at D. Therefore, to find the generator impedance, it is necessary to enter the Smith Chart at the top along the R+j0 line and rotate along the generator VSWR circle a distance ℓ_1/λ_o toward the load.

4.3.3 Experimental Data

The technique described above has been used experimentally with a stub tuner in series with the generator. The load consisted of a 100 ohm coaxial termination and a short (random) length of transmission line. Experimental data is given in Fig. 102. No data points corresponding to large values of stub reactance appear in Fig. 102. The mismatch between the generator and tuning stub was so great in this region that the energy transfer to the line was insufficiently large to make accurate measurements. It will be noted that the data in Fig. 102, obtained with a complex load, is in excellent agreement with the data in Fig. 97, which is an impedance measurement of the same generator and tuning stub utilizing a short circuit termination.

The technique described above should prove useful for measuring complex generator impedances using a complex load, provided all harmonics or spurious outputs are far below the level of the fundamental frequency. Techniques for measuring the generator impedance at spurious and harmonic frequencies with energy being generated simultaneously at these frequencies are presently under consideration.

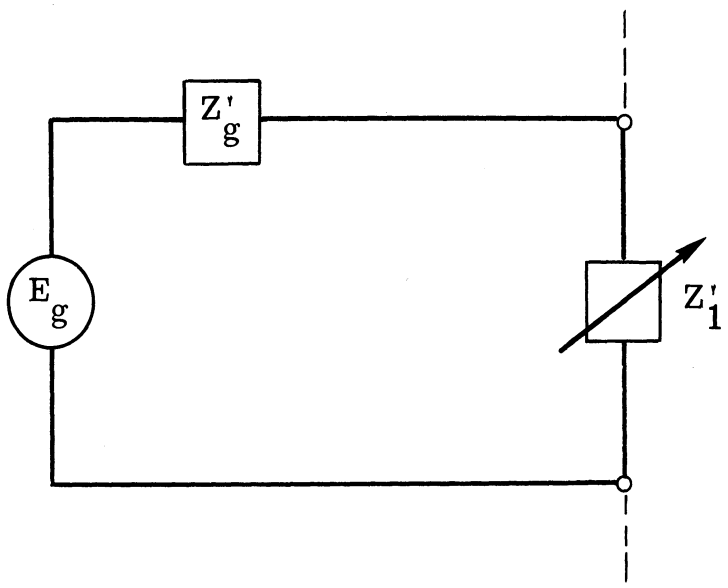

FIG. 101: EQUIVALENT CIRCUIT OF FIG. 100

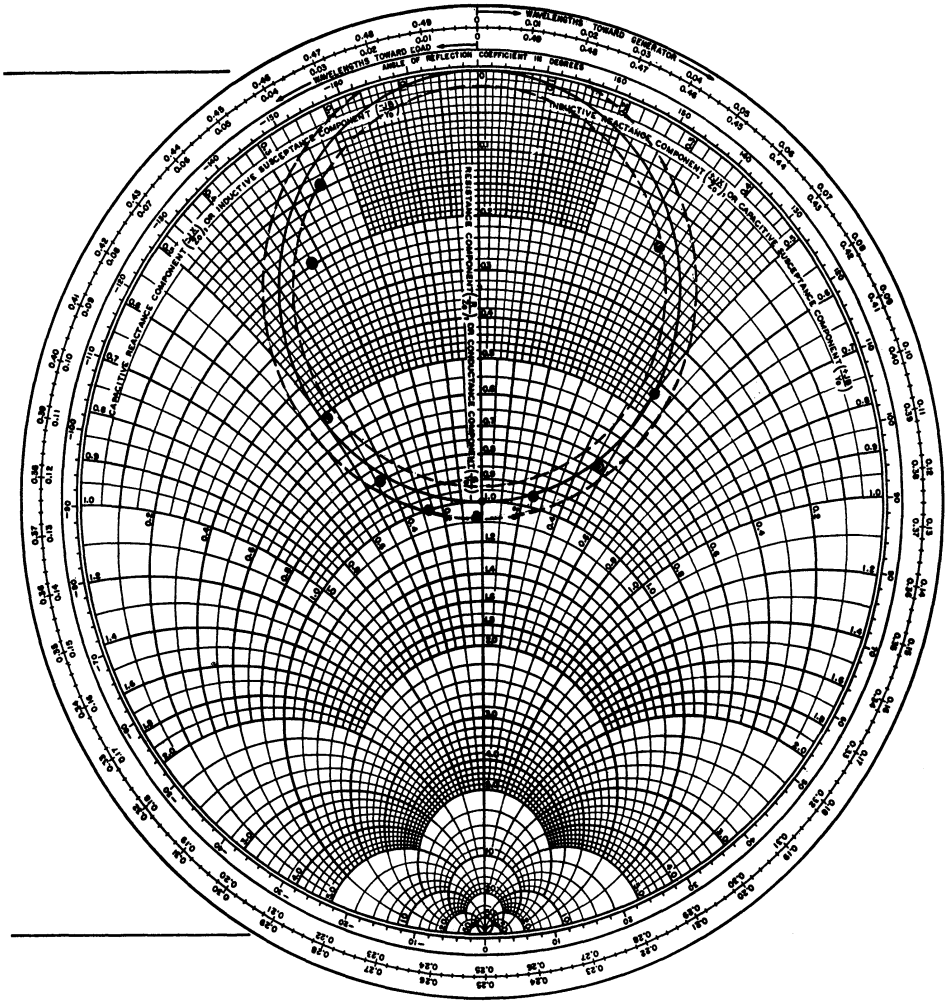

— $\frac{Z}{Z_o} = 1 + jx$ ---- Area of Uncertainty Due to Minimum VSWR > 1 : 1

FIG. 102: IMPEDANCE OF GENERATOR IN SERIES WITH STUB TUNER
(using a complex load)

V
CONCLUSIONS AND RECOMMENDATIONS

A simplified modeling technique applicable to obtaining three-dimensional spectrum signatures of airborne antennas has been presented. Employing this technique, three antenna configurations have been used, and typical data shown. The three antenna configurations were a modified monopole, $\lambda/4$ monopole and a slot antenna. The modified and $\lambda/4$ monopoles operated at a full scale frequency of approximately 300 MHz, and the slot antenna at 1.0 GHz. For the purposes of this study these antennas were scaled by a factor of 8 such that the VHF antennas operated at 2.4 GHz and the UHF antenna at 8.0 GHz. Data was collected at the fundamental and four harmonics of each of these antennas and is presented in both analog and statistical form. From a rewiew of this data, it can be seen that simplified modeling is an acceptable low cost technique for obtaining antenna spectrum signature data for future interference predictions.

A second aspect of the program has been an investigation of recording techniques applicable to obtaining spectrum signature data in a digital format. Three techniques were considered; 1) manual, 2) semi-automatic and 3) automatic. Limitations of these are discussed in the report along with a discussion of the automatic technique developed and employed by The University of Michigan. From this study, a recommendation can be made that automatic recording techniques be employed to obtain antenna spectrum signature data in a digital format. This digital data can then be placed in a universal format for storage at ECAC. Therefore, a standard data format is presented to ensure that all antenna signature data sent to ECAC is the same. Here, it is recommended this data be placed on IBM cards.

A third aspect of the study has been an investigation of an improved signature collection technique applicable to transmitters. An analysis of the problem is presented together with possible techniques of acquiring the needed data. From

this analysis it has been determined that three items of information should be collected and stored by ECAC:

1) the transmitter VSWR
2) antenna VSWR
3) maximum power available from the transmitter.

It is felt that the antenna VSWR and transmitter power can easily be obtained by standard measurement techniques. However, a new technique is required to obtain the transmitter VSWR. A suggested technique is described, from which the transmitter VSWR may be obtained at the fundamental and harmonic frequencies, along with some experimental verification. It is recommended that this work be continued since, at the present time, only the VSWR of laboratory type generators have been measured. To further evaluate the technique it will be necessary to measure the VSWR of typical transmitters used by the military. The purpose for carrying on this study is that more accurate transmitter spectrum signature data is required from which interference prediction analyses can be made. Presently, because the data collected is relatively crude and inaccurate, interference prediction analyses are inaccurate.

APPENDIX

Referring to Fig. 93, we can write equations for the impedance seen at points P, Z_g' and Z_a'. Z_g' is the impedance at P seen looking toward the source, and Z_a' is the impedance seen at P looking toward the antenna. Expressions for the resistive and reactive components on transmission lines are well known. A particularly clear and compact form is given in Montogomery et al (1948).

Let

$$Z_g' = R_g' + X_g' \tag{A1}$$

and

$$Z_a' = R_a' + X_a' \tag{A2}$$

For the source

$$R_g' = Z_o \frac{r_g}{r_g^2 \cos^2 kd_g + \sin^2 kd_g} \tag{A3}$$

$$X_g' = Z_o \frac{(1 - r_g^2) \sin kd_g \cos kd_g}{r_g^2 \cos^2 kd_g + \sin^2 kd_g} \tag{A4}$$

and for the antenna

$$R_a' = Z_o \frac{r_a}{r_a^2 \cos^2 kd_a + \sin^2 kd_a} \tag{A5}$$

$$X_a' = Z_o \frac{(1 - r_a^2) \sin kd_a \cos kd_a}{r_a^2 \cos^2 kd_a + \sin^2 kd_a} \tag{A6}$$

In these equations, r_g is the standing wave ratio on a line of characteristic impedance Z_o terminated in Z_g, k is the propagation constant of this line. Likewise, r_a is the standing wave ratio on the same line terminated in Z_a.

Now let $kd_g = \pi/2$ to establish point P, then

$$R_g' = Z_o r_g \tag{A7}$$

$$X_g' = 0 . \tag{A8}$$

For any arbitrary length of transmission line between the source and the antenna, the antenna impedance seen at point P will be

$$Z_a' = R_a' + j X_a' . \tag{A9}$$

Now let us compute the power absorbed by the antenna. The equivalent circuit is as shown in Fig. A-1. Note that in Fig. A-1, E_g' is not, in general, the same as E_g in Figs. 92 and 93. The equivalent source voltage has been transformed by the transmission line. As will be shown presently, this transformation need not be calculated; a measurement of maximum power available from the source will suffice to define E_g' so that the E_g or E_g' need be measured explicitly.

From Fig. A-1 the power absorbed by the antenna is

$$I = \frac{E_g'}{\sqrt{(R_g' + R_a)^2 + (X_a')^2}} \tag{A10}$$

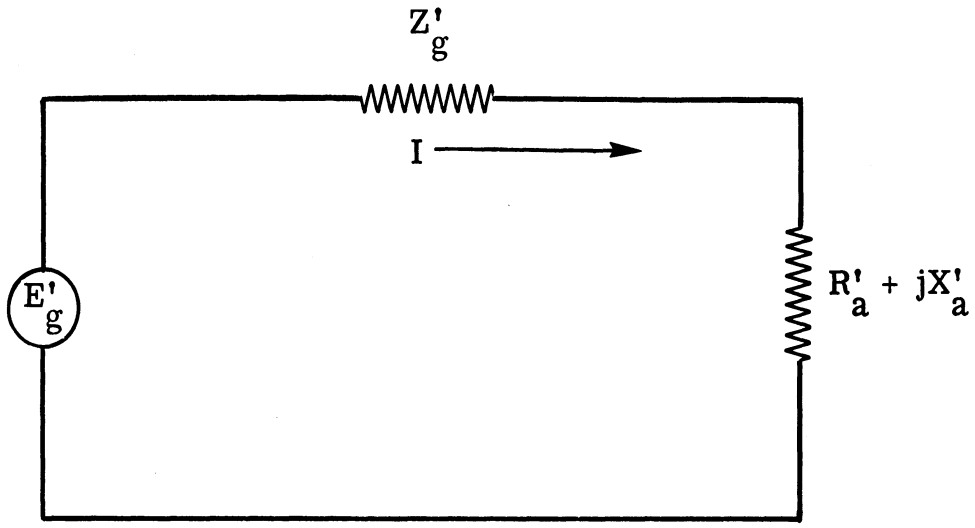

FIG. A-1: EQUIVALENT CIRCUIT FOR THE TRANSMISSION LINE PROBLEM

$$P = I^2 R_a' = \frac{E_g'^2 R_a}{(R_s' + R_a')^2 + (X_a')^2} \tag{A11}$$

Equation (A11) may be normalized by computing the maximum power that any load might draw from the source. For the maximum power, the transmission line should be terminated by a load R_g' at $kd_g = \pi/2$. For this condition the maximum power is given by

$$P_M = I^2 R_g' \tag{A12}$$

$$I = \frac{E_g'}{2R_g'} \tag{A13}$$

$$P_M = \frac{E_g'^2}{4R_g'} \tag{A14}$$

Now, Equation (A11) can be written in normalized form.

$$\frac{P}{P_M} = \frac{E_g'^2 R_a'}{(R_g' + R_a')^2 + (X_a')^2} = \frac{4R_g'}{E_g'^2} \tag{A15}$$

$$\frac{P}{P_M} = \frac{4R_g' R_a'}{(R_g' + R_a')^2 + (X_a')^2} \tag{A16}$$

Substituting the relations (A3), (A5), and (A6) (remembering that $kd_g = \pi/2$) Equation (A16) becomes

$$\frac{P}{P_M} = \frac{4 Z_o r_g \dfrac{Z_o r_a}{r_a^2 \cos^2 kd_a + \sin^2 kd_a}}{\left(Z_o r_g + \dfrac{Z_o r_a}{r_a^2 \cos^2 kd_a + \sin^2 kd_a} \right)^2 + \left(\dfrac{Z_o (1 - r_a^2) \cos kd_a \sin kd_a}{r_a^2 \cos^2 d_a + \sin^2 kd_a} \right)^2} \tag{A17}$$

Simplifying Equation (A17) results in

$$\frac{P}{P_M} = \frac{4 r_g r_a (r_a^2 \cos^2 kd_a + \sin^2 kd_a)}{\left[r_g (r_a^2 \cos^2 kd_a + \sin^2 kd_a) + r_a \right]^2 + (1 - r_a^2)^2 \cos^2 kd_a \sin^2 kd_a} \tag{A18}$$

Now for certain values of d_a P/P_M will be maximum or minimum.

if $kd_a = n\pi$ $\qquad n = 0, 1, 2, \ldots\ldots$

$$P\Big|_{n\pi} = P_{min} = P_M \frac{4 r_s r_a r_a^2}{(r_g r_a^2 + r_a)^2 + 0} \tag{A19}$$

$$= P_M \frac{4 r_g r_a}{(r_g r_a + 1)^2} \tag{A20}$$

If $kd_a = \frac{2n+1}{2}\pi$ $\qquad n = 0, 1, 2, \ldots\ldots$

$$P\Big|_{\frac{(2n+1)\pi}{2}} = P_{max} = P_M \frac{4r_g r_a}{(r_g + r_a)^2} \tag{A21}$$

$$\frac{P_{max}}{P_{min}} = \alpha^2 = \frac{r_g r_a + 1}{r_g + r_a}^2 \tag{A22}$$

Equation (A22) is a simple equation that determines the ratio of the maximum power to the minimum power delivered to an antenna from a course using any aribtrary length of the transmission line. The only quantities that need to be measured are the standing wave ratios for the antenna and the source impedance. Equation (A21) gives the ratio of the maximum power delivered to an arbitrary impedance to the maximum power available from the source using an impedance matched to the source.

The equations of greatest interest at this point are Eqs. (A14), (A18), and (A22). First, Eq. (A14).

$$P_M = \frac{E'^2_g}{4R'_g} \tag{A14}$$

This equation establishes the absolute maximum power available from the sources using a matched load; no other load can extract more power from the source.

Now consider Eq. (A18):

$$\frac{P}{P_M} = \frac{4r_g r_a (r_a^2 \cos^2 kd_a + \sin^2 kd_a)}{\left[r_g (r_a^2 \cos^2 kd_a + \sin^2 kd_a) + r_a\right]^2 + (1 - r_a^2)^2 \cos^2 kd_a \sin^2 kd_a} \tag{A18}$$

For fixed r_g and r_a, the power, P, absorbed by the load will vary between the two values given by Eqs. (A20) and (A21).

$$P_{min} = P_M \frac{4 r_g r_a}{(r_g r_a + 1)^2} \qquad \text{(A20)}$$

$$P_{max} = P_M \frac{4 r_g r_a}{(r_g + r_a)^2} \qquad \text{(A21)}$$

Thus, P can never be greater than P_{max} no less than P_{min} regardless of the transmission line length*.

These equations (A20 and A21) are relatively simple and will predict the maximum and minimum power radiated by an antenna when connected to a specified source. The data necessary from measurements consists of two standing wave ratio measurements and one power measurement.

Predicting the power delivered to the antenna as a function of the transmission line length is somewhat more complicated and requires additional work.

For this problem, we have to turn our attention to Eqs. (A18) and (A21).

---

*Recall the assumption that the transmission line is lossless and contains no reflection from connectors or other discontinuities. This lossless condition can be removed if the standing wave ratio r_g and the power available, P_M, are measured through a length of transmission line approximately equal to the length used in a typical installation. The reflectionless condition will also be removed for a given installation by this technique, but the variation from one installation to another will not. Normal connector reflections are small and should not affect the prediction appreciably.

$$\frac{P}{P_M} = \frac{4\, r_g\, r_a\, (r_a^2 \cos^2 kd_a + \sin^2 kd_a)}{\left[r_g (r_a^2 \cos^2 kd_a + \sin^2 kd_a) + r_a\right]^2 + (1 - r_a^2)^2 \cos^2 kd_a \sin^2 kd_a} \qquad \text{(A18)}$$

$$\frac{P_{max}}{P_M} = \frac{4 r_g\, r_a}{(r_g + r_a)^2} \qquad \text{(A21)}$$

Dividing Equation (A18) by Equation (A21), we obtain

$$\frac{P}{P_{max}} = \frac{(r_g + r_a)^2 (r_a^2 \cos^2 kd_a + \sin^2 kd_a)}{\left[r_g (r_a^2 \cos^2 kd_a + \sin^2 kd_a) + r_a\right]^2 + (r_a^2 - 1)^2 \cos^2 kd_a \sin^2 kd_a} \qquad \text{(A23)}$$

Fortunately, this expression can be simplified greatly to the following:

$$\frac{P}{P_{max}} = \frac{1}{\alpha^2 \cos^2 kd_a + \sin^2 kd_a} \qquad \text{(A24)}$$

in which

$$\alpha^2 = \left(\frac{r_g\, r_a + 1}{r_g + r_a}\right)^2 = \frac{P_{max}}{P_{min}} \qquad \text{(A22)}$$

In Figure 94, a set of universal curves calculated from Equation (A24) show the variation of power delivered to the antenna as a function of the transmission line length, d_a.

REFERENCES

1. Dute, J. C., J. E. Ferris and R. B. Harris (1966), "Antenna Spectrum Signature Data Recording Techniques," The University of Michigan Radiation Laboratory Report 7274-4-T, AFAL-TR-66-169, Supplement I (June 1966).

2. Ferris, J. E., S. E. Stone and R. L. Wolford (1965), "Investigation of Measurement Techniques for Obtaining Airborne Antenna Spectrum Signatures," The University of Michigan Radiation Laboratory Report 6664-1-F, AFAL-TR-104. UNCLASSIFIED. 105 pp.

3. Montgomery, C. G., R. H. Dicke and E. M. Purcell (1948), "Waveguides as Transmission Lines," Chapter 3, p. 72, Principles of Microwave Circuits, 8, Radiation Laboratory Series, Boston Technical Lithographers, Inc., Lexington, Massachusetts.

unclassified

Security Classification

DOCUMENT CONTROL DATA - R&D

(Security classification of title, body of abstract and indexing annotation must be entered when the overall report is classified)

1. ORIGINATING ACTIVITY *(Corporate author)* The University of Michigan Department of Electrical Engineering Radiation Laboratory	2a. REPORT SECURITY CLASSIFICATION unclassified 2b. GROUP

3. REPORT TITLE

Investigation of Measurement Techniques for Obtaining Airborne Antenna Spectrum Signatures

4. DESCRIPTIVE NOTES *(Type of report and inclusive dates)*

Final Technical Report

5. AUTHOR(S) *(Last name, first name, initial)*

Ferris, Joseph E., DeHart, Wilbur R., Wolford, Ronald L., Henry, William B.

6. REPORT DATE	7a. TOTAL NO. OF PAGES	7b. NO. OF REFS
June 1966	139	3

8a. CONTRACT OR GRANT NO. AF 33(615)-2606 b. PROJECT NO. 4357 c. Task No. 435703 d.	9a. ORIGINATOR'S REPORT NUMBER(S) 7274-1-F 9b. OTHER REPORT NO(S) *(Any other numbers that may be assigned this report)*

10. AVAILABILITY/LIMITATION NOTICES Qualified requesters may obtain copies of this report from DDC This document is subject to special export controls and each transmittal to foreign governments or foreign nationals may be made only with prior approval of AFAL (AVPT), Wright-Patterson AFB Ohio 45433.

11. SUPPLEMENTARY NOTES	12. SPONSORING MILITARY ACTIVITY Air Force Avionics Laboratory Air Force Systems Command Wright Patterson AFB, Ohio

13. ABSTRACT

This report discusses three areas which are of importance to the Electromagnetic Compatibility program presently being conducted by the U. S. Government. The areas discussed in this report are: 1) methods for obtaining spectrum signatures at a minimum of cost, 2) data recording techniques, and 3) methods for obtaining transmitter signature characteristics.

The methods for obtaining antenna spectrum signatures discusses the use of simplified models along with typical results for three different antenna configurations. The three antenna configurations were tested on both a simplified and a precision model of a jet aircraft at a fundamental and four harmonic frequencies. In the data recording section the data format for antenna signature is presented. A recommendation as to the format in which the data should be collected and forwarded to ECAC for prediction analysis is made. A discussion of a technique for digitally recording signature data at a minimum of cost is presented. Under the final section techniques for determining the signature characteristics of a communications type system is discussed and some preliminary results.

DD FORM 1 JAN 64 1473

unclassified

Security Classification

unclassified

Security Classification

14. KEY WORDS	LINK A		LINK B		LINK C	
	ROLE	WT	ROLE	WT	ROLE	WT
Spectrum signatures						
Antenna						
Measurements						

INSTRUCTIONS

1. ORIGINATING ACTIVITY: Enter the name and address of the contractor, subcontractor, grantee, Department of Defense activity or other organization *(corporate author)* issuing the report.

2*a*. REPORT SECURITY CLASSIFICATION: Enter the overall security classification of the report. Indicate whether "Restricted Data" is included. Marking is to be in accordance with appropriate security regulations.

2*b*. GROUP: Automatic downgrading is specified in DoD Directive 5200.10 and Armed Forces Industrial Manual. Enter the group number. Also, when applicable, show that optional markings have been used for Group 3 and Group 4 as authorized.

3. REPORT TITLE: Enter the complete report title in all capital letters. Titles in all cases should be unclassified. If a meaningful title cannot be selected without classification, show title classification in all capitals in parenthesis immediately following the title.

4. DESCRIPTIVE NOTES: If appropriate, enter the type of report, e.g., interim, progress, summary, annual, or final. Give the inclusive dates when a specific reporting period is covered.

5. AUTHOR(S): Enter the name(s) of author(s) as shown on or in the report. Enter last name, first name, middle initial. If military, show rank and branch of service. The name of the principal author is an absolute minimum requirement.

6. REPORT DATE: Enter the date of the report as day, month, year; or month, year. If more than one date appears on the report, use date of publication.

7*a*. TOTAL NUMBER OF PAGES: The total page count should follow normal pagination procedures, i.e., enter the number of pages containing information.

7*b*. NUMBER OF REFERENCES: Enter the total number of references cited in the report.

8*a*. CONTRACT OR GRANT NUMBER: If appropriate, enter the applicable number of the contract or grant under which the report was written.

8*b*, 8*c*, & 8*d*. PROJECT NUMBER: Enter the appropriate military department identification, such as project number, subproject number, system numbers, task number, etc.

9*a*. ORIGINATOR'S REPORT NUMBER(S): Enter the official report number by which the document will be identified and controlled by the originating activity. This number must be unique to this report.

9*b*. OTHER REPORT NUMBER(S): If the report has been assigned any other report numbers *(either by the originator or by the sponsor)*, also enter this number(s).

10. AVAILABILITY/LIMITATION NOTICES: Enter any limitations on further dissemination of the report, other than those imposed by security classification, using standard statements such as:

(1) "Qualified requesters may obtain copies of this report from DDC."

(2) "Foreign announcement and dissemination of this report by DDC is not authorized."

(3) "U. S. Government agencies may obtain copies of this report directly from DDC. Other qualified DDC users shall request through

_____."

(4) "U. S. military agencies may obtain copies of this report directly from DDC. Other qualified users shall request through

_____."

(5) "All distribution of this report is controlled. Qualified DDC users shall request through

_____."

If the report has been furnished to the Office of Technical Services, Department of Commerce, for sale to the public, indicate this fact and enter the price, if known.

11. SUPPLEMENTARY NOTES: Use for additional explanatory notes.

12. SPONSORING MILITARY ACTIVITY: Enter the name of the departmental project office or laboratory sponsoring *(paying for)* the research and development. Include address.

13. ABSTRACT: Enter an abstract giving a brief and factual summary of the document indicative of the report, even though it may also appear elsewhere in the body of the technical report. If additional space is required, a continuation sheet shall be attached.

It is highly desirable that the abstract of classified reports be unclassified. Each paragraph of the abstract shall end with an indication of the military security classification of the information in the paragraph, represented as *(TS)*, *(S)*, *(C)*, *or (U)*.

There is no limitation on the length of the abstract. However, the suggested length is from 150 to 225 words.

14. KEY WORDS: Key words are technically meaningful terms or short phrases that characterize a report and may be used as index entries for cataloging the report. Key words must be selected so that no security classification is required. Identifiers, such as equipment model designation, trade name, military project code name, geographic location, may be used as key words but will be followed by an indication of technical context. The assignment of links, rules, and weights is optional.

unclassified

Security Classification